ESD-TR-70-123

THE EFFECT OF METEOROLOGICAL CONDITIONS ON THE TRADE WIND DUCT AND RELATED RADIO WAVE PROPAGATION

L. G. Rowlandson
H. W. Meredith

February 1970

AEROSPACE INSTRUMENTATION PROGRAM OFFICE
HQ ELECTRONIC SYSTEMS DIVISION (AFSC)
L. G. Hanscom Field, Bedford, Massachusetts 01730

(Prepared under Contract No. F19628-69-C-0208 by Syracuse University Research Corp., Merrill Lane, University Heights, Syracuse, New York 13210.)

LEGAL NOTICE

When U. S. Government drawings, specifications or other data are used for any purpose other than a definitely related government procurement operation, the government thereby incurs no responsibility nor any obligation whatsoever; and the fact that the government may have formulated, furnished, or in any way supplied the said drawings, specifications, or other data is not to be regarded by implication or otherwise as in any manner licensing the holder or any other person or conveying any rights or permission to manufacture, use, or sell any patented invention that may in any way be related thereto.

OTHER NOTICES

Do not return this copy. Retain or destroy.

ESD-TR-70-123

THE EFFECT OF METEOROLOGICAL CONDITIONS ON THE TRADE WIND DUCT AND RELATED RADIO WAVE PROPAGATION

L. G. Rowlandson
H. W. Meredith

February 1970

AEROSPACE INSTRUMENTATION PROGRAM OFFICE
HQ ELECTRONIC SYSTEMS DIVISION (AFSC)
L. G. Hanscom Field, Bedford, Massachusetts 01730

(Prepared under Contract No. F19628-69-C-0208 by Syracuse University Research Corp., Merrill Lane, University Heights, Syracuse, New York 13210.)

FOREWORD

This report is prepared for the

Aerospace Instrumentation Program Office
Electronic Systems Division
Air Force Systems Command of the United States Air Force
Bedford, Massachusetts

Air Force Program Monitor - Lt. C. Schafer, ESD/ESSIE

Project Number 6684, Task 6684.08

covering research over the period

1969 March 1 to 1970 February 28.

Prepared under Contract No. F19628-69-C-0208 by

Syracuse University Research Corporation
Merrill Lane, University Heights
Syracuse, New York.

This report was reviewed and approved.

C. Schafer, Lieutenant, USAF
Program Manager for ESD/ESSIE/6684.

ABSTRACT

The horizontal extent and the intensity of the Trade Wind Inversion are controlled by meteorological conditions. The subtropical area of the Caribbean is influenced by subsiding air which tends to produce a temperature inversion around one kilometer above the sea surface. The vertical transport of water vapor is thereby inhibited and a boundary forms along the inversion with moist air below and dry air above. The index of radio refraction therefore decreases rapidly with height through this layer to form an elevated duct. The meteorological situation controlling the characteristics of this duct varies from the normal high pressure condition. Interest is therefore centered on the variability of the inversion layer as affected by weather systems and local geographical conditions.

ACKNOWLEDGEMENT

We wish to acknowledge the support provided by Mr. John Herlihy in the areas of flight planning and the supervision of data collection and processing. Mr. Herlihy formerly of SURC is now with Telcomp Corporation, Cambridge, Massachusetts.

We also wish to commend the support received from the Air Base Wing at L. G. Hanscom Field, Bedford, Massachusetts for the operation and maintenance of the USAF, C-131 aircraft used to make the meteorological measurements.

Our appreciation is also extended to Mrs. R. Aldrich and Mr. N. Gerson of SURC for their efforts and recommendations during the preparation of the respective reports.

TABLE OF CONTENTS

		Page
Section I	Introduction	1
1.1	Thermodynamic Processes in the Trade Wind Structure	3
1.2	The Experimental Program	4
Section II	A Description of Available Data and Their Presentation	7
Section III	The Temporal and Spatial Variations of Refractivity Within Limited Geographical Areas (Missions 1 and 2, 6 March)	11
3.1	Measurement in the Key West Area, Mission 1	11
3.2	Measurements in the Key West Area, Mission 2	17
3.3	Comments on Missions 1 and 2	20
Section IV	The Characteristics of the Inversion and Associated Weather From Key West to New Orleans (Mission 3, 9 March)	25
Section V	The Characteristics of the Inversion and Associated Weather From Eglin to Merida (Mission 4, 10 March)	31
Section VI	The Characteristics of the Trade Wind Duct and Associated Weather From Merida to the Caymans (Mission 5, 11 March)	39
Section VII	The Temporal and Spatial Variations of Refractivity in the Area of Puerto Rico (Mission 6, 14 March)	49
Section VIII	The Characteristics of the Trade Wind Duct and Associated Weather From San Juan to Grand Turk (Mission 7, 17 March)	63
Section IX	The Characteristics of the Trade Wind Duct and Associated Weather From Grand Turk to Nassau (Mission 8, 18 March)	69

		Page
Section X	Spatial Variations of Refractivity in the Vicinity of Key West (Missions 9, 10, and 11 21 March)	77
Section XI	Variations of Refractivity in the Key West Area (Missions 12, 13, and 14)	85
11.1	Mission 12	85
11.2	Mission 13	89
11.3	Mission 14	93
Section XII	The Characteristics of Elevated Layers Measured During the Test Period	107
Section XIII	Radiosonde Lag Constants	124
13.1	Absolute Errors	126
13.2	Relative Errors	127
13.3	Summary	129
Section XIV	Meteorological Analysis and Related Inversion Characteristics Along Two Planes in the Caribbean	131
14.1	Jacksonville, Florida, to Allbrook Air Force Base, Panama	131
14.2	Merida, Mexico, to Guadelupe by Way of Grand Turk	135
14.3	Summary	136
Section XV	Conclusions	140
Section XVI	Recommendations	143
Appendix A	Correction Procedures for the Sensor Time Lag in Radiosonde Data (After Dougherty)	144
References		150

SECTION I

INTRODUCTION

The Caribbean Sea is within the subtropical area wherein dry air from high altitudes descends and flows toward the equatorial trough. This flow replaces the air rising from the equatorial region due to thermal convection. A circulation pattern is shown in Figure 1, which also includes a high altitude northward flow to replace the dense surface air draining from the polar region. Due to the earth's rotation, the air moving towards the equatorial trough becomes directed towards the west. This combination of effects produces a flow of air from the northeast across the Caribbean with the direction increasing toward the west as the flow approaches the equatorial region.

The dry subsiding air within this flow is heated due to the pressure increase as it descends. In the vicinity of one kilometer above sea level, a temperature inversion generally occurs where the air temperature becomes greater than the temperature of the underlying maritime air. This temperature inversion retards the upward movement of moist air and a boundary is formed with dry air above and moist air below. Since the index of radio refractivity is directly affected by the water vapor pressure, the inversion produces a region wherein the refractivity decreases rapidly with height. In terms of the effect of this layer on radio propagation, two significant conditions are produced. First, the rapid decrease of refractivity with height produces an elevated duct. Radio signals introduced into this duct can be propagated with very small attenuation if the energy is constrained to remain with the duct. Second, this layer represents an above normal change of dielectric constant with height. This dielectric change permits a significant amount of radio energy to be reflected from the layer, thereby affording another mechanism to obtain propagation beyond the radio horizon.

The characteristics of this layer are changed due to orographic and thermal effects which can generate sufficient vertical momentum to cause moisture to break through the layer. Therefore, the layer is generally not continuous and homogeneous because of these effects. Any frontal system, usually off the continent from the northwest, will break up the layer and make it unrecognizable as the front passes. Of course, large scale low pressure cells which may come off the continent or from the hurricane generation area of the southeast can destroy the inversion. These cells cause large quantities of water vapor to be carried aloft which may not dissipate for several days following the passage of the weather system.

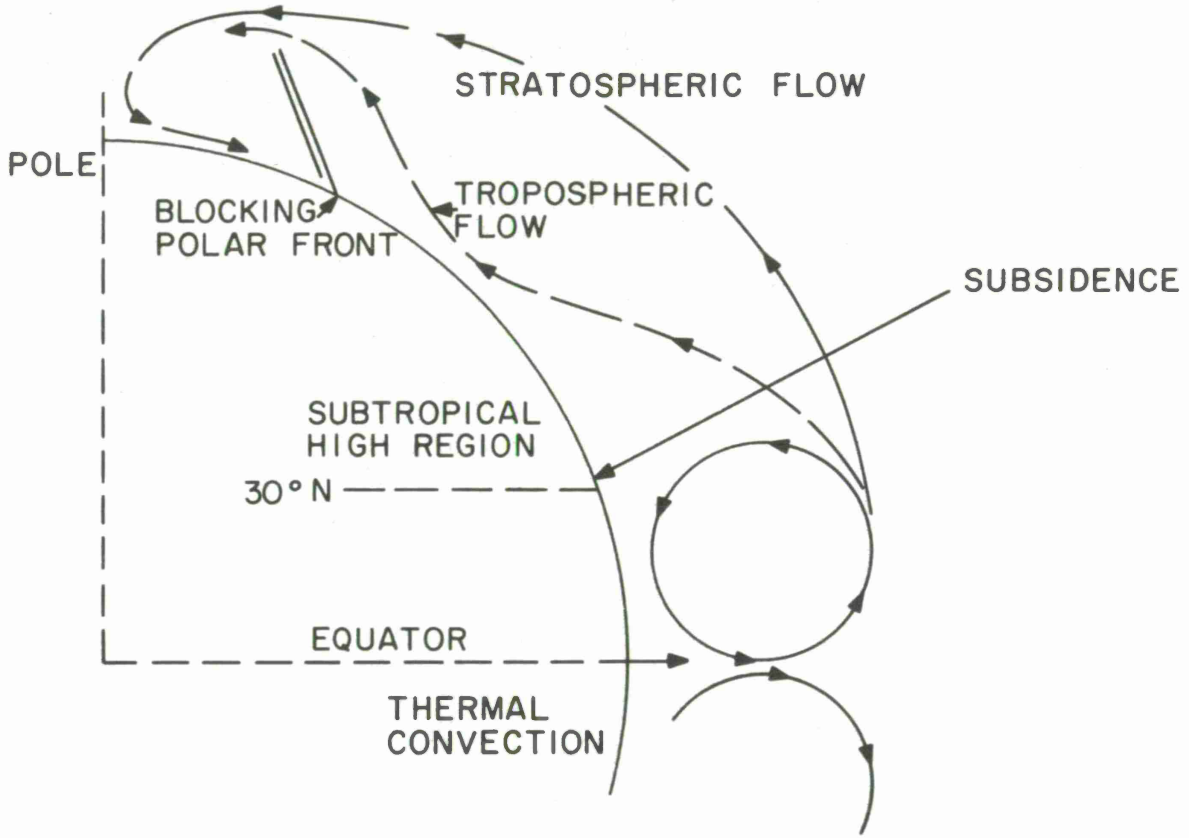
STRATOSPHERIC FLOW
POLE
BLOCKING
POLAR FRONT
TROPOSPHERIC
FLOW
SUBSIDENCE
SUBTROPICAL
HIGH REGION
30° N
EQUATOR
THERMAL
CONVECTION

FIGURE 1.

1.1 Thermodynamic Processes in the Trade Wind Structure

Several effects are present in determining the formation and the characteristic thermodynamic and moisture structure of the Trade Wind Regime. First, there is an exchange of heat and water vapor between the ocean and the atmosphere. Second, the latent heat exchanged in this transfer of momentum determines the general circulation patterns (Montgomery, 1936, 1948).

At the boundary layer of the air and sea water molecules are continually diffusing into a very thin air film at the surface. Above this the air flow becomes turbulent due to the fact that the flow is in friction with the laminar layer of air at the surface. The continuing vertical exchange of momentum is then largely produced by this dynamic turbulence.

In addition, there may exist composite convection, particularly where the Westerly Trades initially begin to overflow the warmer waters of the Caribbean Sea. The superadiabatic layer, which then forms near the sea surface, is a region of great instability wherein the vertical transfer of moist air is not only unrestircted but is in fact enhanced. Above this near-surface layer the temperature lapse rate is essentially adiabatic and it is found that the specific humidity is nearly constant and the air-water mixture seems to be completely mixed and homogeneous (Gentilli, 1958; Hill, 1962).

Experimental data indicates that on the average the homogeneous layer extends to about 550 meters and about 80 percent of the level of condensation under cloudy conditions.

As the vertical stability of the air increases because of subsidence of the air aloft, the marine layer is therefore constrained in its vertical thickness. Further experimental data presented herein shows that the lifting produced by the release of latent heat of condensation can overcome the subsidence stability and lift the water vapor above the local, average height of the marine layer. The occasion of cellular convection, coupled with wind shear, often produces longitudinal roll vortices with their axes parallel to the direction of shear (Benard, 1900). When overflying the Caribbean, one may frequently see extensive areas where these clouds produce a corrugated roof appearance.

Extensive analytical and experimental studies on the Trades cloud structure are documented and it is unreasonable to attempt to cover this material herein. The publication by Roll is very comprehensive in this area and is recommended reading for anyone wishing to pursue this subject (Roll, 1965).

1.2 The Experimental Program

This report attempts to associate the meteorological conditions, including thermal and orographic effects, storm systems and fronts, with the intensity and horizontal extent of the inversion layer.

The experimental program was initiated on 6 March 1969 and continued through 25 March 1969. An instrumental USAF C-131 Convair was used to obtain detailed measurements on the characteristics of the Trade Wind Inversion [Rowlandson, et al, 1969]. An extended flight was made from Key West, Florida, in a counter-clockwise direction extending through the areas of New Orleans, Merida, Grand Caymans, Puerto Rico, the Bahamas and back to Key West. Figure 2 shows the flight plan with vertical soundings indicated by the circles along the various legs. At Key West and Puerto Rico, additional local measurements were made in an attempt to determine how the inversion could be affected by local climatological features.

Whenever possible the flights were made to coincide with a local radiosonde observation. This was done, in part, to determine to what extent radiosonde data could be used to define the inversion characteristics. Radiosonde data were also used to support the analysis of temporal and spatial effects.


MASTER FLIGHT RECORD
UNITED STATES
MOBILE
EGLIN AFB
ATLANTIC OCEAN
PATRICK AFB
GULF OF MEXICO
PATH II
PATH IIII
PATH III
KEY WEST NAS
PATH I
NASSAU
BAHAMA ISLANDS
GRAND TURK ISLAND
PATH IIII
HAVANA
CUBA
MERIDA
MEXICO
GEORGE TOWN
CAYMAN ISLANDS
PATH III
GREATER ANTILLES
JAMAICA
KINGSTON
DOMINICAN REPUBLIC
HAITI
RAMEY AFB
SAN JUAN
PUERTO RICO
PATH II
LESSER ANTILLES
BRITISH HONDURAS
CARIBBEAN SEA
GUATEMALA
HONDURAS
EL SALVADOR
NICARAGUA
COSTA RICA
PANAMA
COLUMBIA
VENEZUELA
GULF OF MEXICO – CARIBBEAN AREA
SCALE 1:5,702,400 OR 90 MILES TO 1 INCH
STATUTE MILES
KILOMETERS
TRACED FROM NATIONAL GEOGRAPHIC SOCIETY MAP, WASHINGTON, DECEMBER 1959

FIGURE 2.

SECTION II

A DESCRIPTION OF AVAILABLE DATA AND THEIR PRESENTATION

Measurements were made of air temperature, relative humidity and radio refractivity over a large part of the northern Caribbean Sea. The airborne instrumentation and data collected were described in earlier reports. In addition, the weather maps (surface and 850 millibar) describing the meteorological conditions were presented with these airborne measurements. On many occasions, radiosonde launches were made in conjunctionwith local aircraft measurements providing a direct comparison of data. In general, the radiosonde data over the northern Caribbean areawere used to assist in defining the meteorological conditions, such as the description of a frontal system, andwere generally not directly related to the airborne measurements.

Cloud photographs were obtained from the aircraft as frequently as possible. These photographs indicate the presence of weather systems and the local meteorological forces at work. In the presence of a strong, extensive, inversion, the cloud tops tend to lie along the inversion and are broken only by local thermal convection. The moist air rises but as it reaches the temperature inversion it then sinks causing a circulation of air at the inversion height. Strong turbulence in flight at the inversion height is therefore a good indication that the layer is well formed and intense.

The following data presentation associate the meteorological and local geographical effects with the inversion characteristics measured by the instrumentation. Radiosonde and cloud conditions are included, whenever possible, to corroborate the discussions.

These data will be presented in a chronological order within each section and identified by aircraft mission numbers so they may be related to measurements and data presented in the earlier reports.

Several parameters associated with these measurements should be clearly defined. The first is the radio refractivity, N, and the modified index of refraction, M, both of which play an important role in determining the relationship of the inversion characteristics to radio wave propagation.

The index of refraction, n, for air is related to the refractivity, N, and free air variables by the expression, [Smith and Weintraub, 1953]

$$(n - 1) \cdot 10^6 = N \tag{1}$$

$$= \frac{77.6P}{T} + \frac{3.73 \times 10^5 e}{T^2} \tag{2}$$

where P = the air pressure (mb)

T = the air temperature ($^{\circ}$ K)

e = the water vapor pressure in the associated sample of air (mb)

To maintain hydrostatic equilibrium, the pressure, P, decreases almost exponentially with height and has such an overwhelming influence on N, that in general it is found that N also decreases exponentially with height [Bean and Dutton, 1966]. Variations from this average behavior are primarily due to the water vapor pressure term, e. This subject will be discussed further in the report.

When a radio signal is propagated and its travel defined by a single ray, the variations of N along its path produce changes in its velocity and its direction of travel. These considerations are well documented and do not need to be presented herein [Bean and Dutton, 1966]. In the study of radio ray propagation, it is frequently convenient to transform the geometry to a flat earth and treat the problem in Cartesian rather than in polar coordinates. This transformation changes the normal decrease of N with height over the flat earth.

The new index, M, resulting from this transformation then becomes

$$M(h) = N(h) + h/a \cdot 10^{6} \tag{3}$$

where h = the height above the earth's surface

a = the earth radius

Another parameter, the potential temperature, θ, is of particular importance when studying the Trade Wind Inversion [Fleagle and Businger, 1963]. The potential temperature is given by

$$\theta = T\left(\frac{P}{1000}\right)^{-R/C_p} \tag{4}$$

where T = the air temperature ($^{\circ}$ K)

P = the air pressure (mb)

R = the specific gas constant for air

C_p = the specific heat capacity for air at constant pressure

therefore,

$$R/C_p = 0.286 \text{ for dry air} \qquad (5)$$

The potential temperature may be considered to be the temperature a sample of dry air would have if it were compressed (or expanded) adiabatically from a given state, P and T, to a pressure of 1000 mb. Therefore, θ, is a conservative property of a parcel of air which is invariant during adiabatic processes.

When an inversion occurs, such as in the case of the Trade Wind Inversion, the potential temperature increases very rapidly with height through the layer. This condition indicates that abnormal (non-adiabatic) heating occurs which is produced by the subsidence of the upper air. The vertical stability of the air is then greatly increased in the layer. Therefore, the vertical transfer of air from the region below the layer is strongly inhibited.

It will be seen that any temperature advection that modifies the air, except for normal adiabatic processes, will have a marked effect on the vertical variation of potential temperature. Greater or lesser stability then occurs depending on the temperature change of the air from adiabatic.

SECTION III

THE TEMPORAL AND SPATIAL VARIATIONS OF REFRACTIVITY WITHIN LIMITED GEOGRAPHICAL AREAS
(Missions 1 and 2, 6 March)

Variations in the characteristic of the Trade Wind Inversion over large geographical areas, that is hundreds of miles, are associated with the changing meteorological conditions. Attempting to describe these effects from measurements using an instrumented aircraft can be frustrated because of the time and space rate of change of conditions when such large areas are concerned.

The characteristic of the inversion can be more readily determined if the area of investigation is severely restricted. In this case, spatial variations can be discerned within a time frame of a few hours and a check on the magnitude of temporal variations is possible by repeating measurements at the same location.

The following subsections attempt to describe such local variations and relate the radio refractivity profiles to associated meteorological conditions.

3.1 Measurements in the Key West Area, Mission 1

Missions 1 and 2 were flown on the same day and separated by about nine hours. It is meaningful to discuss these missions together since they reveal information on temporal effects between early morning and later in the afternoon on 6 March.

Figure 3 shows the flight plans.

Spiral	Location	Spiral Start Time Z	Local
A	a. Key West NAS	1131	0631
B	b. 25-06 N, 81-51 W	1214	0714
C	c. 24-06 N, 81-08 W	1315	0815

Taking a vertical slice through the locations of Spirals a, b, and c, the refractivity profiles are shown on Figure 4 for the morning mission. It is interesting to note that two layers are present. The lower one, usually identified as the Trade Wind Inversion, is about 1500 meters above sea level and decreases in altitude in the eastward direction. A second layer, around 2500 meters, is equally intense and also decreases in altitude in correspondence with the lower layer.

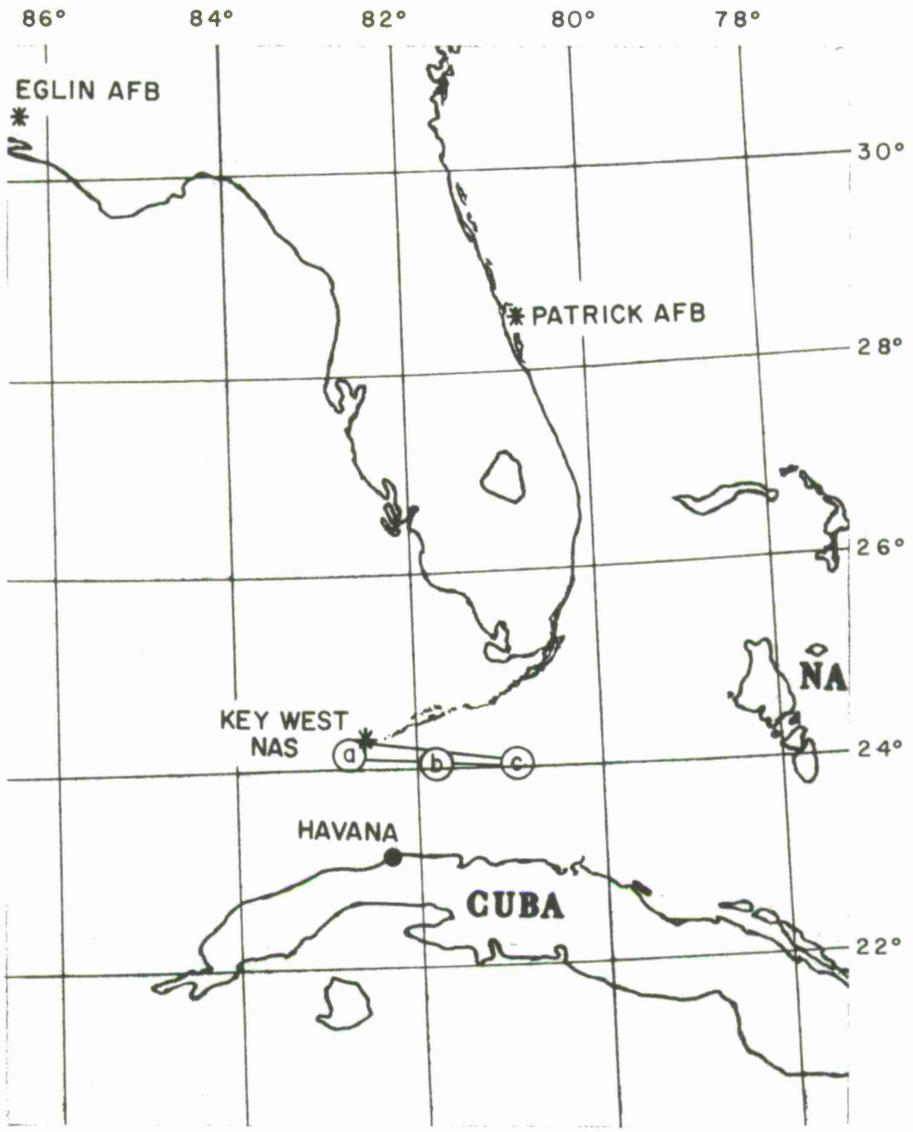

SCALE 1:5,702,400 OR 90 MILES TO 1 INCH

100 50 0 100 200 300

STATUTE MILES

100 50 0 100 200 300 400

KILOMETERS

FLIGHT PATH I

MISSIONS 1 AND 2 — 6 MARCH 1969

MISSIONS 9, 10, AND 11 — 21 MARCH 1969

FIGURE 3.

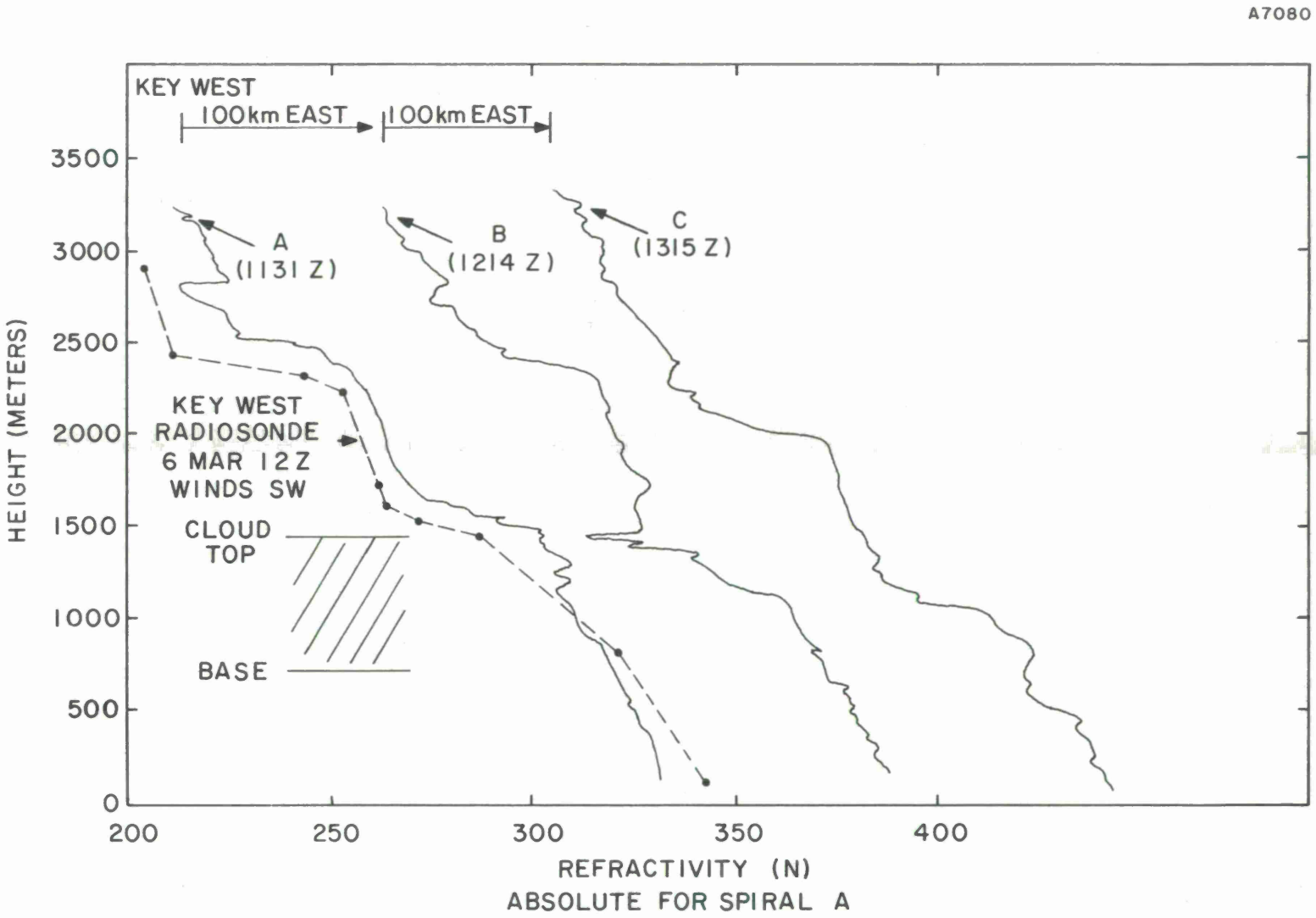
A7080
KEY WEST
100km EAST
100km EAST
A
(1131 Z)
B
(1214 Z)
C
(1315 Z)
KEY WEST
RADIOSONDE
6 MAR 12Z
WINDS SW
CLOUD
TOP
BASE
HEIGHT (METERS)
3500
3000
2500
2000
1500
1000
500
0
200
250
300
350
400
REFRACTIVITY (N)
ABSOLUTE FOR SPIRAL A

FIGURE 4.

This double layer condition was observed some years earlier at Curacao, N. A., during mid-February to mid-March 1965 Rowlandson, 1966. It does not appear to be a usual feature of the Caribbean area since there is little mention of it in the literature. However, examination of the potential temperature, θ, profiles shows that there are many instances where a marked increase in stability occurs in the region of 3000 meters. Therefore, a refractivity layer could form at these altitudes if a significant amount of moisture escaped from the maritime layer. The above report shows that strong thermal convection and orographic effects produced by land can produce sufficient momentum for water vapor to be driven aloft through what is normally defined as the inversion.

Figure 5 shows the profiles of water vapor, labeled E, and potential temperature, θ, associated with Spiral A. It is noted that the vertical increase of potential temperature is very small beneath the lower inversion. In fact conditions are almost completely adiabatic and moisture is filling the region with almost equal concentration in height. These conditions would optimize the chance that moisture be displaced into the next higher level by thermal and/or orographic effects.

The surface weather map, Figure 6, shows a high pressure cell east of Key West. The increased subsidence associated with this cell would cause the height of the inversions to lower, as it does, in a direction eastward from Key West. In any case, the normal flow of the Trade Winds from the northeast causes the concentration of water vapor to increase in the direction of the wind with a thickening of the maritime layer. This effect is produced by a continuous transfer of water vapor through the inversion largely due to thermal convection. The advection of water vapor not only weakens the strength of the refractivity gradient but tends to raise the mean height of the layer in the downwind direction. However, if the high pressure system was located southwest of Key West, the associated increase in subsidence could constrain this normal tendency for the Trade Wind Duct to rise with distance.

It is apparent from Figure 4 that the aircraft and radiosonde measurements taken at Key West are similar in shape. However, the radiosonde shows the inversion layer to be less intense at the lower level but more intense at the higher level. During the sounding, the aircraft covers a circular diameter of several miles, depending on its altitude, therefore, horizontal variations in refractivity, N, would appear as vertical variations on the profiles. For this reason, one cannot attach significance to the small variations represented by the aircraft measurements.

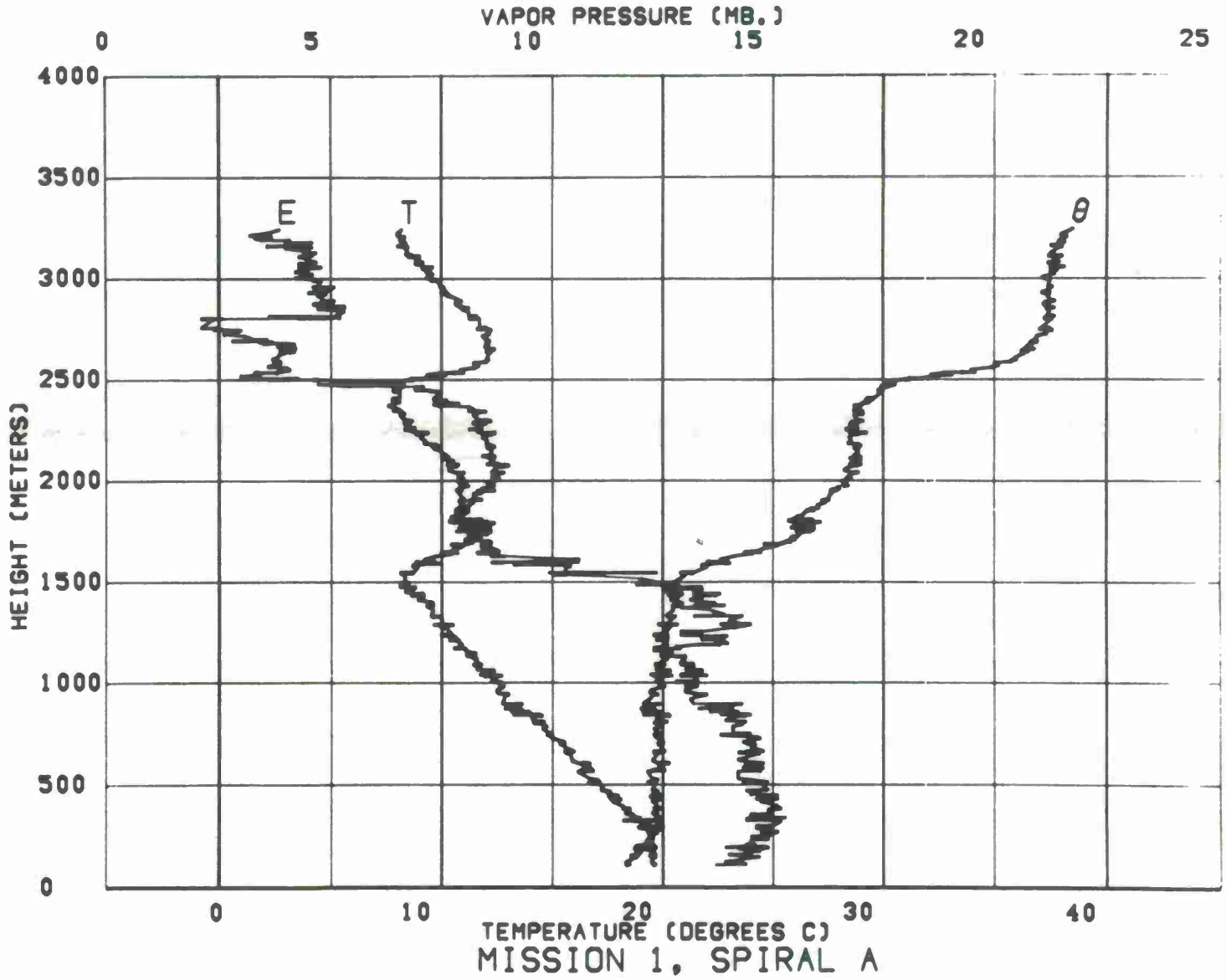
VAPOR PRESSURE (MB.)
0
5
10
15
20
25
4000
3500
3000
2500
2000
1500
1000
500
0
HEIGHT (METERS)
E
T
θ
0
10
20
30
40
TEMPERATURE (DEGREES C)
MISSION 1, SPIRAL A

FIGURE 5.

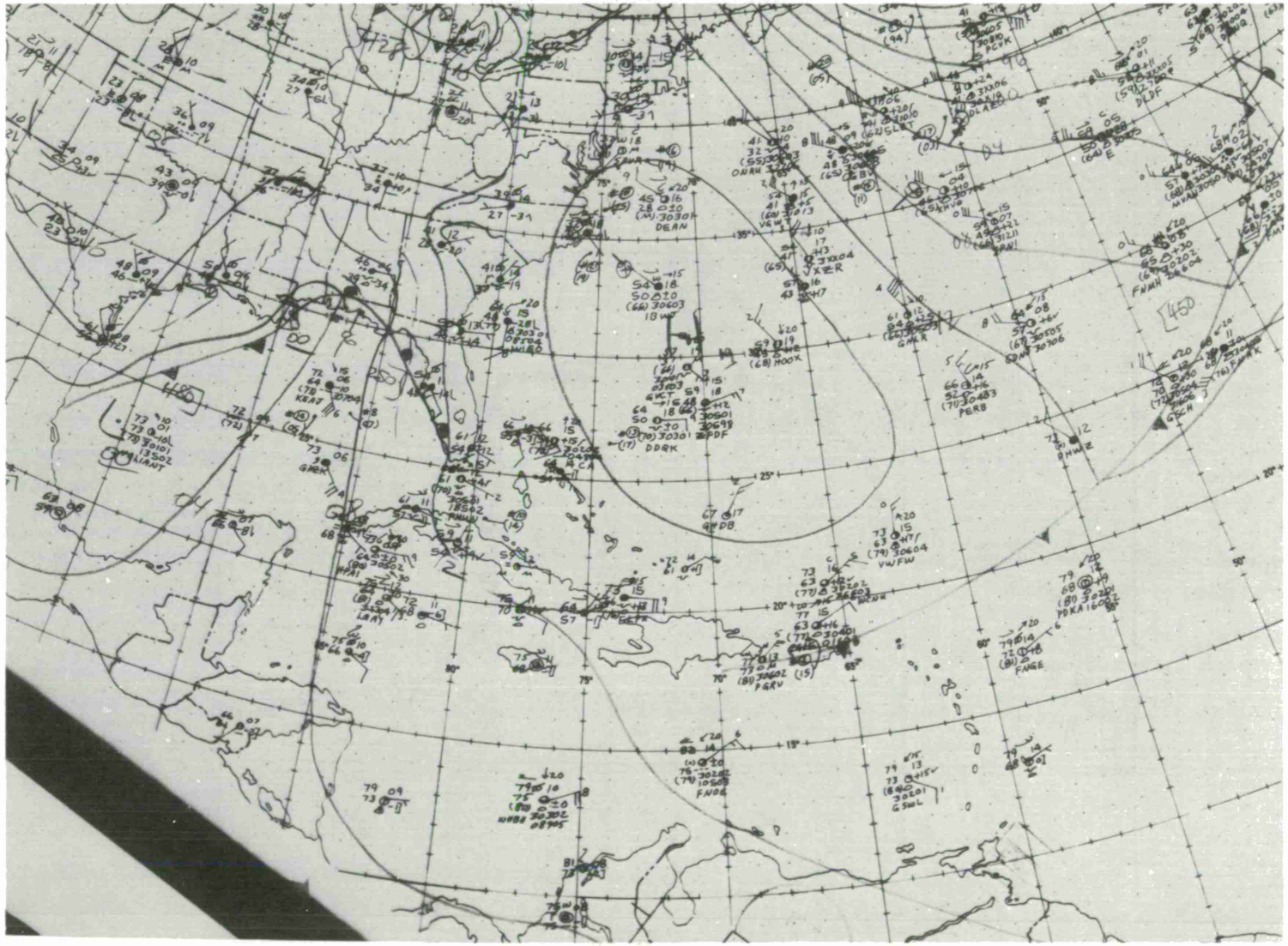

FIGURE 6

SURFACE CHART 6 March 1969

An additional effect is produced by the leeward drift of the radiosonde. At a nominal rate of ascent of 300 meters per minute it takes the radiosonde about five minutes to reach the height of the inversion. Therefore, depending upon the magnitude and direction of the near-surface winds, the radiosonde can be many miles away from the aircraft, at any particular time.

Large spatial variations which generally occur around land/sea interfaces can, therefore, severely limit any comparisons between respective measurements. The aircraft measurements (Figure 4) indicate significant spatial variations even for the large scale features shown on the profiles. Therefore, one cannot tacitly assume that the radiosonde data are less significant than the aircraft measurement even though by its method of operation it provides less detail.

3.2 Measurements in the Key West Area, Mission 2

The flight plan for Mission 2 is the same as before except that the soundings were taken in a different order. As shown directly below, Spiral A was flown at Position C, Spiral B at Key West, and so on. This was done to get two soundings at two separated locations to check for temporal effects. The rather unusual order in which these measurements were conducted was set by requirements for rest and refueling for the following morning's mission.

Spiral	Location	Spiral Start Time Z	Local
A	c. 24-06 N, 81-08 W	2019	1519
B	a. Key West NAS	2107	1607
C	b. 24-06 N, 81-51 W	2156	1657
D	c. 24-06 N, 81-08 W	2235	1735
E	a. Key West NAS	2313	1813

Mission 2, flown later in the afternoon of 6 March, indicates (Figure 7) that the inversion at the upper elevation has weakened with a corresponding increase in the intensity of the gradient at the lower level. Considering the times and locations of the aircraft measurements, it is apparent that the inversion, now at 1000 meters, shows little variation.

The weather map for 7 March, which is shown in an abbreviated form on Figure 8, indicates that the high pressure cell has moved South West. The effect of this movement is clearly evident on the aircraft measurements, above. Increased subsidence and greater horizontal stratification and

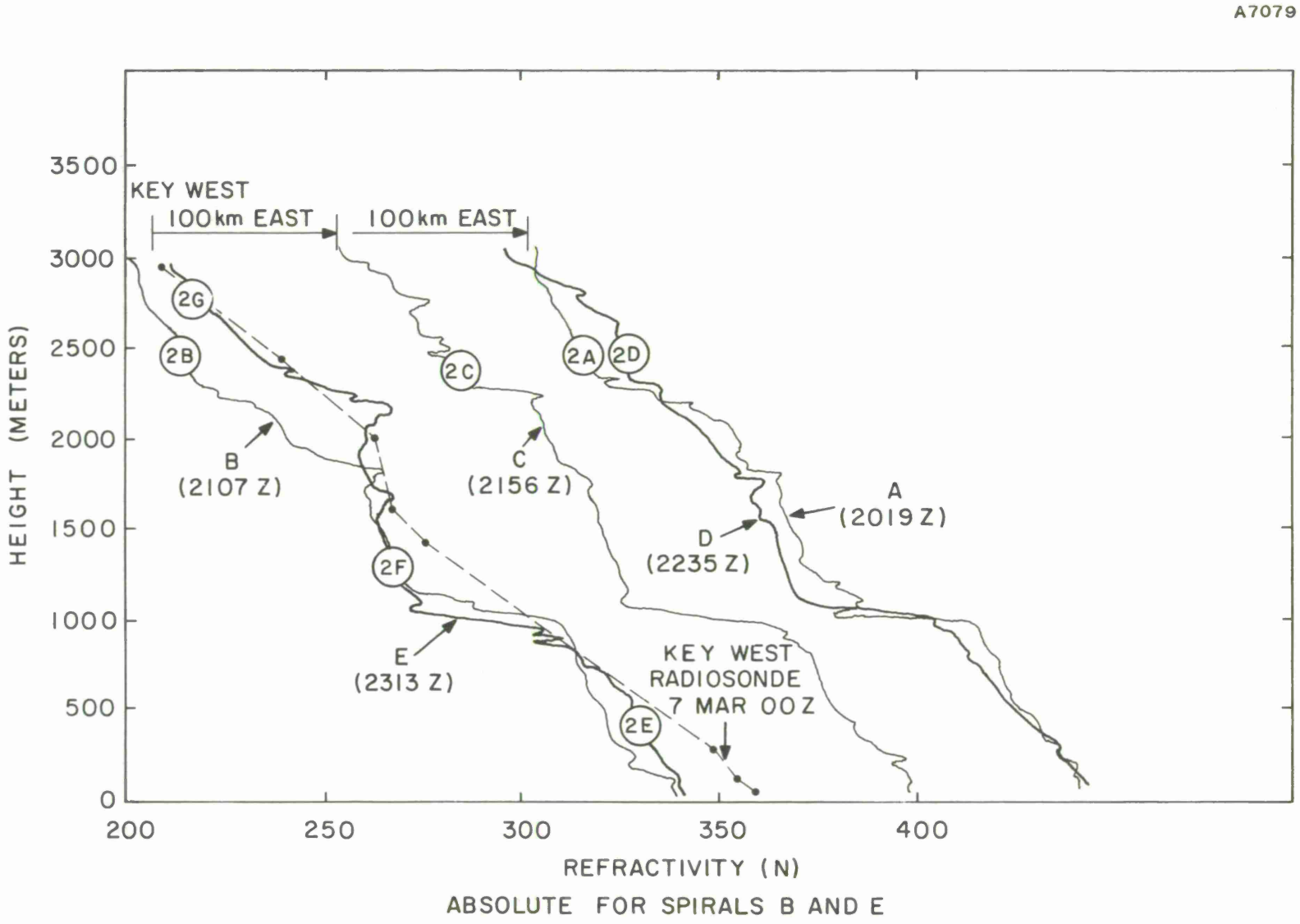
A7079
HEIGHT (METERS)
3500
3000
2500
2000
1500
1000
500
0
KEY WEST
100km EAST
100km EAST
2G
2B
2C
2A
2D
2F
2E
B
(2107 Z)
C
(2156 Z)
A
(2019 Z)
D
(2235 Z)
E
(2313 Z)
KEY WEST
RADIOSONDE
7 MAR 00Z
200
250
300
350
400
REFRACTIVITY (N)
ABSOLUTE FOR SPIRALS B AND E

FIGURE 7.

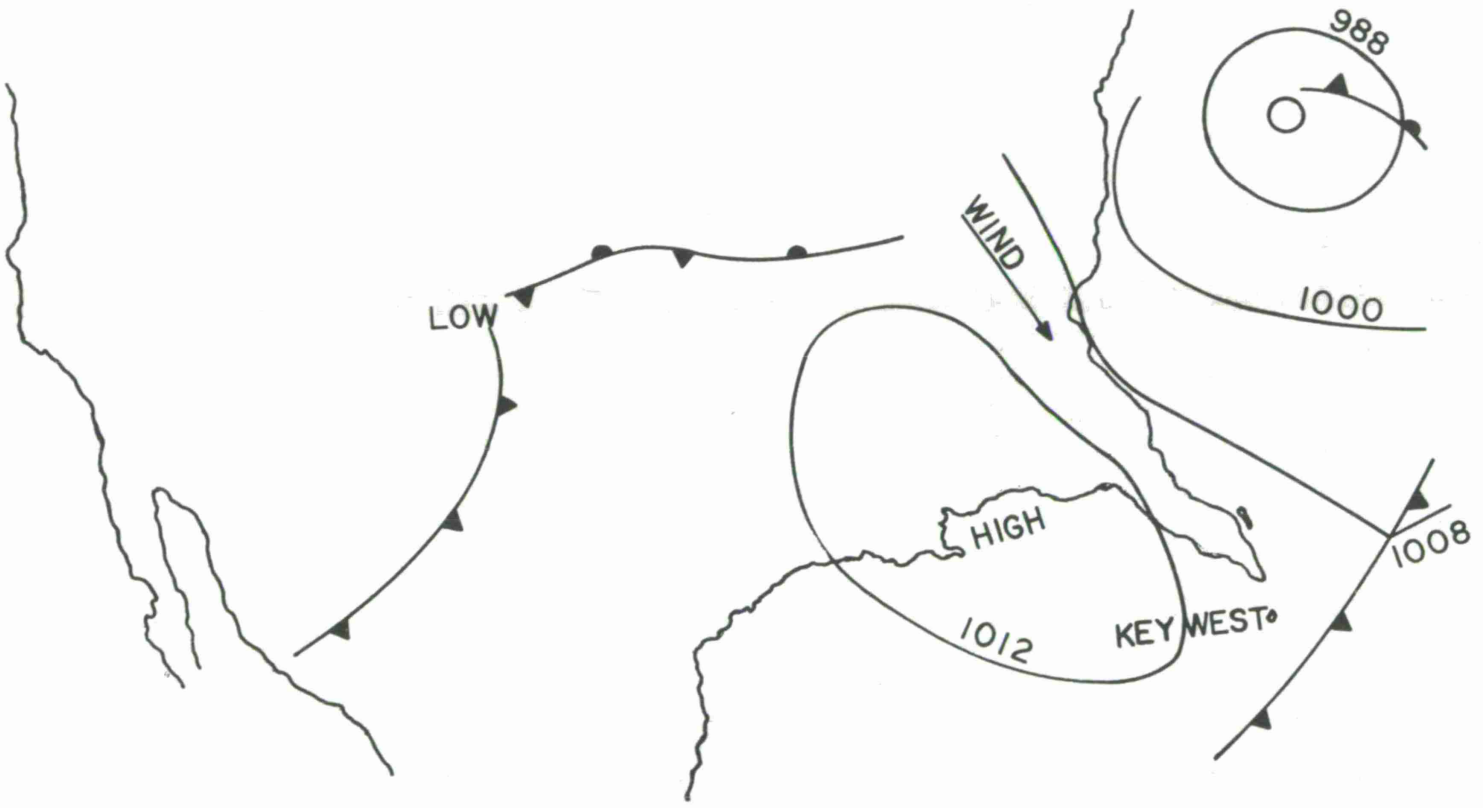

FIGURE 8.

stability is evident over the time and extent of Mission 2. With this general stability evident, it is indeed unfortunate that the radiosonde profile, shown on Figure 7, is missing significant data in the region of the inversion height.

It may be of interest to note that on the 2313 Z profile, a moisture layer is evident around 2300 meters which weakens toward the east. This may be a precursor of events to follow.

During Mission 2, several cloud photographs were made which can be associated, from Figure 7, with the height in a given sounding. Photographs 2B, E, F, and G were taken during the soundings made at Key West. In particular, 2B indicates generally clear conditions with a few high scattered clouds. By the time 2E, F, and G were taken in sounding E (2313 Z) one can begin to see, particularly in 2F, some clouds building up at high elevations, indicating the advection of moisture.

Moving eastward from Key West, photographs 2C through 2D clearly show the presence of moisture at high altitudes. In particular, 2A shows the presence of light cumulus.

From Figure 8, it is apparent that the circulation, clockwise around the high pressure cell is fortified by the low to the northeast. This would start to draw moisture southward from the continental shelf area and then later on 6 March could account for the advection of moisture at high levels.

3.3 Comments on Missions 1 and 2

The behavior of the inversion in terms of its intensity and horizontal stability is directly related to the intensity and position of the high pressure system. High pressure associated with subtropical subsidence in these areas causes the formation of the temperature inversion, that is, the character of the Trade Wind Duct. The profiles obtained during Missions 1 and 2 are, therefore, completely subject to the meteorological conditions. However, in Mission 1 it is interesting to see the uncommon formation of a higher layer which may be attributed to the fact that the local air mass was just slightly stable at the lower levels if one excludes advection.

The two radiosonde profiles show the contrast between a useful set of data (6 March, 1200 Z) and a disappointing lack of significant data (7 March, 0000 Z).

A7020

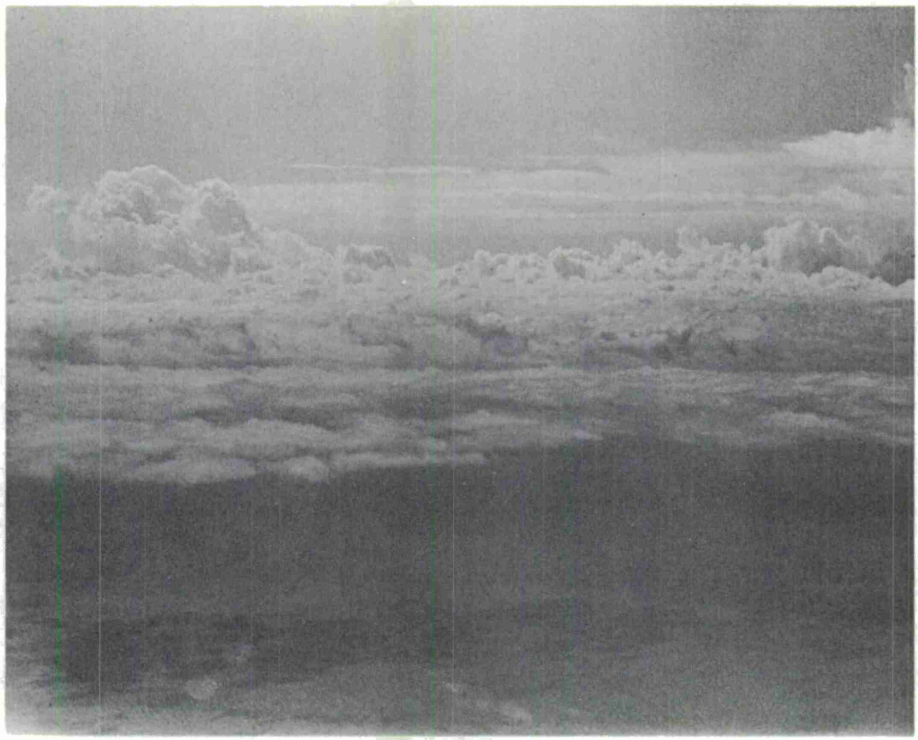

2A 6 March 1969-SPIRAL A-8K

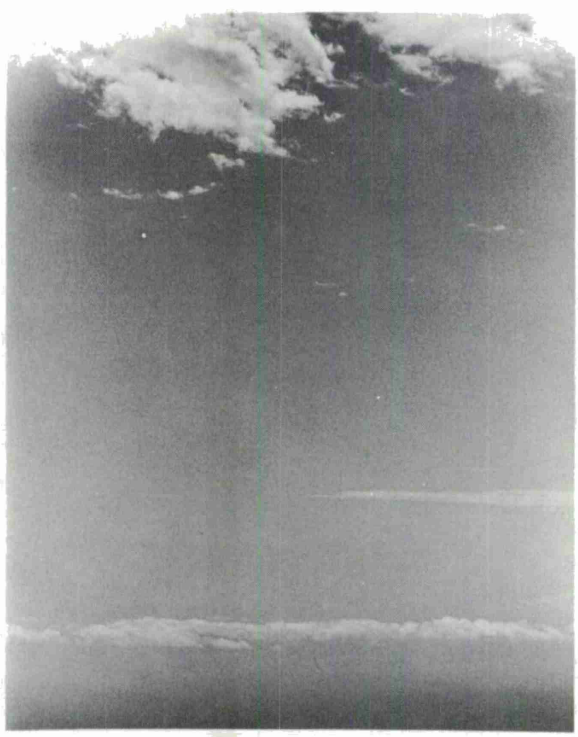

2B 6 March 1969-SPIRAL B-8K

A7021

2C 6 March 1969-SPIRAL C-7.5K

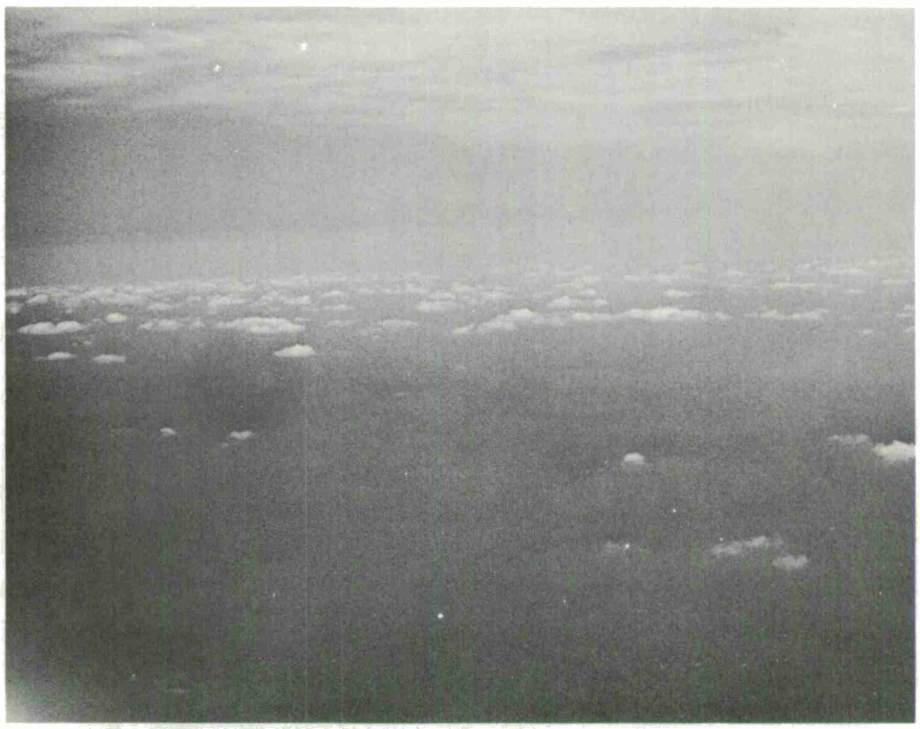

2D 6 March 1969-SPIRAL D-8K

A7022

2E 6 March 1969-SPIRAL E-1K

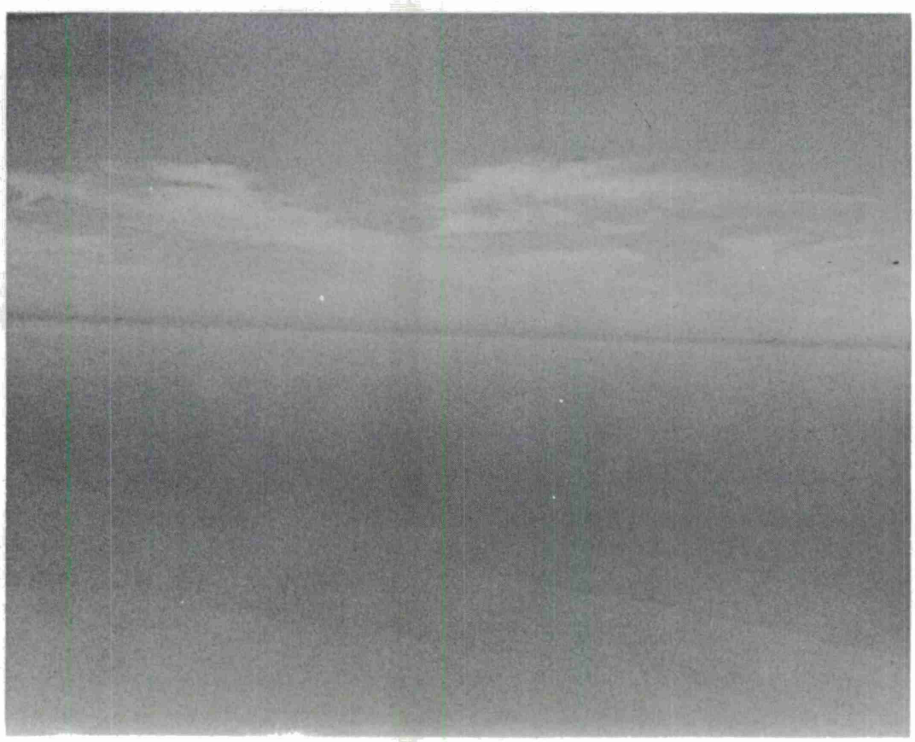

2F 6 March 1969-SPIRAL E-4K

A7023

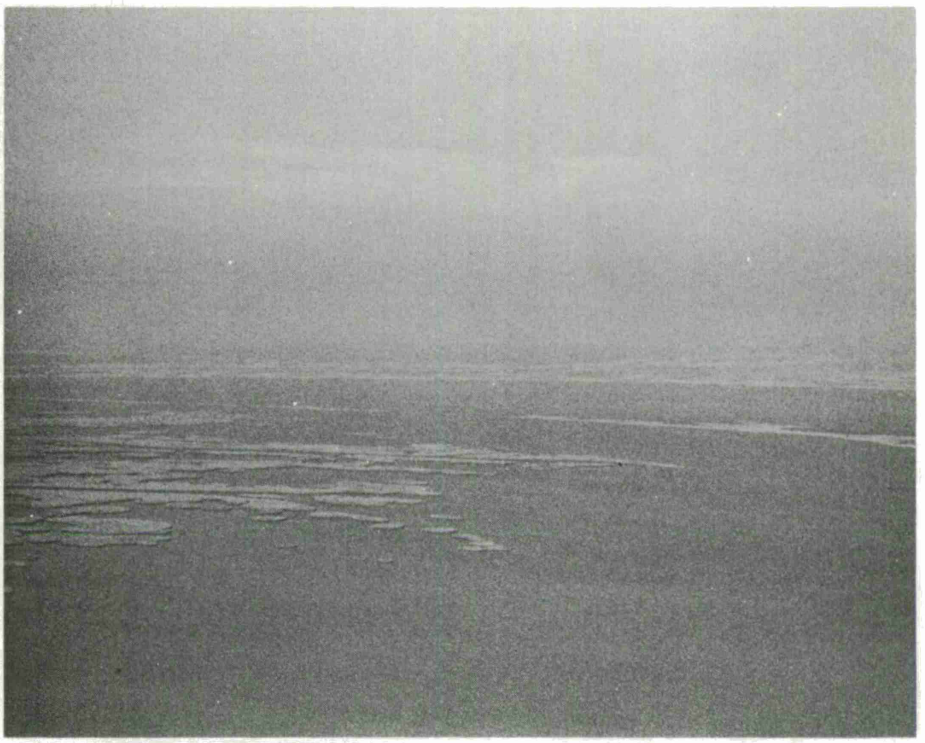

2G 6 March 1969-SPIRAL E-9K

SECTION IV

THE CHARACTERISTICS OF THE INVERSION AND ASSOCIATED WEATHER FROM KEY WEST TO NEW ORLEANS (Mission 3, 9 March)

Aircraft measurements were made from Key West to the weather station at Burwood, which is just southeast from New Orleans. As shown on Figure 9, five profiles were attempted with intervening measurements during the transition periods between these soundings. Malfunction of a pressure recorder caused a loss of data up to the completion of Spiral B. A coincidental lack of radiosonde data from Key West for 9 March (1200 Z) restricts meaningful data to the path from 200 km northeast of Key West.

Spiral	Location	Spiral Start Time Z	Local
A	a. Key West NAS	1555	1055
B	b. 25-15 N, 83-15 W	1635	1135
Climb 1	b-c	1656	1156
C	c. 26-00 N, 85-00 W	1743	1243
Climb 2	c-d	1755	1255
D	d. 27-07 N, 86-20 W	1834	1334
Climb 3	d-e	1856	1356
E	e. 29-10 N, 89-07 W	2016	1516

Figure 10 shows the isopleths of refractivity, N, taken from the aircraft measurements. Neglecting for a moment that the aircraft took over four hours to complete the measurements, the isopleths show the Trade Wind Duct forming around 800 meters at mid-range and then dissipating towards New Orleans. Since the radio refractivity, N, is so dependent upon vapor pressure, (equation (2)), these lines also indicate the spatial variation of moisture.

During the first half of the path from Key West to Burwood, the larger concentrations of moisture are found at higher levels to be closer to Key West. As the inversion intensifies near mid-path, the moisture is constrained to lie within lower levels. The 10 March (0 Z) radiosonde from Burwood was launched a few hours after the aircraft reached Burwood. The moisture concentration at low levels continues to increase. However, the inversion is gone with a more normal distribution of moisture with height.

B6840

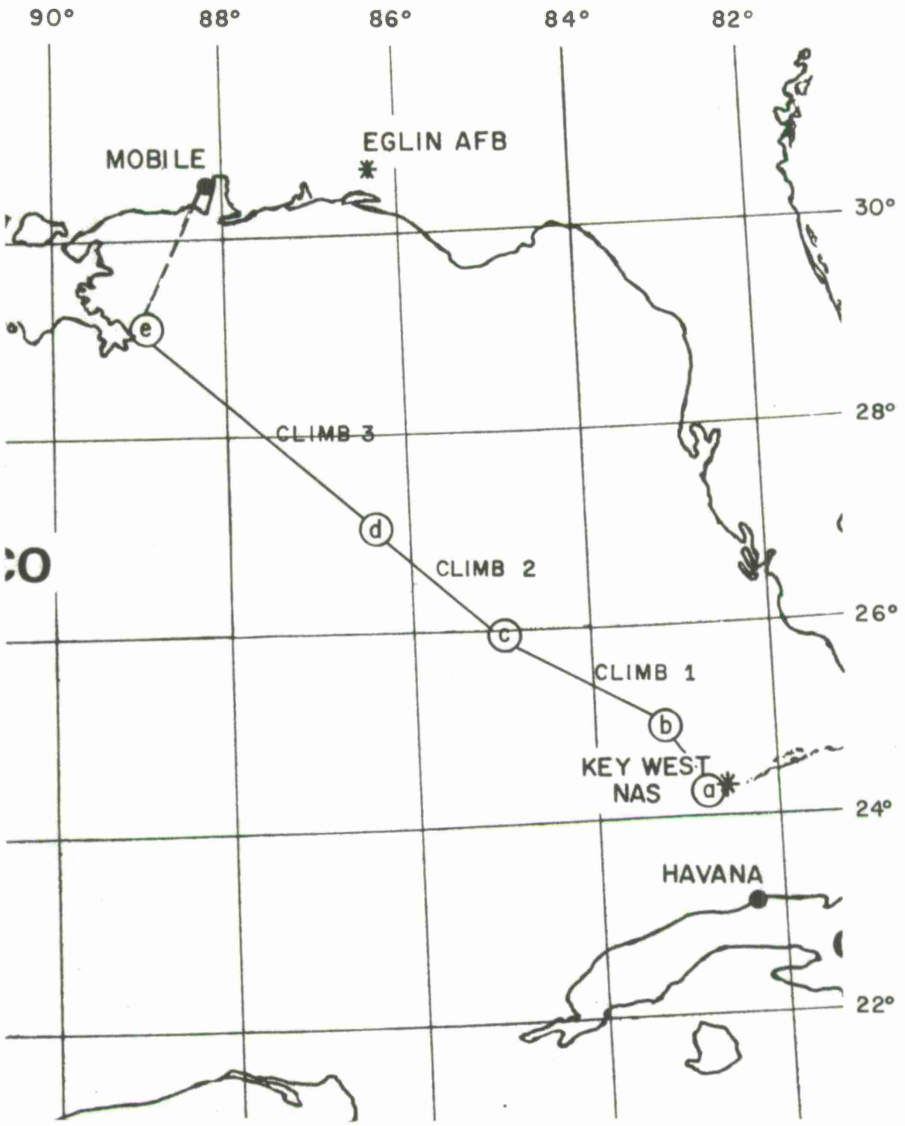

SCALE 1:5,702,400 OR 90 MILES TO 1 INCH

100 50 0 100 200 300

STATUTE MILES

100 50 0 100 200 300 400

KILOMETERS

FLIGHT PATH II

MISSION 3 — 9 MARCH 1969

FIGURE 9.

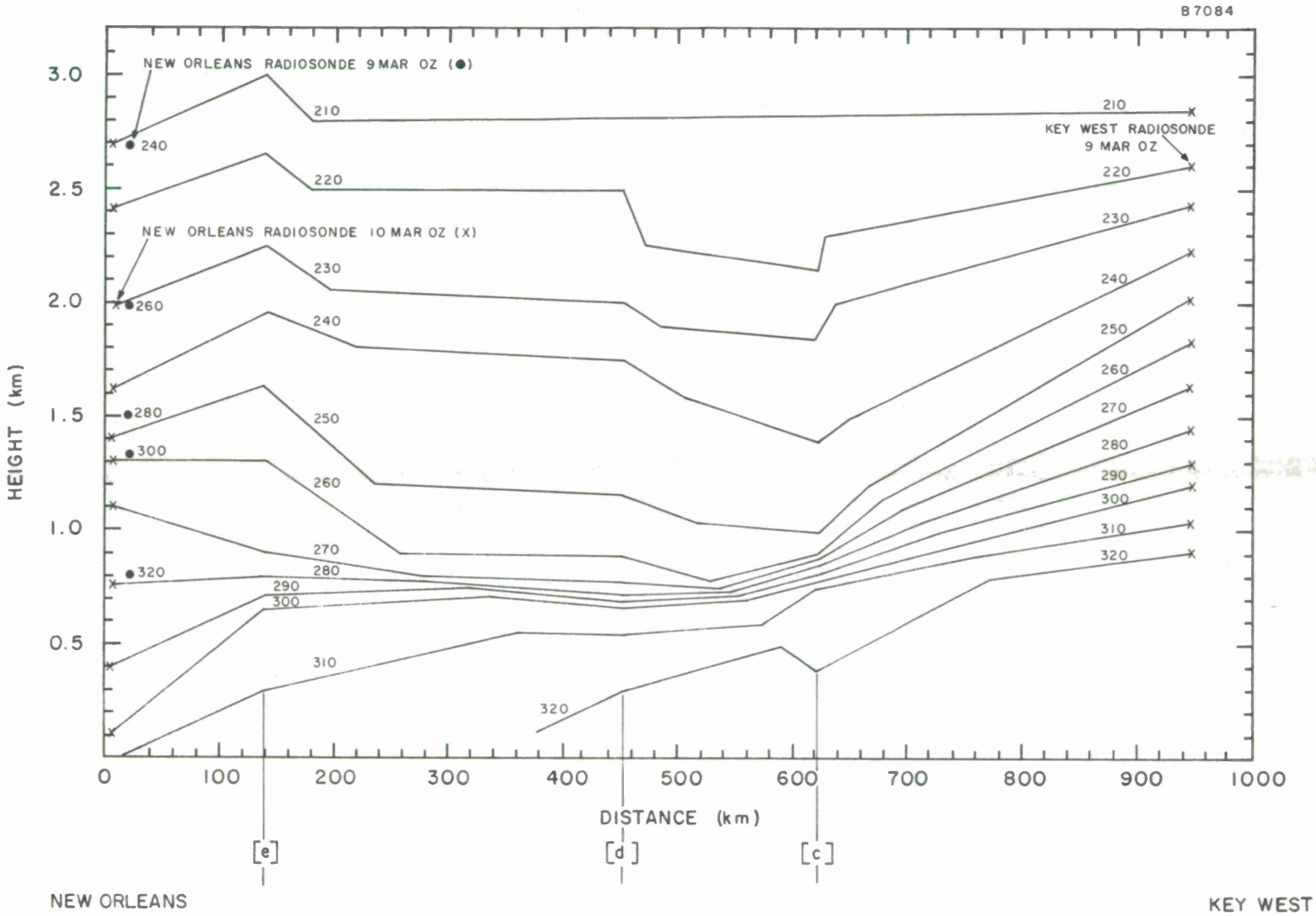
B7084
NEW ORLEANS RADIOSONDE 9 MAR 0Z (●)
NEW ORLEANS RADIOSONDE 10 MAR 0Z (X)
KEY WEST RADIOSONDE
9 MAR 0Z
HEIGHT (km)
3.0
2.5
2.0
1.5
1.0
0.5
0
100
200
300
400
500
600
700
800
900
1000
DISTANCE (km)
[e]
[d]
[c]
NEW ORLEANS
KEY WEST
210
220
230
240
250
260
270
280
290
300
310
320

FIGURE 10.

The previous launch from Burwood (9 March, 0 Z) shows comparatively much larger concentrations of moisture at altitude. In fact, the distribution with height looks very similar to that at Key West, at the same time. It therefore appears that during the flight of the aircraft the degree of subsidence, which would be associated with a high pressure call, was intensifying and had moved through Burwood during the period from 9 March to 10 March (0 Z).

Figure 11 shows the weather analysis along the path at 0 Z on 9 March corresponding to 0700 EST Key West, 9 March. It was about four hours later when the aircraft began the flight. Figure 12 shows the surface weather map at this same time. It is apparent that a cold front in advance of a high pressure cell is crossing through the region. Dry subsiding air follows in the wake of the front which accounts for the restoration of the inversion near mid-path.

On Figure 11 the solid lines, according to convention, show the air temperature which is much cooler in the wake of the front. The dashed lines show the dew point temperatures with a large spread indicating dry air and a small spread indicating near-saturation conditions. In the dry region, the spread between the air temperature and the dew point temperature is about 25 degrees centigrade. Near Burwood, and close to the surface, it is noted that the 10 degree air temperature line is essentially the same as the dew point temperature indicating high humidity and possibly fog and/or precipitation.

Cold air near the surface over warm Gulf water causes instability which supports the vertical transfer of moisture [Roll, 1965, p 247]. This results from the fact that air in proximity with the water reaches a temperature greater than the cooler air above. It, therefore, rises into the more dense air above the surface and carries water vapor aloft.

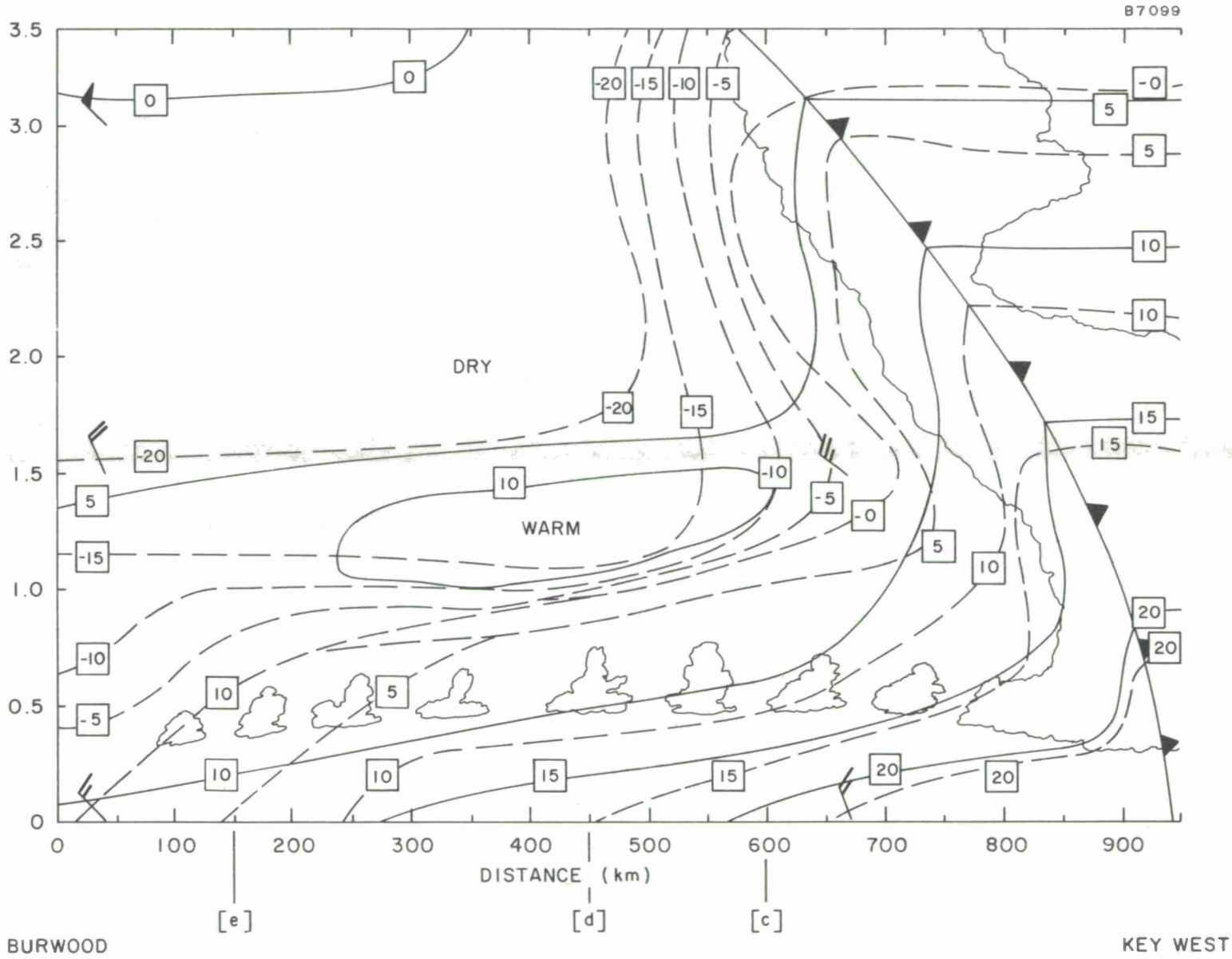
B7099
3.5
3.0
2.5
2.0
1.5
1.0
0.5
0
DRY
WARM
0
100
200
300
400
500
600
700
800
900
DISTANCE (km)
[e]
[d]
[c]
BURWOOD
KEY WEST

FIGURE 11.

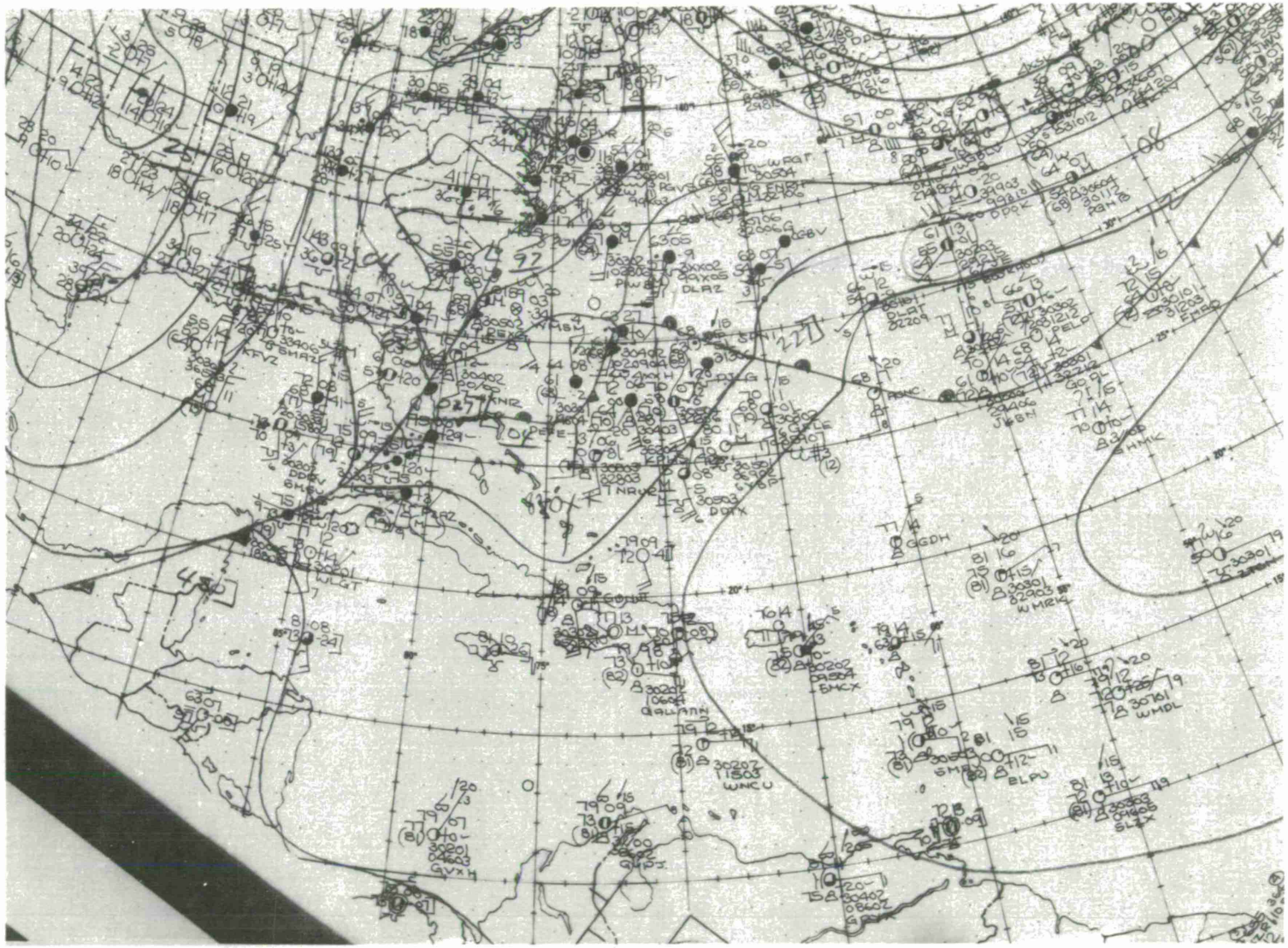

FIGURE 12

SURFACE CHART 9 March 1969

SECTION V

THE CHARACTERISTICS OF THE INVERSION AND ASSOCIATED WEATHER FROM EGLIN TO MERIDA (Mission 4, 10 March)

Figure 13 shows the location of spirals for the flight from Eglin AFB to Merida, Mexico, on 10 March. Data were also recorded in the sections marked by climbs between spirals.

Spiral	Location	Spiral Start Time Z	Local
A	a. 29-00 N, 87-00 W	2032	1432
Climb 1	a-b	2050	1450
B	b. 25-00 N, 88-13 W	2217	1617
Climb 2	b-c	2235	1635
C	c. 23-00 N, 89-00 W	2315	1715

For the previous mission, the refractivity structure was presented first and then justified on the basis of the weather system. This time let us examine the weather data and attempt to postulate the refractivity structure.

Figure 14 shows the surface map for 0700 EST on 10 March. The cold, high pressure wave has almost cleared Cuba and leaves behind a large mass of cool, dry air. From Eglin to Merida, surface winds are light and generally in a southward direction. The center of this massive high pressure system is still northwest of the Gulf. These conditions would suggest stronger subsidence in the northern part of the flight path. The inversion should be present but weakening towards Merida. Because the winds would be cool there should be a considerable amount of moisture upwelling which would produce a low level cloud buildup.

Figure 15 shows the isopleths of refractivity obtained from aircraft measurements. The measurements made during the final climb towards Merida are in good agreement with the radiosonde launch at 0000 Z, 11 March. It is apparent that an elevated layer is formed around 700 meters elevation at the northern part of the track. This layer weakens and rises as the track continues southward. As the aircraft approaches the land, the layer is destroyed, probably through strong thermal convection.

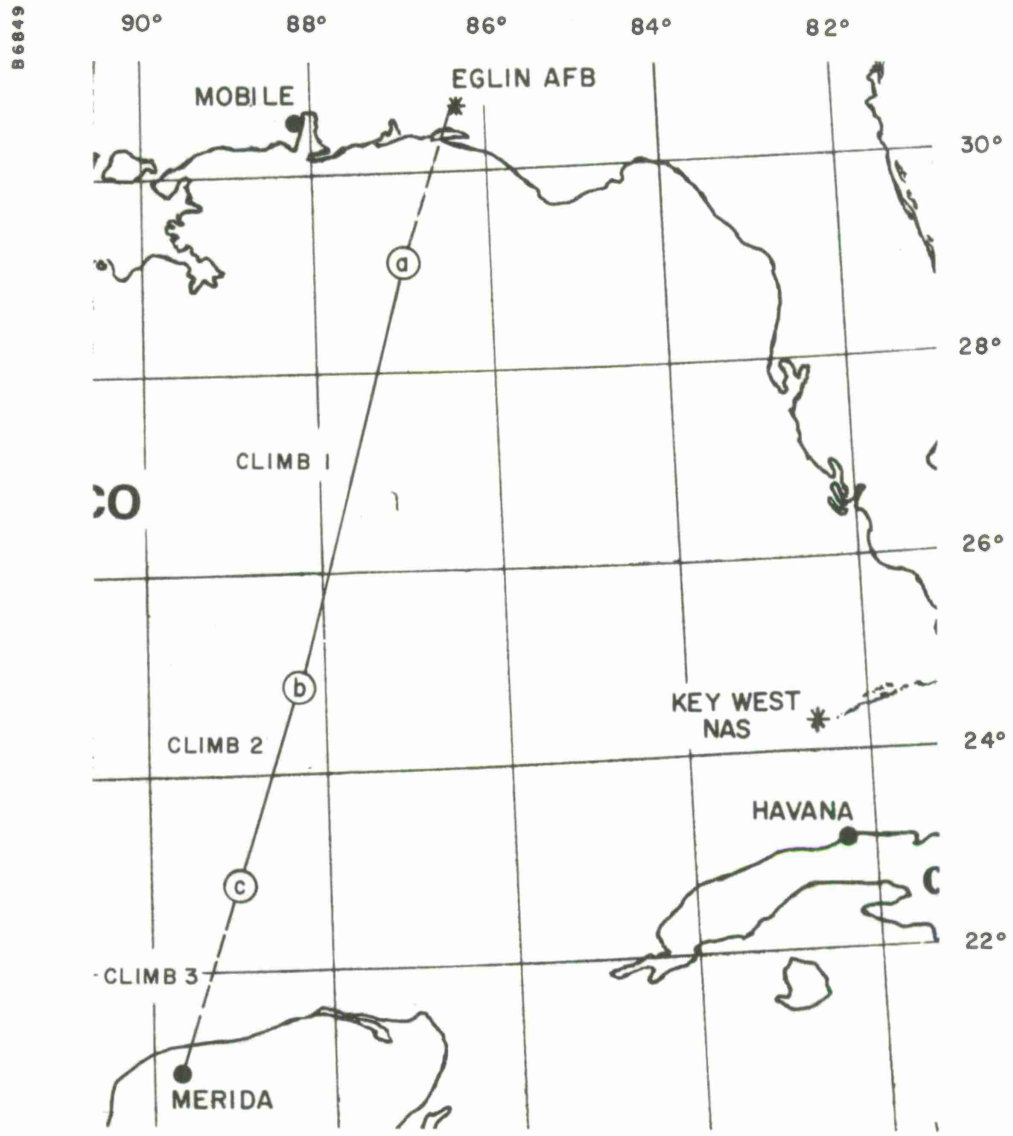

FLIGHT PATH III

MISSION 4 — 10 MARCH 1969

FIGURE 13.

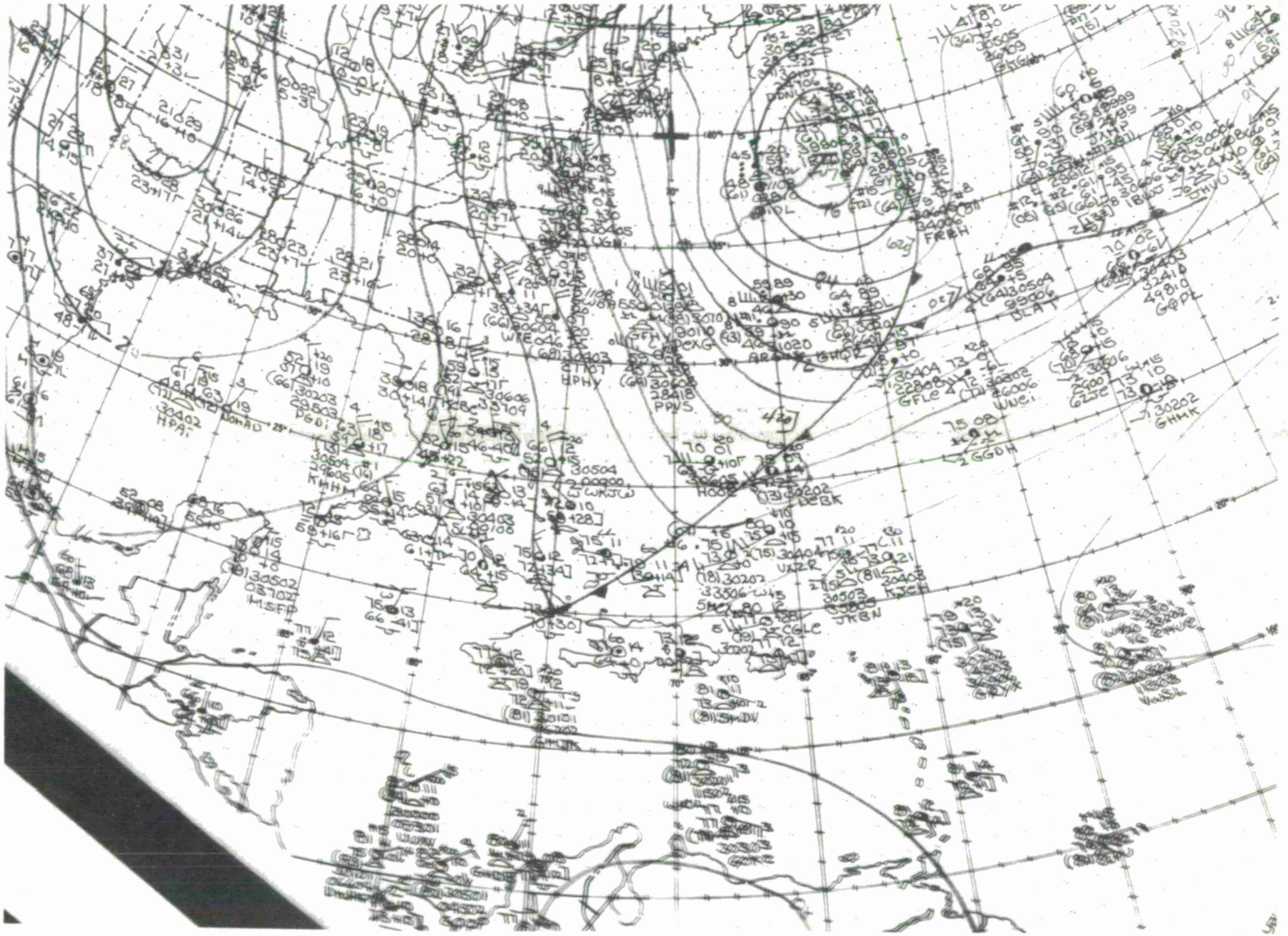

FIGURE 14

SURFACE CHART 10 March 1969

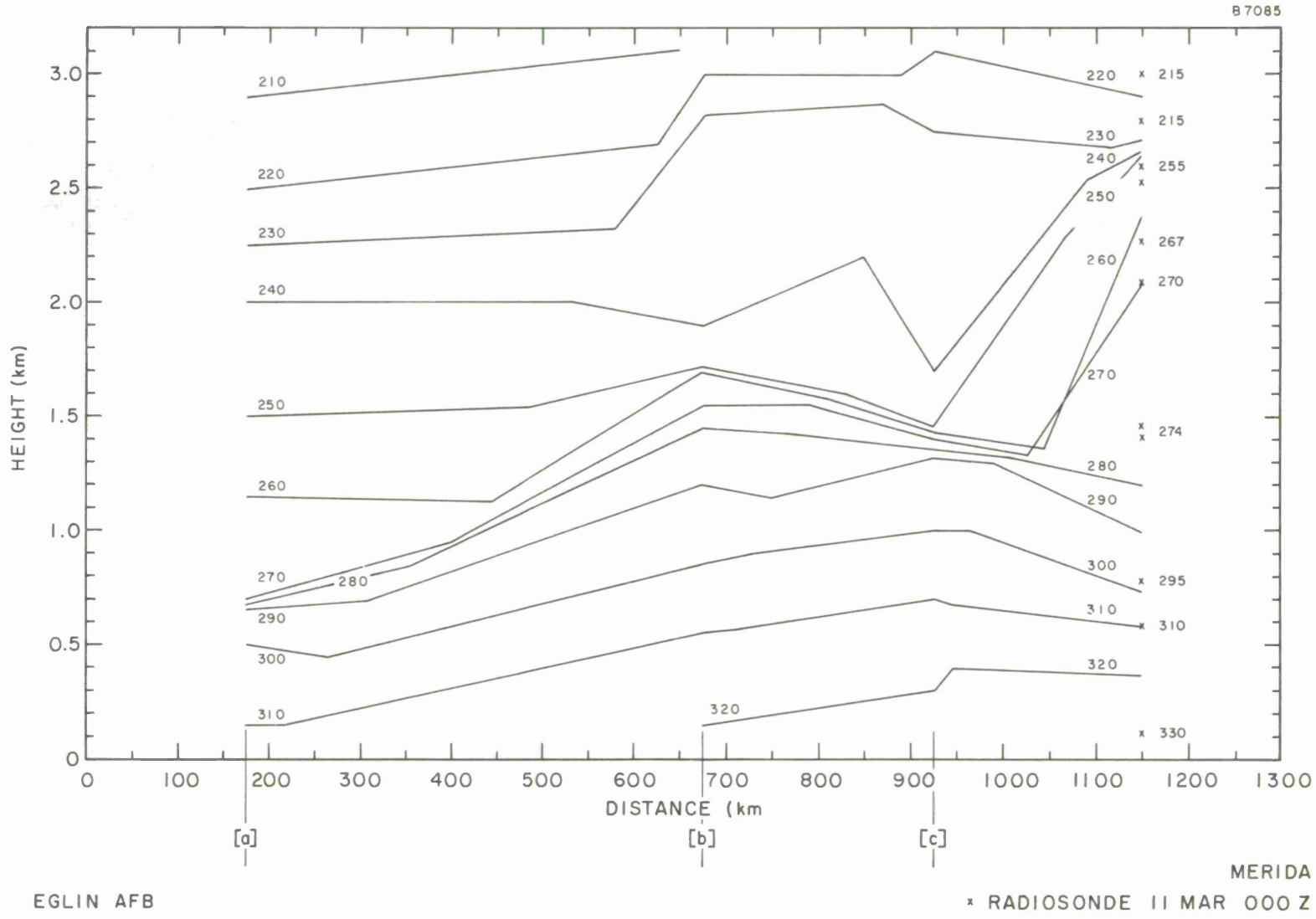
B7085
HEIGHT (km)
3.0
2.5
2.0
1.5
1.0
0.5
0
0
100
200
300
400
500
600
700
800
900
1000
1100
1200
1300
DISTANCE (km
[a]
[b]
[c]
210
220
230
240
250
260
270
280
290
300
310
320
220 x 215
x 215
230
240
x 255
250
x 267
260
x 270
270
x x 274
280
290
300
x 295
310
x 310
320
x 330
EGLIN AFB
MERIDA
x RADIOSONDE 11 MAR 000 Z

FIGURE 15.

A weather analysis is shown on Figure 16, where surface, upper air, and aircraft measurements were all used to give the greatest possible detail. Dry cool air is aloft and has advanced 800 km at 2400 meters towards Merida. At lower levels, around 1300 meters, the advance is retarded by the buildup of moisture from the sea. The condensation of this moisture at altitude produces heat from condensation. The 15 degree air temperature isopleth clearly separates the dry, cool air above from the warm, moist air below. Photograph 4A shows the beginning of a cloud deck as the inversion intensifies. Referring to Figure 16, this photograph was taken near the top of the first Spiral, A.

Near Merida, the transfer of water vapor due to thermal convection is pronounced. The advecting upper tongue of cool air is producing a band of clouds at the 2400 meter level with this condition increasing as warm moist air is reached over the land. Photograph 4B shows the large amounts of water vapor aloft as the aircraft approaches Merida, with the aircraft (Figure 16) located in Spiral B between the upper and lower cloud decks. Photograph 4C was taken at the bottom of Spiral B and shows some of the detail of the lower cloud structure.

This pattern shows in a striking manner how rapidly the vertical transfer of water vapor takes place when cool air overrides warmer water. The second effect when this moist air begins to precipitate and release heat is to increase the buoyancy of the air. The net effect is to cause extremely large transfer of moisture in the vertical, which must destroy the normal characteristics of the Trade Wind Duct.

One might have expected that with the cool air pushing south over warmer water that large amounts of vapor would be transported vertically. Further, that the height of the Duct would increase towards Merida and would weaken because of the moisture transport. However, any detailed information about the characteristics of the Duct appears unobtainable without detailed knowledge of the overriding air temperatures. For example, certainly the surface air temperature will be increased by association with the warm water and the heat of vapor condensation. However, at what rate, in terms of distance traveled, does this air temperature modification occur? Also, at what rate is the dry air modified at greater altitudes by this thermal friction occurring at lower levels?

It appears that one can only make some general comments about how the Duct is modified in the presence of conventionally defined weather systems. Details on the height, thickness, intensity, or in fact, the presence or absence of the duct are generally unknown unless the meteorological parameters are known in detail. This observation can be checked repeatedly as subsequent missions are analyzed.

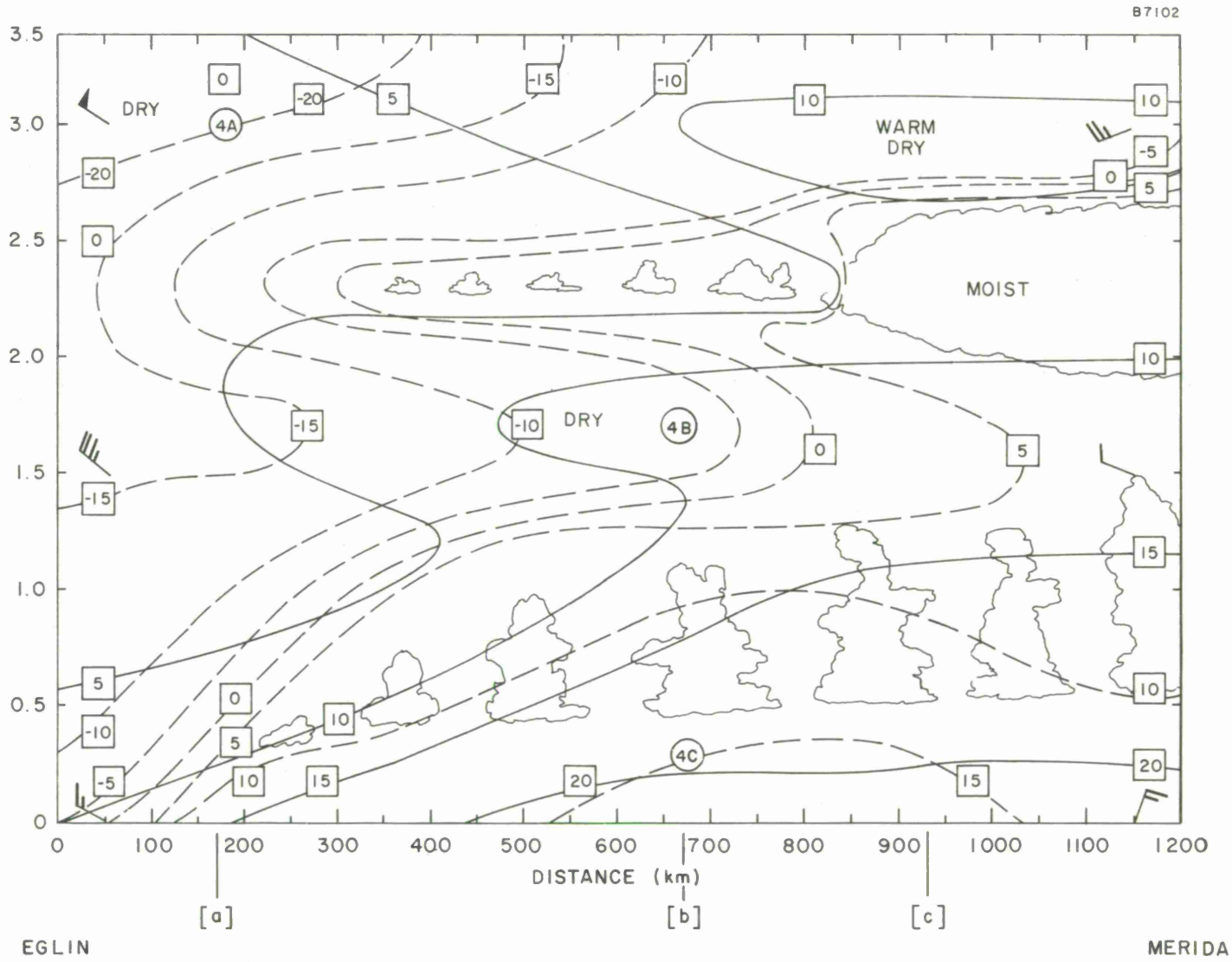
B7102
3.5
3.0
2.5
2.0
1.5
1.0
0.5
0
DRY
4A
WARM
DRY
MOIST
DRY
4B
4C
0
100
200
300
400
500
600
700
800
900
1000
1100
1200
DISTANCE (km)
[a]
[b]
[c]
EGLIN
MERIDA

FIGURE 16.

A7024

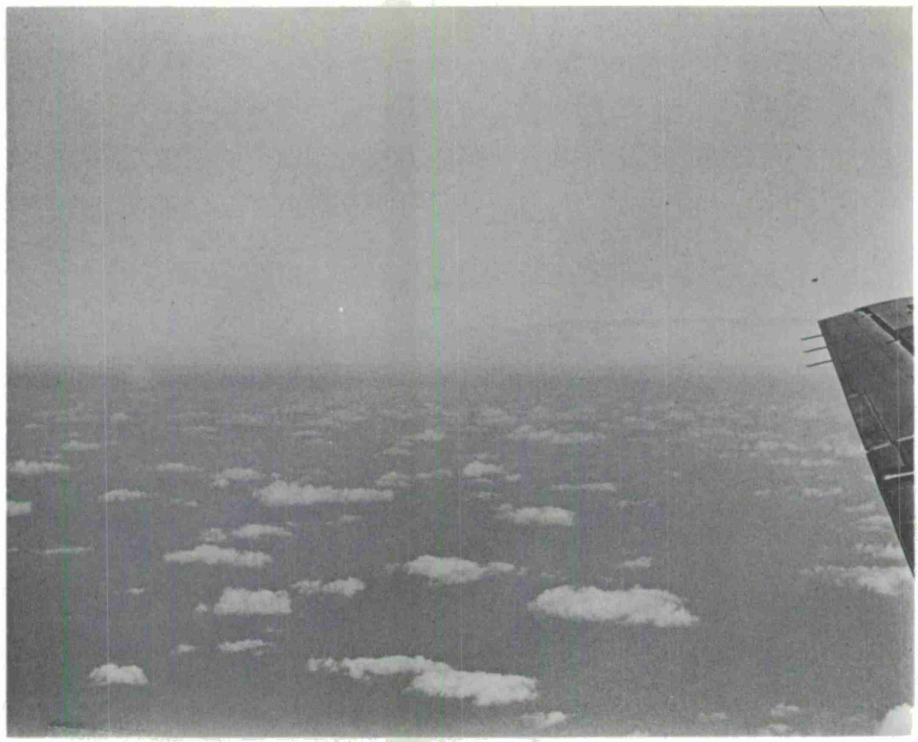

4A 10 March 1969

4B 10 March 1969

A7025

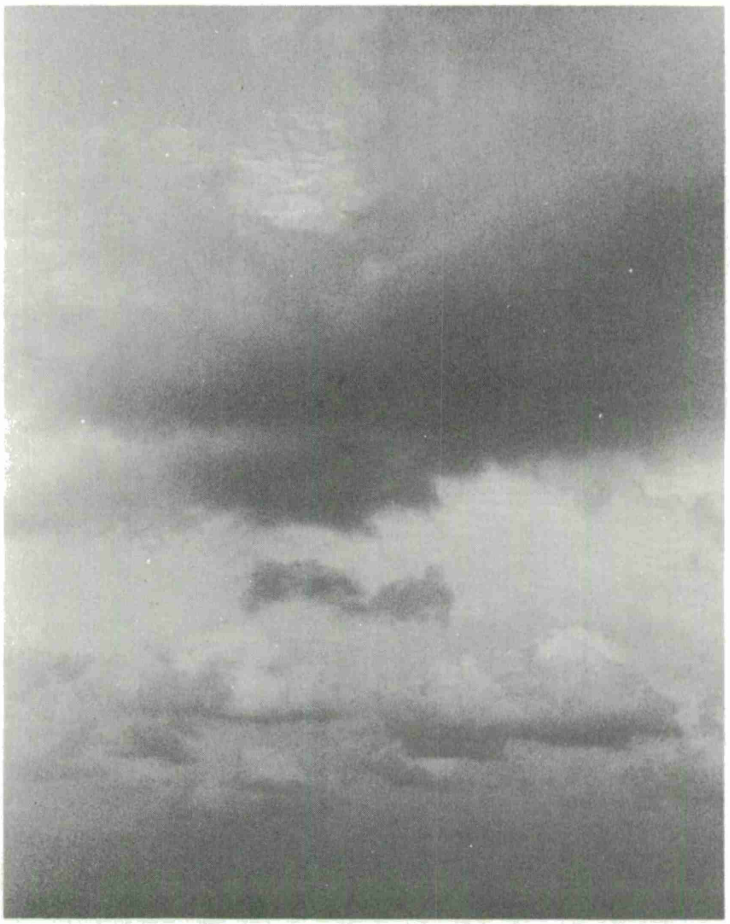

4C 10 March 1969

SECTION VI

THE CHARACTERISTICS OF THE TRADE WIND DUCT AND ASSOCIATED WEATHER FROM MERIDA TO THE CAYMANS
(Mission 5, 11 March)

Figure 17 shows the flight plan from Merida to the Cayman Islands on 11 March. Data was again recorded during spirals and climbs.

Spiral	Location	Spiral Start Time Z	Local
A	a. 20-00 N, 86-25 W	1848	1248
Climb 1	a-b	1908	1308
B	b. 19-00 N, 85-35 W	1935	1335
Climb 2	b-c	1958	1358
C	c. 18-30 N, 84-00 W	2030	1430
D	d. 19-15 N, 81-15 W	2150	1550

The surface weather map, Figure 18 (0700 EST, 11 March), shows the high pressure system further south than on the previous day. In the region between Merida and the Caymans, the surface winds are still southward and light. The edge of the front is east of the Caymans and should not have any influence on the path.

These conditions would suggest a weak inversion present due to the slight influence of high pressure. The map indicates that the pressure is only a few points over normal sea level pressure. The overriding air is by now only slightly cooler than the water and excessive vertical transport of vapor is not likely except by thermal effects.

Now, let us look at Figure 19, showing the refractivity isopleths. It is strikingly apparent that the isopleths are generally at constant altitude. This is not surprising since the measurements were made almost parallel to the pressure isobars. Except near the Caymans there is a general absence of an elevated duct. The vertical bars on the isopleths indicate there was more than one altitude having a given refractivity. Such hooking in the refractivity profiles usually indicates the presence of strong concentrations of moisture aloft. The isopleth pattern generally indicates a very normal lapse rate of refractivity not usually found in these areas. If anything, the plot is striking in its absence of any interesting features.

FLIGHT PATH IV

MISSION 5 — 11 MARCH 1969

FIGURE 17.

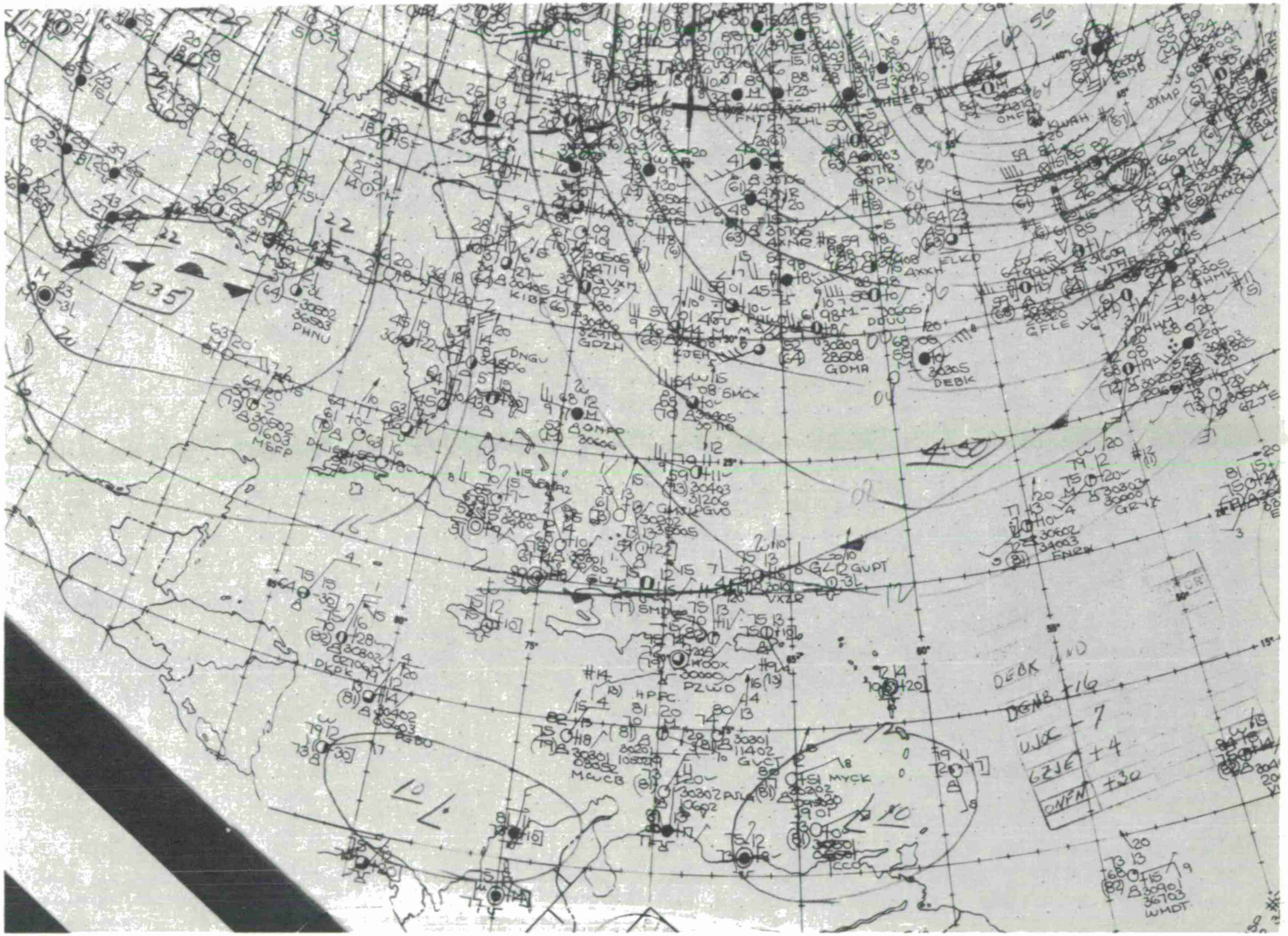

FIGURE 14

SURFACE CHART 11 March 1969

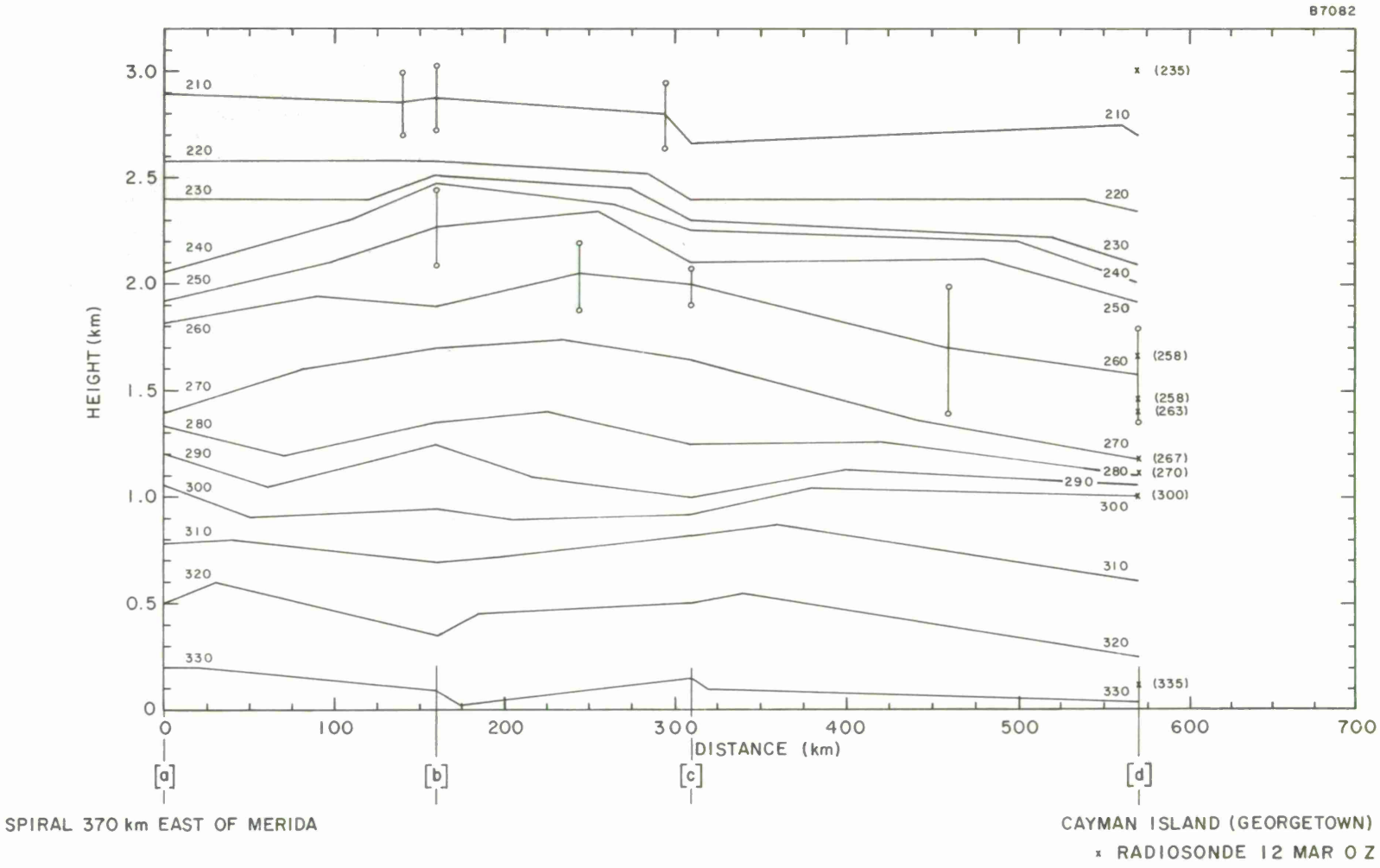
87082
HEIGHT (km)
3.0
2.5
2.0
1.5
1.0
0.5
0
210
220
230
240
250
260
270
280
290
300
310
320
330
x (235)
(258)
(258)
(263)
(267)
(270)
(300)
(335)
0
100
200
300
400
500
600
700
DISTANCE (km)
[a]
[b]
[c]
[d]
SPIRAL 370 km EAST OF MERIDA
CAYMAN ISLAND (GEORGETOWN)
x RADIOSONDE 12 MAR 0 Z

FIGURE 19.

The detailed weather analysis, Figure 20, shows warm dry air aloft extending from Merida over the first half of the path. Nearer to Georgetown in the Caymans, the lapse rate of temperature with height is much larger. The air temperature near the surface is not sufficiently cool to cause great up-welling of water vapor, Therefore, the cloud structure should be largely produced by normal, thermal convection.

In relation to the first conjectures, the absence of the inversion and the associated Trade Wind Duct was unexpected. The subsidence associated with the high pressure system is too weak to have any influence in the area. The air aloft is generally very warm and able to contain a significant vapor pressure. In other words, the region of air marked, "Warm Dry," on Figure 20 is warm but not very dry. The temperature spread between air temperature and dew point does not exceed 15 degrees. Referring to Figure 11, for Mission 3, the dry air shows a spread of about 25 degrees which is more representative for subsidence of stratospheric air.

Here, again, it is evident that it is extremely difficult to define the characteristics of the Duct using limited and inexact data. A variation of the dew point temperature of a few degrees, the strength and direction of the wind pattern, the variations in sea temperature, all interplay to produce a very complicated moisture pattern.

Photographs 5A through 5G were taken at the locations shown on Figure 20, with the latter three, E, F, and G, over Cayman Island. These cloud pictures clearly support the weather analysis, and 5E is a good presentation of a weak inversion layer looking down on it from 2500 meters.

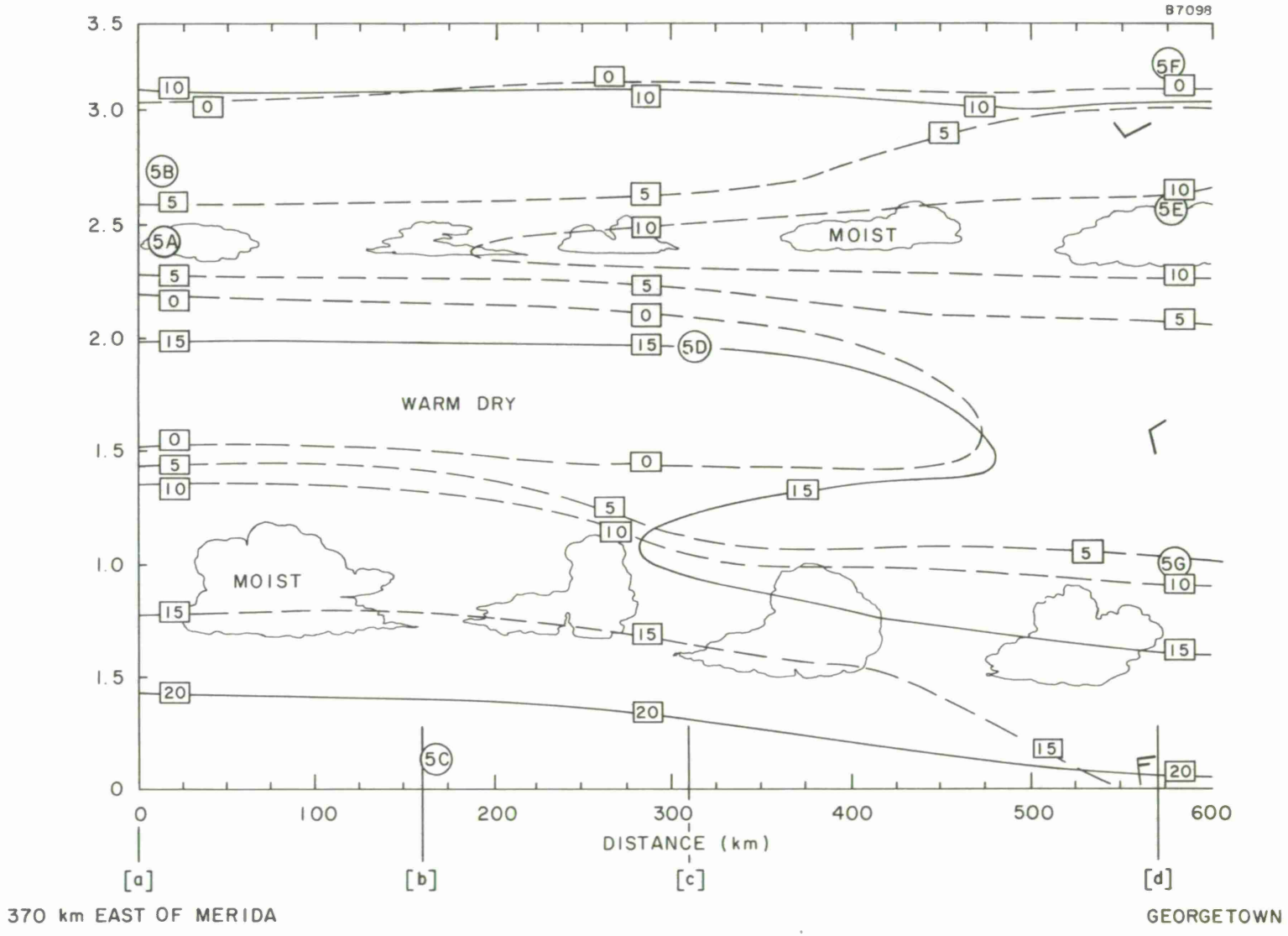
B7098
3.5
3.0
2.5
2.0
1.5
1.0
1.5
0
5A
5B
5C
5D
5E
5F
5G
MOIST
WARM DRY
MOIST
0
100
200
300
400
500
600
DISTANCE (km)
[a]
[b]
[c]
[d]
370 km EAST OF MERIDA
GEORGETOWN

FIGURE 20.

5A 11 March 1969-SPIRAL A-8K

5B 11 March 1969-SPIRAL A-9K

A7027

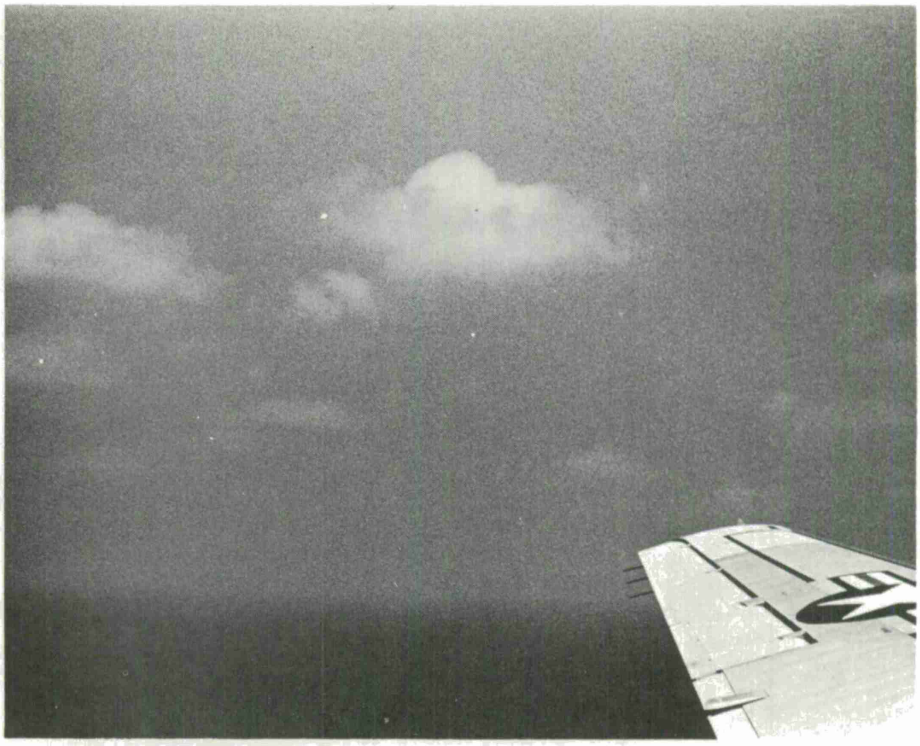

5C 11 March 1969-SPIRAL B-1K

5D 11 March 1969-SPIRAL C-6.5K

A7028

5E 11 March 1969-SPIRAL D

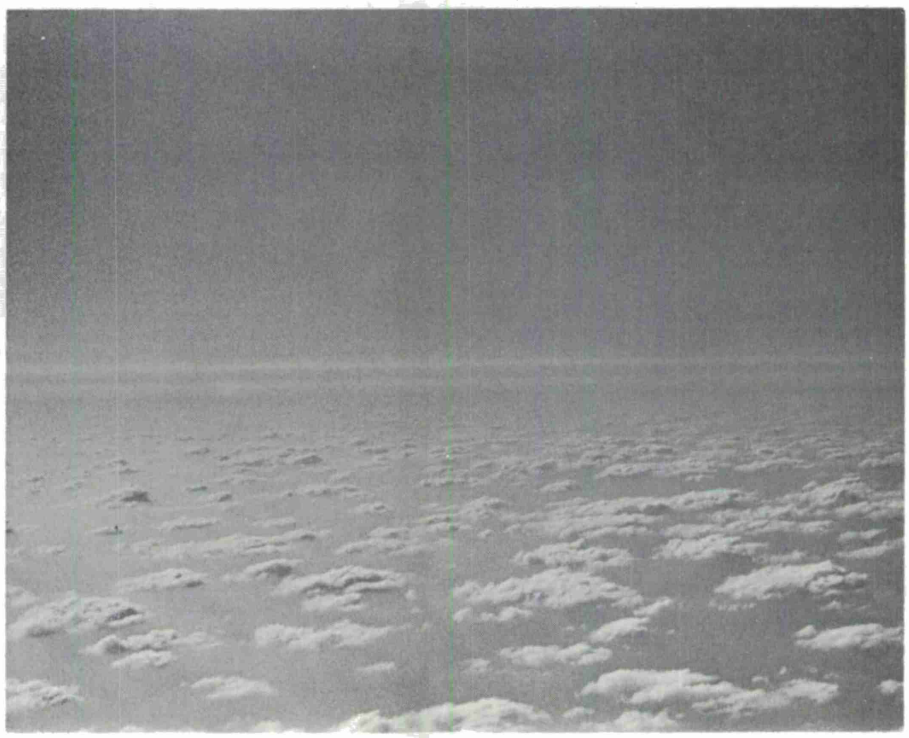

5F 11 March 1969-SPIRAL D

A7029

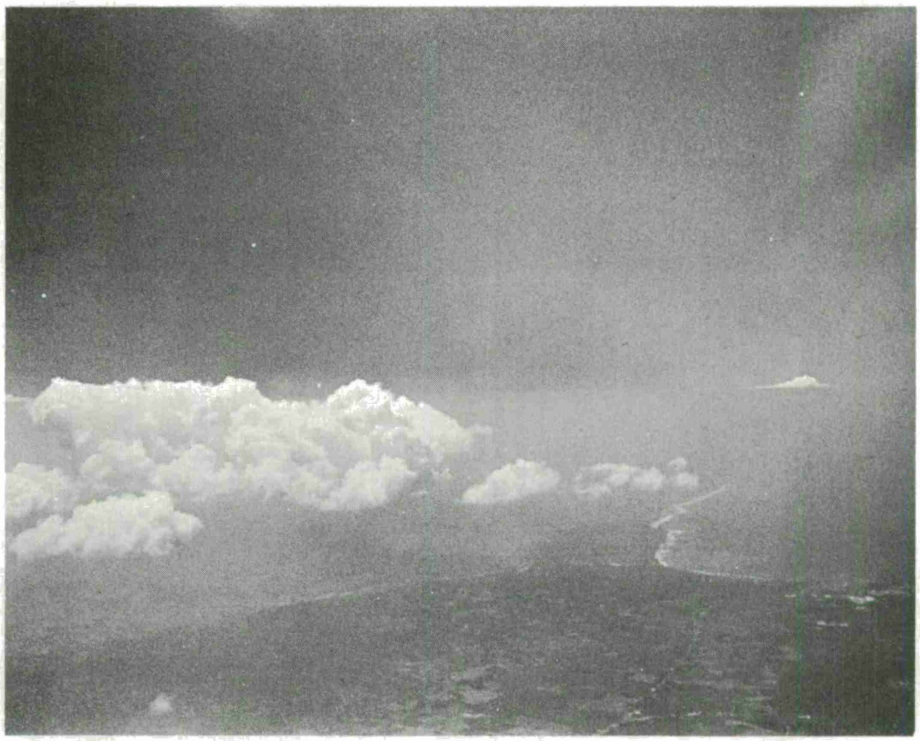

5G 11 March 1969-SPIRAL D

SECTION VII

THE TEMPORAL AND SPATIAL VARIATIONS OF REFRACTIVITY IN THE AREA OF PUERTO RICO
(Mission 6, 14 March)

Figure 21 shows the flight plan for measurements made in the vicinity of Puerto Rico.

Spiral	Location	Spiral Start Time Z	Local
A	a. 18-36 N, 62-00 W	1629	1229
B	b. 17-30 N, 67-00 W	1706	1306
Climb 1	b-c	1726	1326
C	c. 16-17 N, 67-17 W	1810	1410
Climb 2	c-d	1828	1428
D	d. 15-37 N, 67-23 W	1848	1448
Climb 3	d-e	1905	1505
E	e. 17-03 N, 66-14 W	1945	1545
Climb 4	e-f	2003	1603
F	f. 18-34 N, 65-37 W	2033	1633

The surface weather chart, Figure 22, shows the high pressure system centered north of the Caribbean Sea and a low pressure trough in the northeast beginning to influence the area east of Puerto Rico.

In the immediate vicinity of Puerto Rico there is no significant influence from either system. Therefore, one would not expect any degree of spatial variation of the Trade Wind Duct except for thermal and orographic effects from the Islands. Since subsidence is not pronounced, the inversion should be weak and possibly non-existent. The winds are indicated to be light and from the south. Therefore, orographic effects should be minimal south of the Island.

Figure 23 shows the isopleths of refractivity on a north-south cross-section. Spirals A and B bracket the Island. Low-level data are, of course, missing for Spiral A since it was flown in a location which took the aircraft overland.

Photographs 6A and 6B, taken on Spiral B, show a weak inversion present at lower altitude. From Figure 23, this effect is probably around 700 meters above sea level.

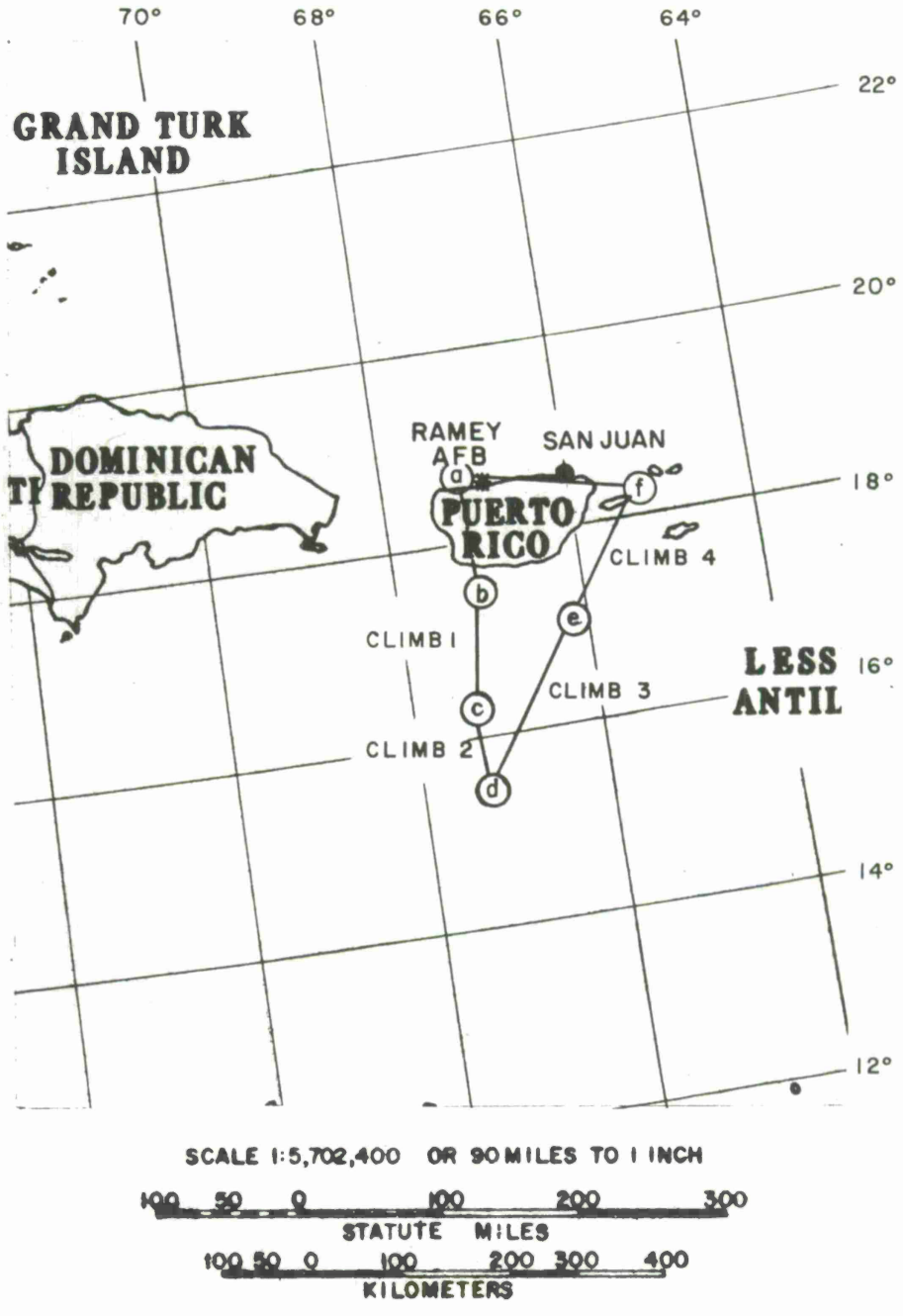

FLIGHT PATH V
MISSION 6 — 14 MARCH 1969

FIGURE 21.

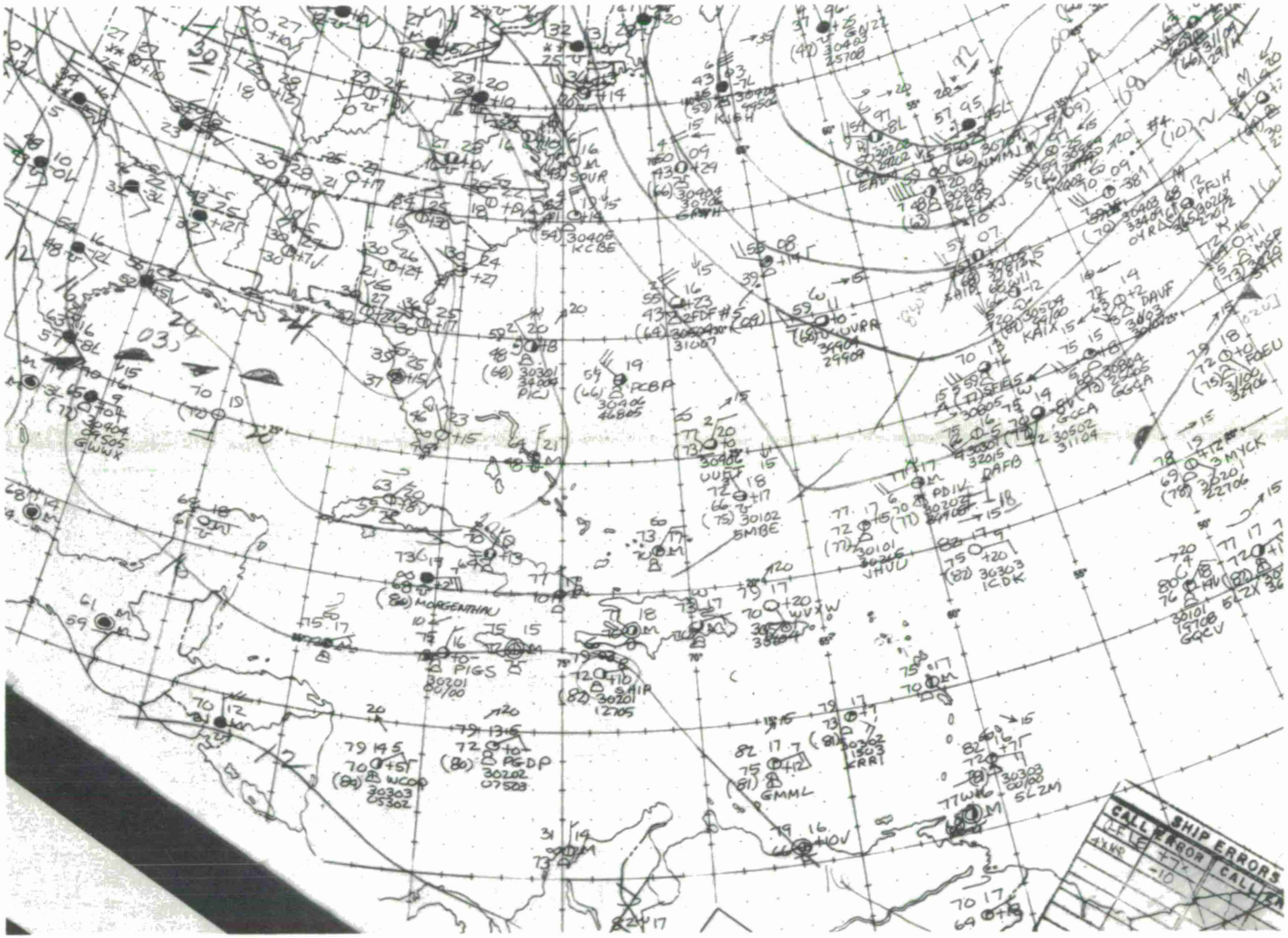

FIGURE 22

SURFACE CHART 14 March 1969

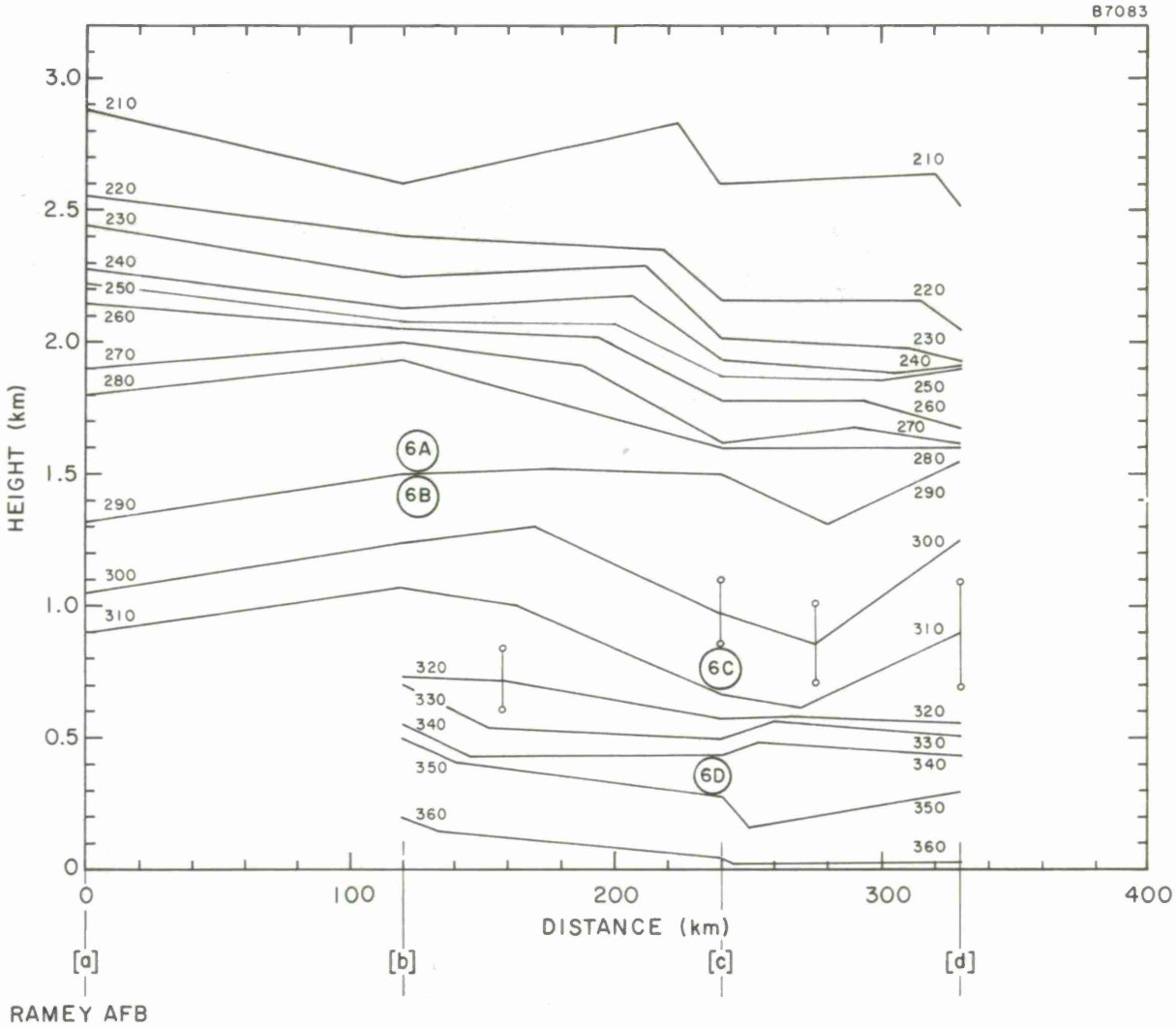
B7083
HEIGHT (km)
3.0
2.5
2.0
1.5
1.0
0.5
0
210
220
230
240
250
260
270
280
290
300
310
320
330
340
350
360
6A
6B
6C
6D
0
100
200
300
400
DISTANCE (km)
[a]
[b]
[c]
[d]
RAMEY AFB

FIGURE 23.

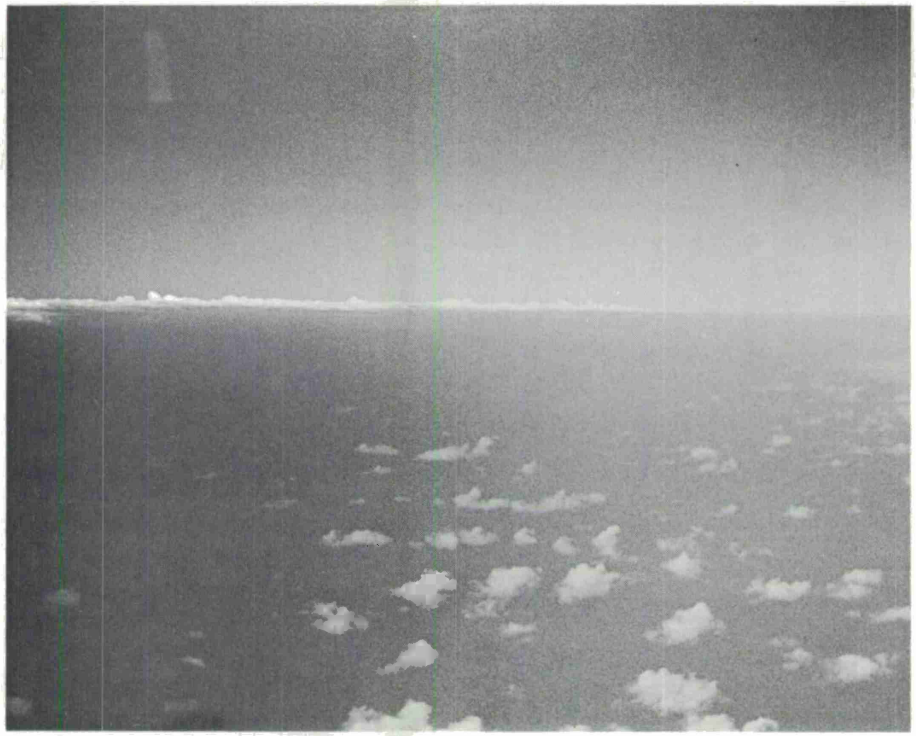

6A 14 March 1969-SPIRAL B

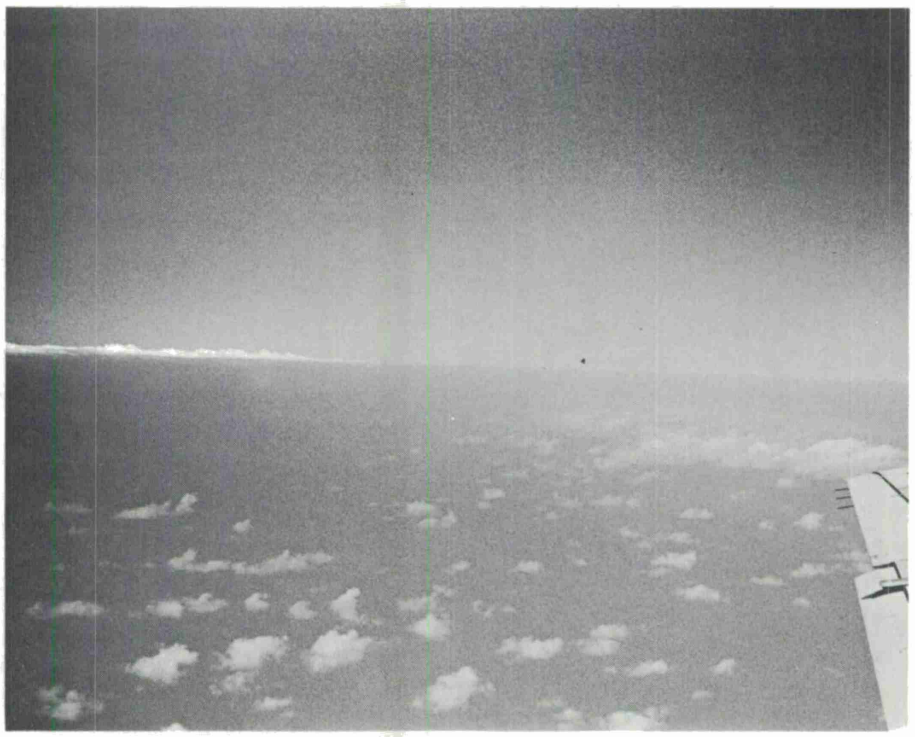

6B 14 March 1969-SPIRAL B-5K

Photographs 6C and 6D, taken at low-level in Spiral C, indicate the presence of very dry air with no noticeable inversion except for a haze layer.

It may be seen that the isopleths of greatest refractivity near the surface are tending to be lifted by the presence of the Island. With light winds from the south the air at low-levels would be expected to lift as the Island is approached. This effect was repeatedly observed in Aruba [Rowlandson, 1966]. At higher levels, the presence of the Island is less influential. The data along the vertical direction indicated by Spiral B, shows a strong vertical refractivity gradient around two kilometers because of the upwelling of the lower air. Downwind from the Island, one generally encounters a low-level jet which is produced by the rapid descent of low-level air.

Information along Spiral D indicates a convergence of isopleths between 1.5 and 2 km altitude which is the average location of the inversion. Toward the Island, the structure becomes wavy producing regions of high and low refractivity gradients. To quote from the Aruba Investigations, "The turbulent pattern of refractivity produced by the Island creates alternating regions of large and small gradients."

Figure 24 shows the refractivity profiles at two locations along the northern coast of the Island. Spirals A and F are almost equally displaced from the radiosonde launch station at San Juan Airport. There is slight evidence of the inversion around 2.3 km which the radiosonde does not detect. However, the turbulence produced by the Island would be expected to destroy the normal inversion. The fact that Spirals A and F were flown at the ends of the Island could account for the fact that some semblance of the inversion is retained. In the center section, at San Juan, the flow of air over the higher land would create stronger turbulence, possibly accounting for the fact that the radiosonde did not observe the inversion. Figure 25 shows the isopleths obtained along another track south from the Island and running to the point F, east of the Island. This track remains off the main Island and the refractivity structure should not be disturbed by orographic effects. In comparison with Figure 23, the isopleths at low altitudes do not rise but remain at almost constant altitude all the way in to Spiral F. Between 0.5 and 1 km, there is a tendency for the isopleths to lower slightly. This could be due, in part, to the fact that the divergent flow over the Island will tend to produce a flow of air in from the East and West directions. Such a flow will tend to reduce the level of any particular parcel of air. For example, the Aruba measurements showed that the inversion tended to lower as measurements were made approaching the Island normal to the Trade Wind flow.

A7031

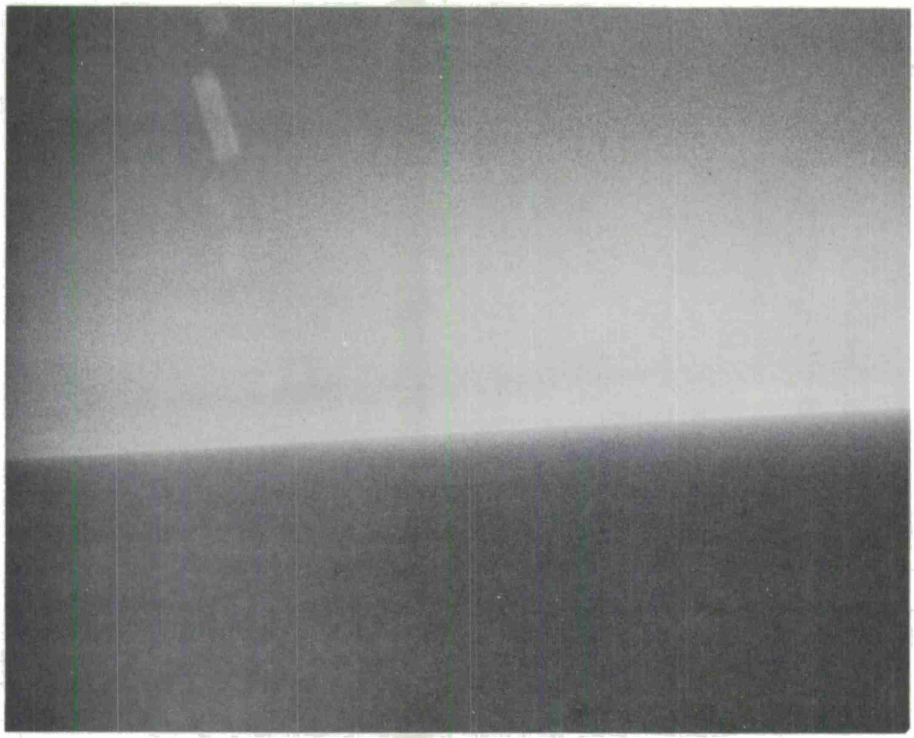

6C 14 March 1969-SPIRAL C-1K

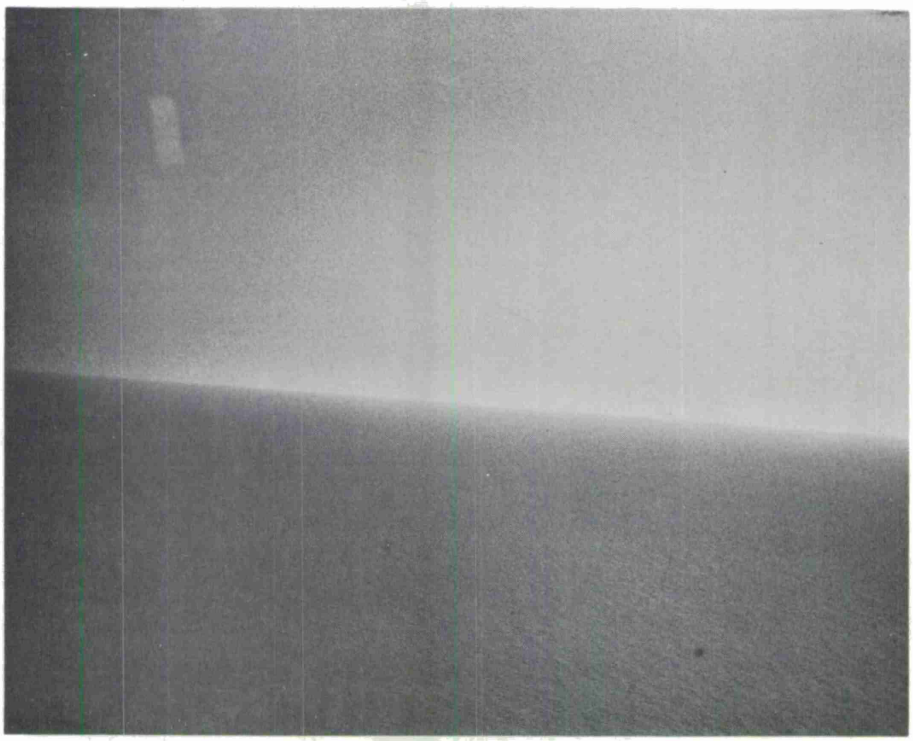

6D 14 March 1969-SPIRAL F

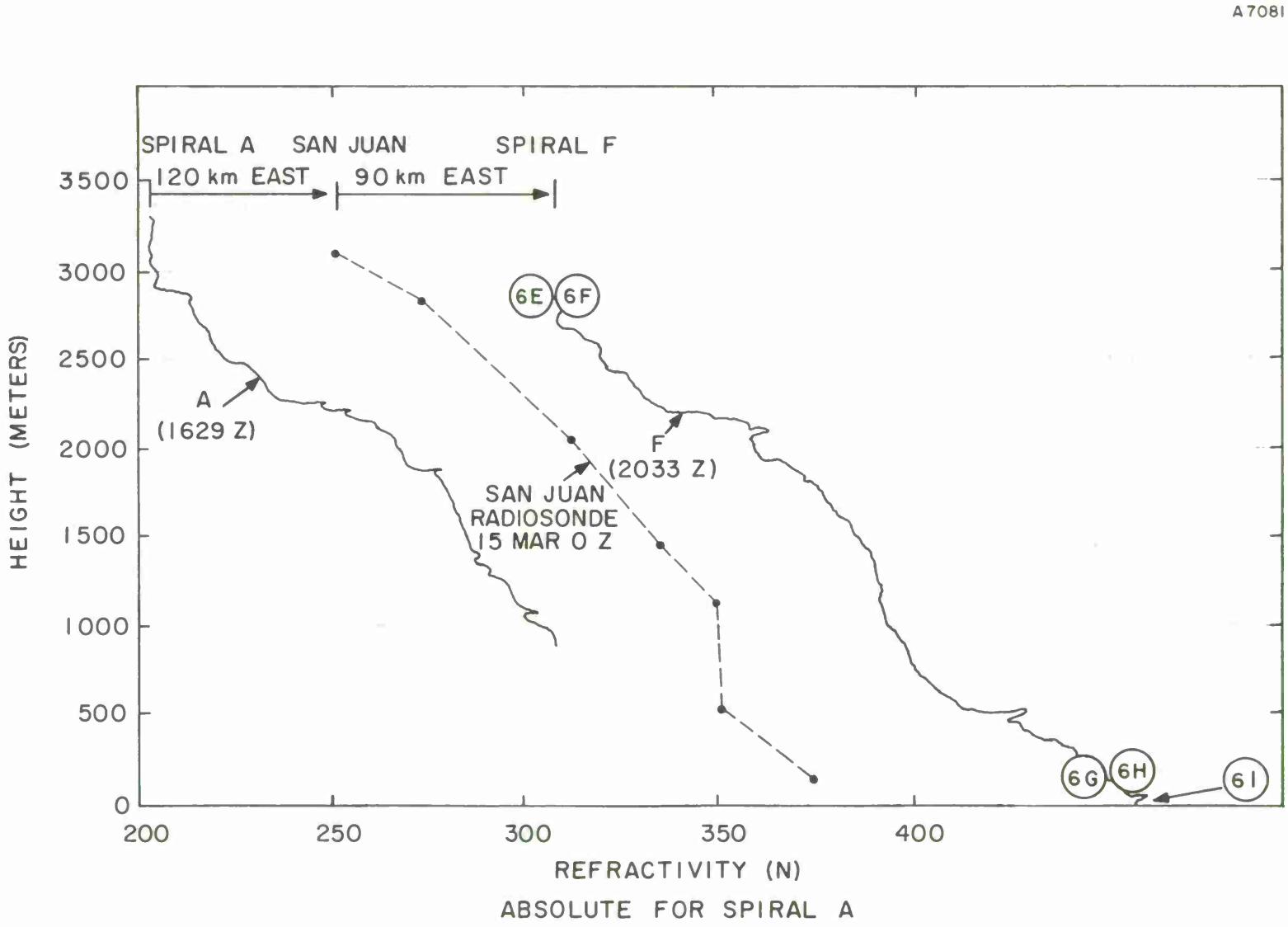
A7081
SPIRAL A
120 km EAST
SAN JUAN
90 km EAST
SPIRAL F
3500
3000
2500
2000
1500
1000
500
0
HEIGHT (METERS)
6E
6F
A
(1629 Z)
F
(2033 Z)
SAN JUAN
RADIOSONDE
15 MAR 0 Z
6G
6H
6I
200
250
300
350
400
REFRACTIVITY (N)
ABSOLUTE FOR SPIRAL A

FIGURE 24.

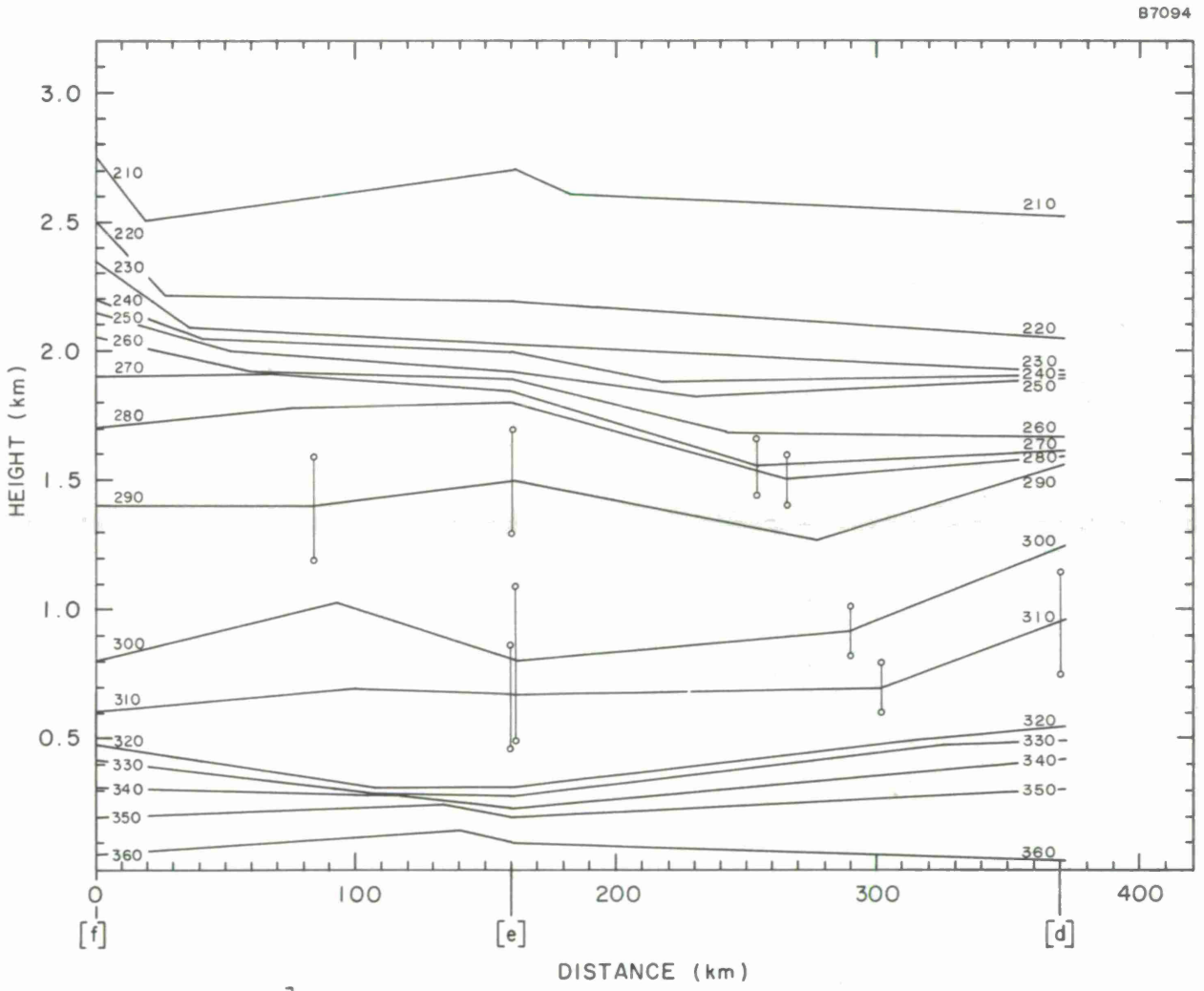
B7094
HEIGHT (km)
3.0
2.5
2.0
1.5
1.0
0.5
210
220
230
240
250
260
270
280
290
300
310
320
330
340
350
360
0
100
200
300
400
[f]
[e]
[d]
DISTANCE (km)
[200 km E OF RAMEY A F B]

FIGURE 25.

It is interesting to look at the cloud structure associated with this mission. Photographs 6E and 6F were taken at the top of Spiral F, off the east end of the Island. Photograph 6E shows the cloud buildup over the Island which is produced by thermal convection and orographic lifting of the air flow over the Island. Photograph 6F shows the normally observed thin layer of stratus clouds which is associated with the inversion. This would indicate that the inversion was formed but broken by the presence of the Island.

Photographs 6G and 6H indicate that Spiral F was made over the few Islands lying off the eastern part of Puerto Rico. It may be noticed that the sea-state is calm and that the surface winds were necessarily light.

Photograph 6I is a very good example of the generation of clouds produced by convection and orographic activity over the eastern tip of the Island. The vertical rise of moisture-laden air during the period of greatest thermal heating usually results in almost daily showers in the high elevations.

A7032

6E 14 March 1969-SPIRAL F-9K

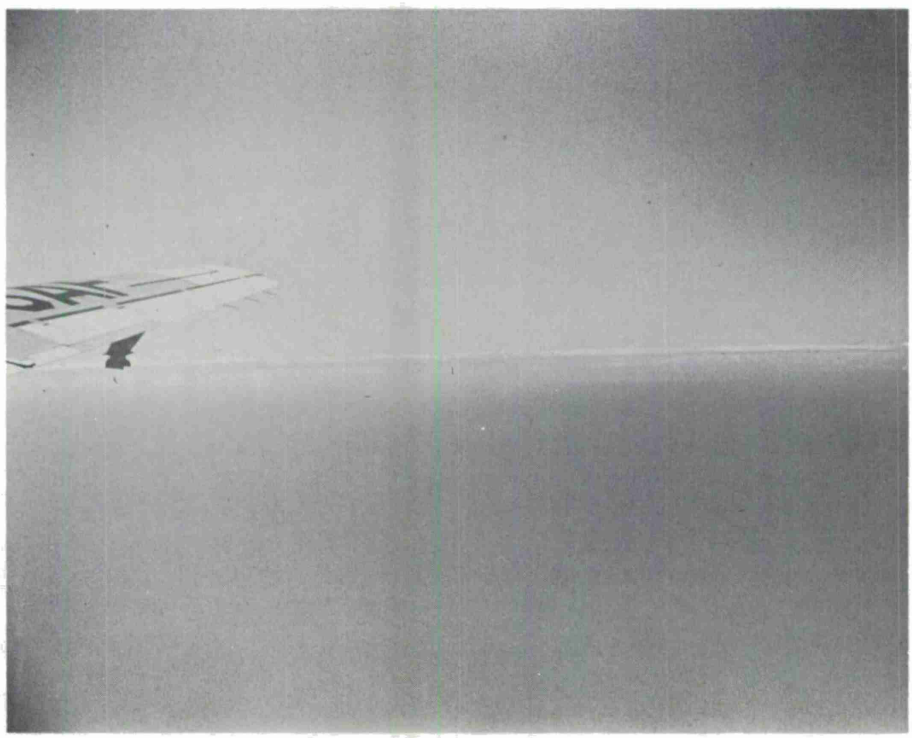

6F 14 March 1969-SPIRAL F-9K

A7033

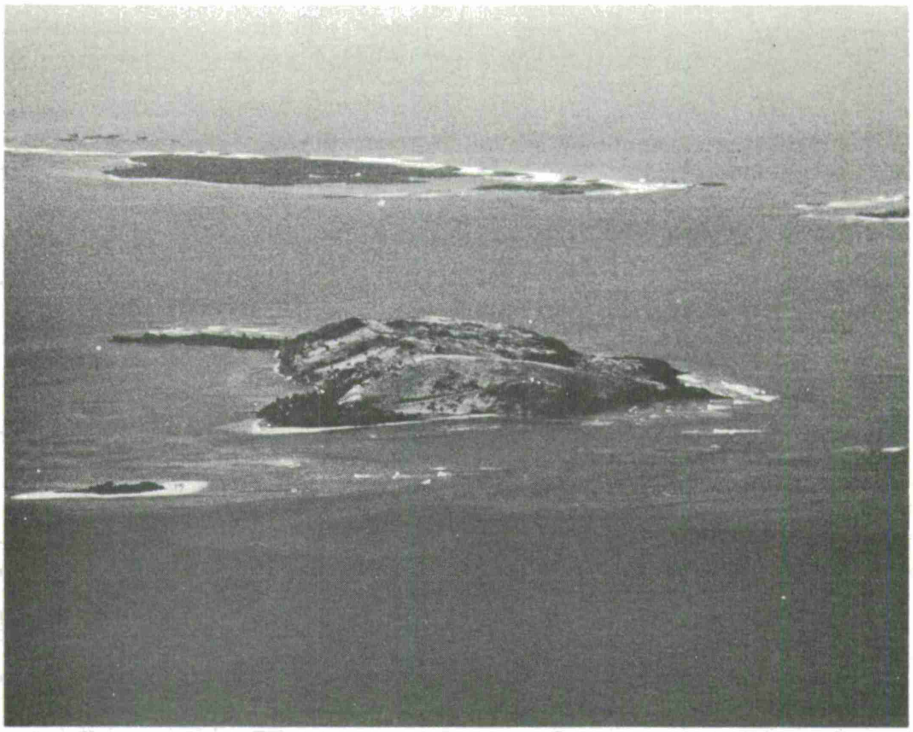

6G 14 March 1969-SPIRAL F-500 feet

6H 14 March 1969-SPIRAL F-500 feet

A7034

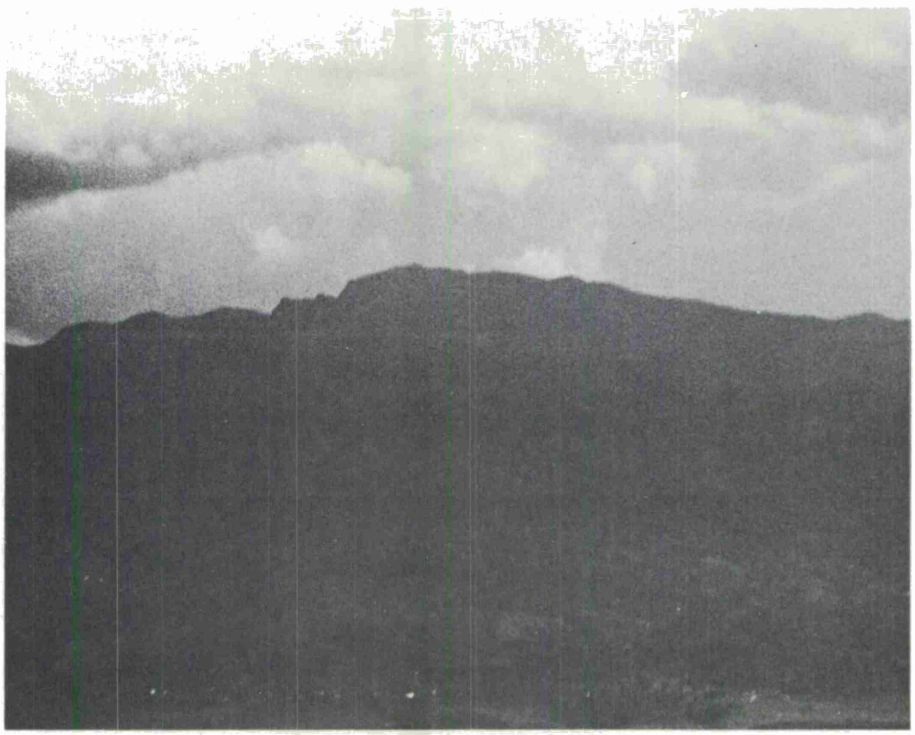

6I 14 March 1969-SPIRAL F
LOOKING TOWARD LAND

SECTION VIII

THE CHARACTERISTICS OF THE TRADE WIND DUCT AND ASSOCIATED WEATHER FROM SAN JUAN TO GRAND TURK
(Mission 7, 17 March)

Figure 26 shows the flight plan for measurements made from San Juan, Puerto Rico, to the Grand Turk Island in the Bahamas.

Spiral	Location	Spiral Start Time Z	Local
A	a. 18-32 N, 67-07 W	1702	1302
B	b. 19-10 N, 68-01 W	1744	1344
Climb 1	b-c	1800	1400
C	c. 1953 N, 69-00 W	1828	1428
Climb 2	c-d	1848	1448
D	d. 20-36 N, 70-00 W	1915	1515
Climb 3	d-e	1932	1532
E	e. 20-34 N, 71-10 W	1955	1555
Climb 4	e-f	2013	1613
F	f. Grand Turk	2033	1633

The surface weather chart, Figure 27, shows a high pressure system just northeast of the flight path. This would cause an increase in subsidence as the system moves from the continent (14 March) into its present position. Winds along the track are from the east to southeast from the Atlantic. The subsidence should intensify as the aircraft moves northward and closer to the center of the system.

Figure 28 shows the refractivity isopleths obtained on this track. The inversion is not well defined anywhere in the area at constant altitude. Initially, a layer is present around 3.5 km altitude which fluctuates in intensity and is absent by the time Spiral D is reached. Near Grand Turk, a weak inversion is indicated around 1.5 km altitude.

The weather profile is shown on Figure 29. The dry air aloft is present near the end of the path at Grand Turk. Warm, moist air is present in two bands, one lying under one km altitude (maritime air) and a second around 2.3 km.

Referring to the previous missions surface chart, it is apparent that the high is replacing the air aloft with dry cool air. However, the trough extending from the Dominican Republic on 14 March had produced an above average water load in the atmosphere.

FLIGHT PATH VI

MISSION 7 — 17 MARCH 1969

FIGURE 26.

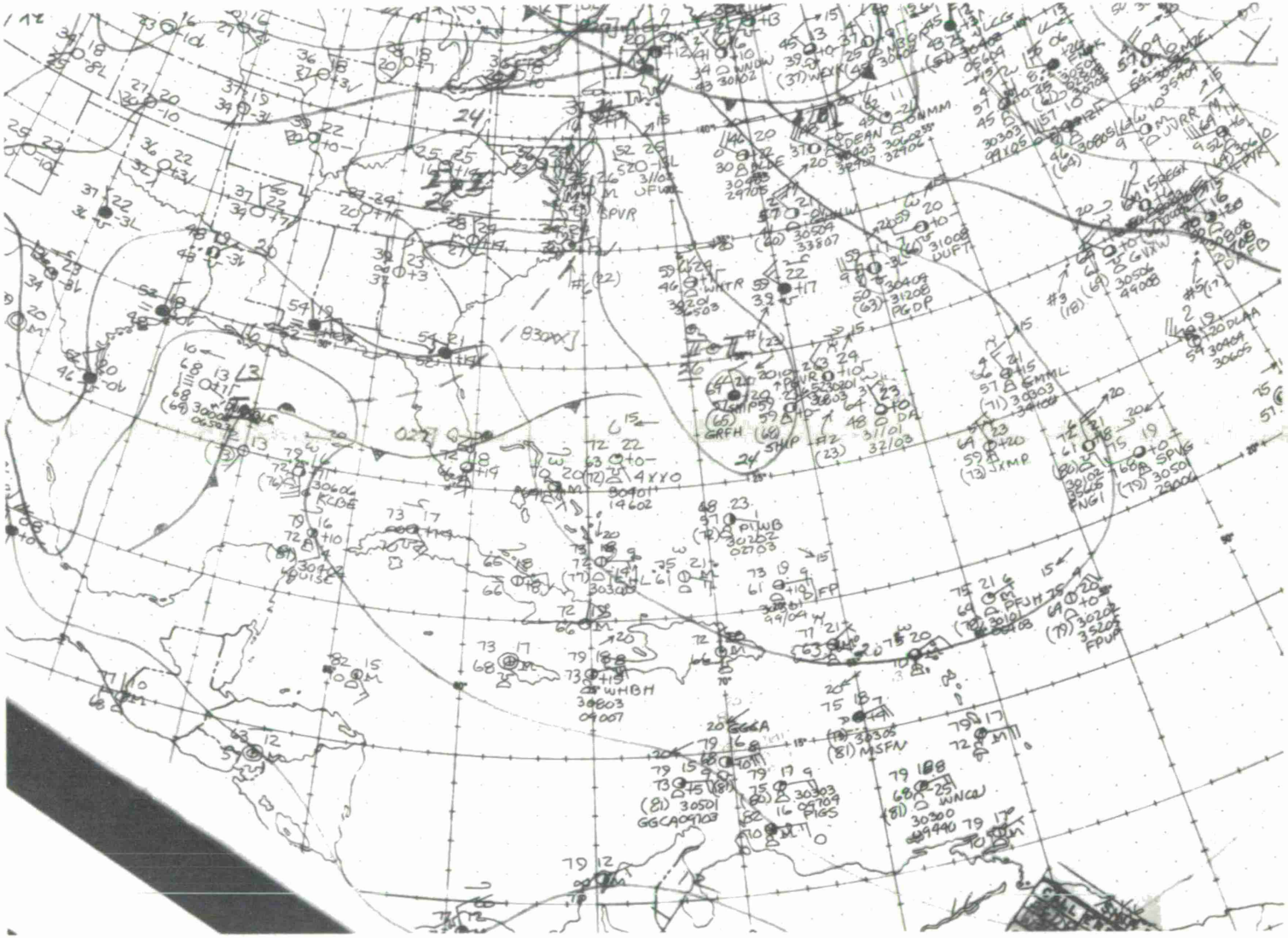

FIGURE 27

SURFACE CHART 17 March 1969

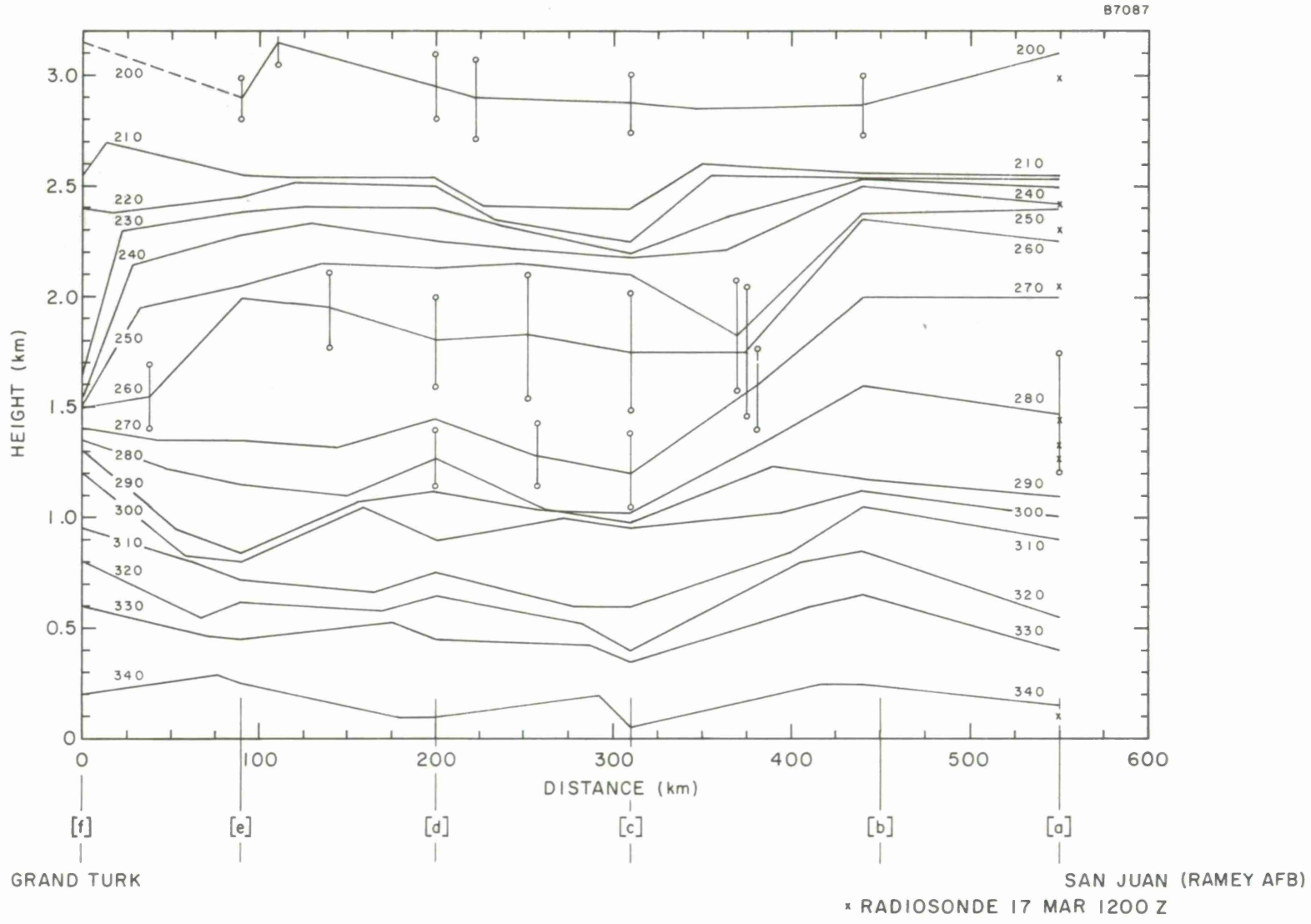
B7087
HEIGHT (km)
3.0
2.5
2.0
1.5
1.0
0.5
0
200
210
220
230
240
250
260
270
280
290
300
310
320
330
340
0
100
200
300
400
500
600
DISTANCE (km)
[f]
[e]
[d]
[c]
[b]
[a]
GRAND TURK
SAN JUAN (RAMEY AFB)
x RADIOSONDE 17 MAR 1200 Z

FIGURE 28.

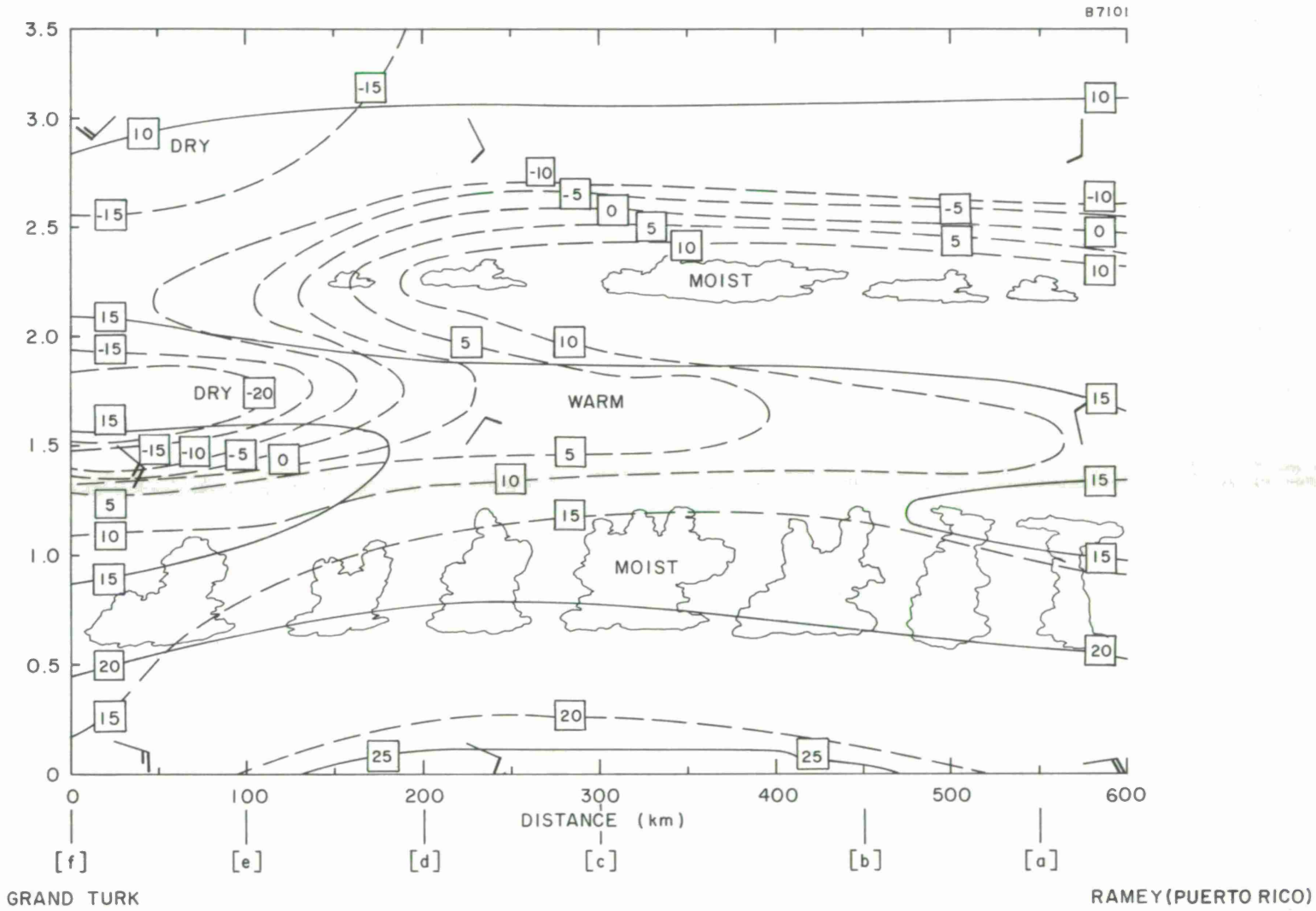
B7101
3.5
3.0
2.5
2.0
1.5
1.0
0.5
0
DRY
MOIST
DRY
WARM
MOIST
0
100
200
300
400
500
600
DISTANCE (km)
[f]
[e]
[d]
[c]
[b]
[a]
GRAND TURK
RAMEY (PUERTO RICO)

FIGURE 29.

The situation presented in this mission is one of normal dry air advection replacing warm, moist air produced by a low pressure trough. Under these conditions, when the two air masses are mixing midway along the path, one observes an unpredictable pattern in the water vapor distribution.

SECTION IX

THE CHARACTERISTICS OF THE TRADE WIND DUCT AND ASSOCIATED WEATHER FROM GRAND TURK TO NASSAU (Mission 8, 18 March)

Figure 30 shows the flight plan from Grand Turk to Nassau on 18 March.

Spiral	Location	Spiral Start Time Z	Local
A	a. Grand Turk	1447	0947
B	b. 22-35 N, 73-07 W	1547	1047
Climb 1	b-c	1606	1106
C	c. 23-08 N, 74-00 W	1630	1130
Climb 2	c-d	1650	1150
D	d. 24-00 N, 75-35 W	1723	1223
Climb 3	d. Nassau	1741	1241

The surface weather map, Figure 31, shows the high pressure system in almost the same location. One would, therefore, expect the advection of dry cool air to have continued from the previous day and the inversion to be much better defined.

Figure 32 shows the refractivity isopleths and it is clearly evident that the Trade Wind Duct is well formed and in its usual location around 1.5 km altitude. Its altitude decreases toward the west and it finally dissipates in the vicinity of Nassau.

The weather profile, Figure 33, shows dry subsiding air over Grand Turk, but with the subsidence intensity falling off in the direction of Nassau. Warm, moist air is present at the lower altitudes in the vicinity of Nassau.

Referring to the surface chart, a low pressure system with a trough through Florida is clearly causing an increase in the water load of the upper air. Its effect is evident at Nassau where the dry air is being under-run with increasing warm, moist air. Increasing cloudiness at the higher altitudes occurs as a result of this advection.

FLIGHT PATH VII

MISSION 8 — 18 MARCH 1969

FIGURE 30.

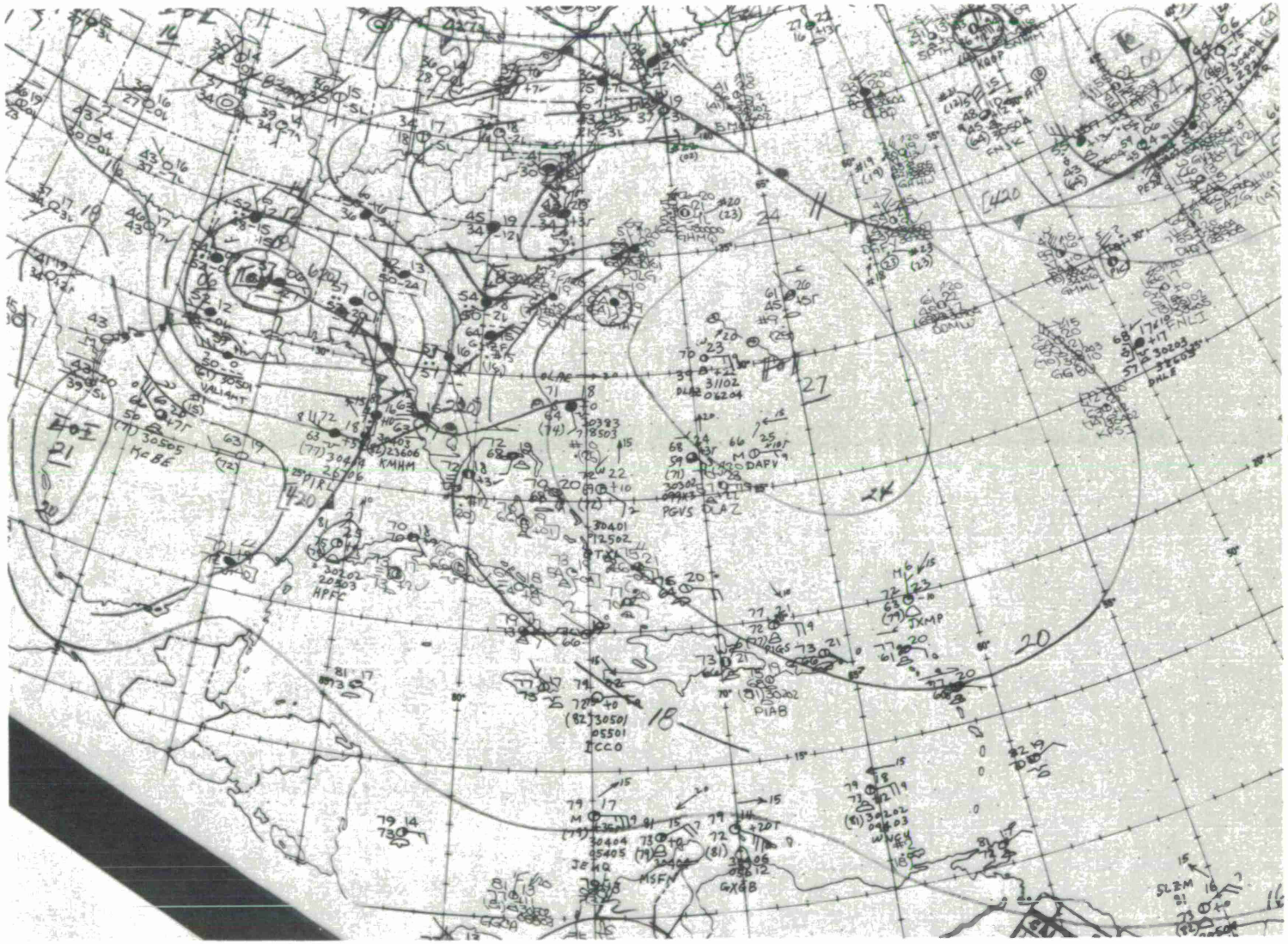

FIGURE 31

SURFACE CHART 18 March 1969

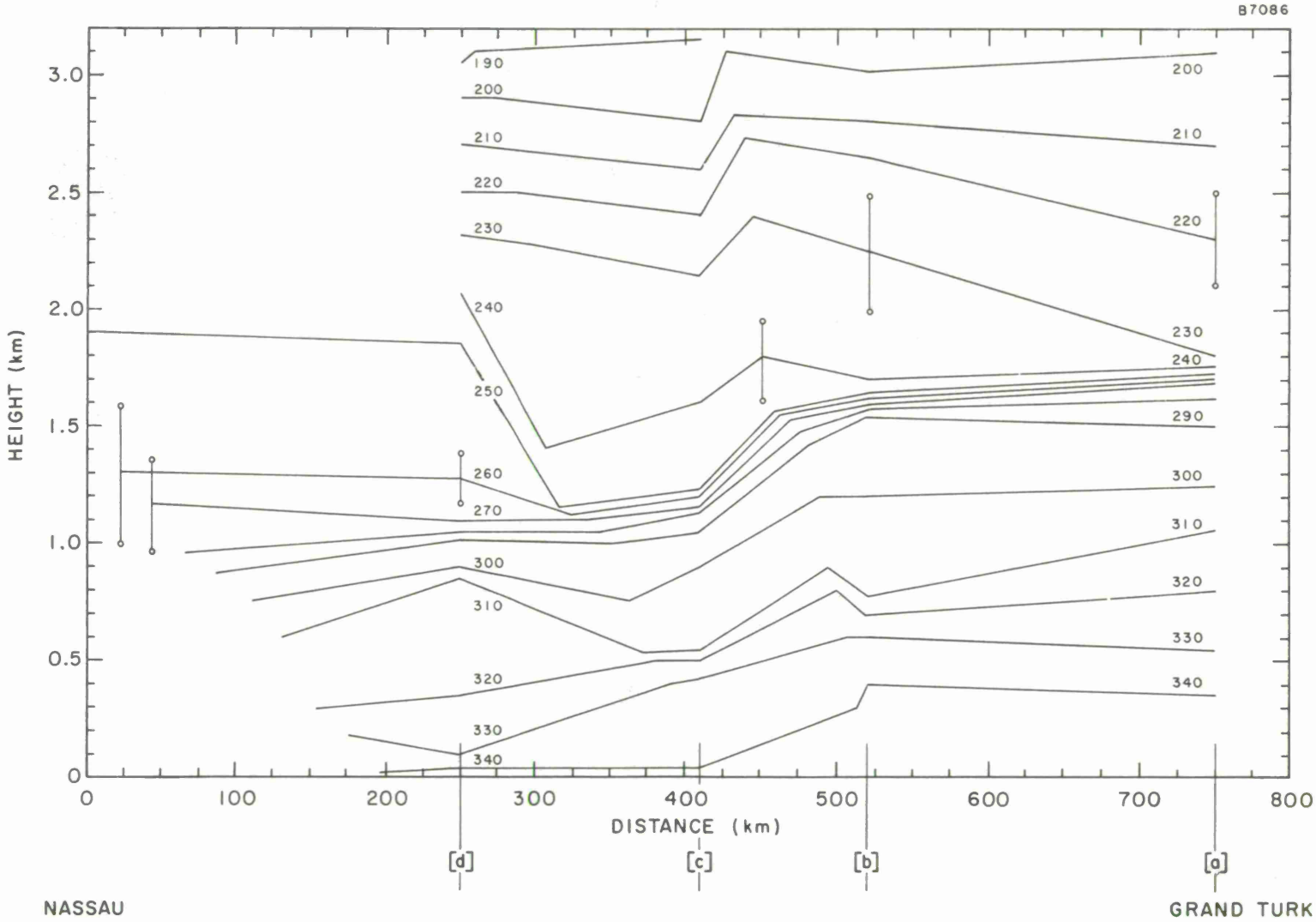
B7086
HEIGHT (km)
3.0
2.5
2.0
1.5
1.0
0.5
0
0
100
200
300
400
500
600
700
800
DISTANCE (km)
190
200
210
220
230
240
250
260
270
300
310
320
330
340
200
210
220
230
240
290
300
310
320
330
340
[d]
[c]
[b]
[a]
NASSAU
GRAND TURK

FIGURE 32.

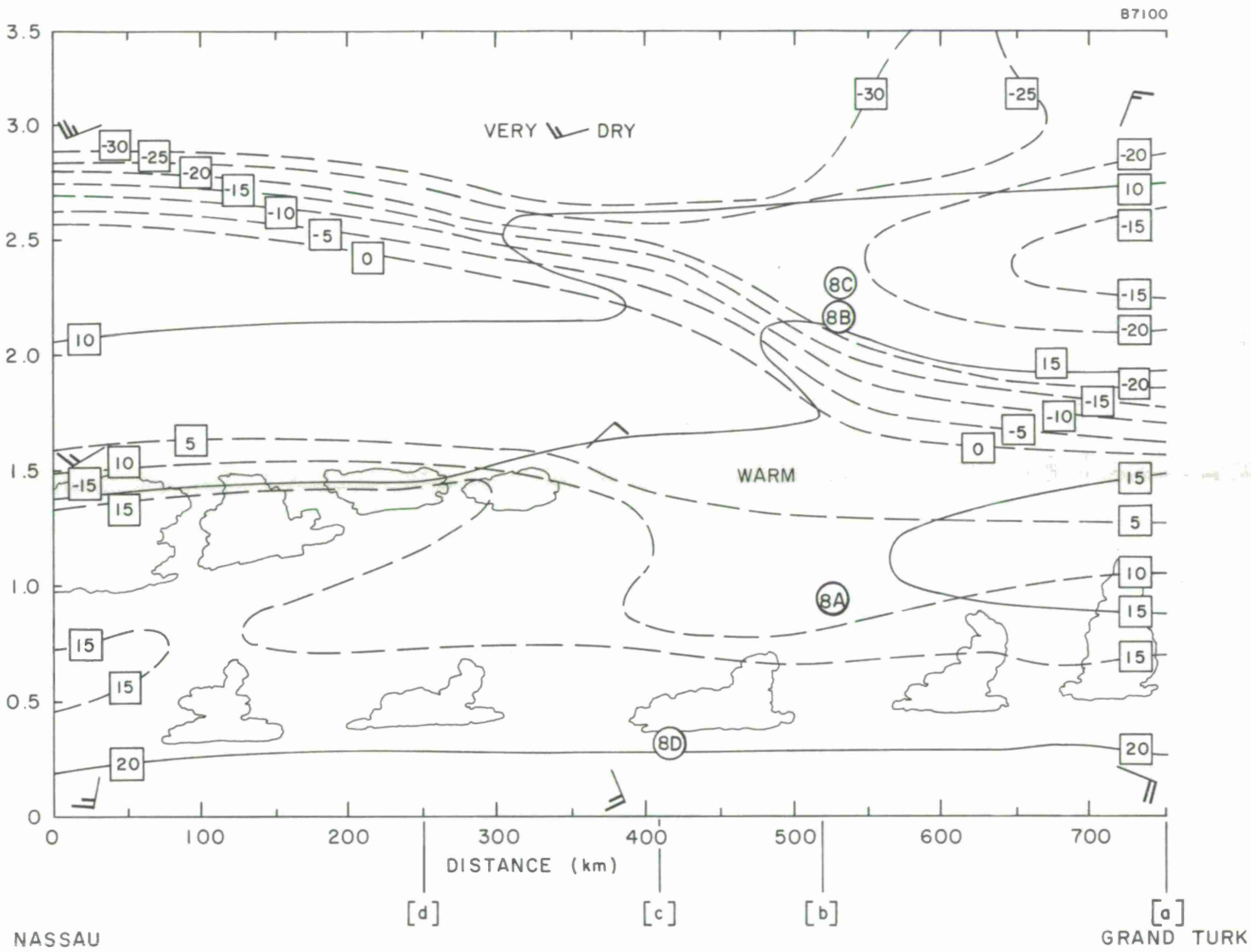
87100
VERY DRY
WARM
8A
8B
8C
8D
-30
-25
-20
-15
-10
-5
0
10
5
15
20
3.5
3.0
2.5
2.0
1.5
1.0
0.5
0
0
100
200
300
400
500
600
700
DISTANCE (km)
[d]
[c]
[b]
[a]
NASSAU
GRAND TURK

FIGURE 33.

Photographs 8A through 8C show little cloud formation as the aircraft leaves the Grand Turk area. In fact, 8B, taken from altitude indicates a haze layer associated with an extensive inversion and very little moisture present at low levels. Photograph 8D was taken at low-level in Spiral C. The air is dry and clear with very thin clouds present. The moisture and haze layer can be seen when looking towards the horizon. There is remarkably little vertical advection of moisture from the sea.

A7035

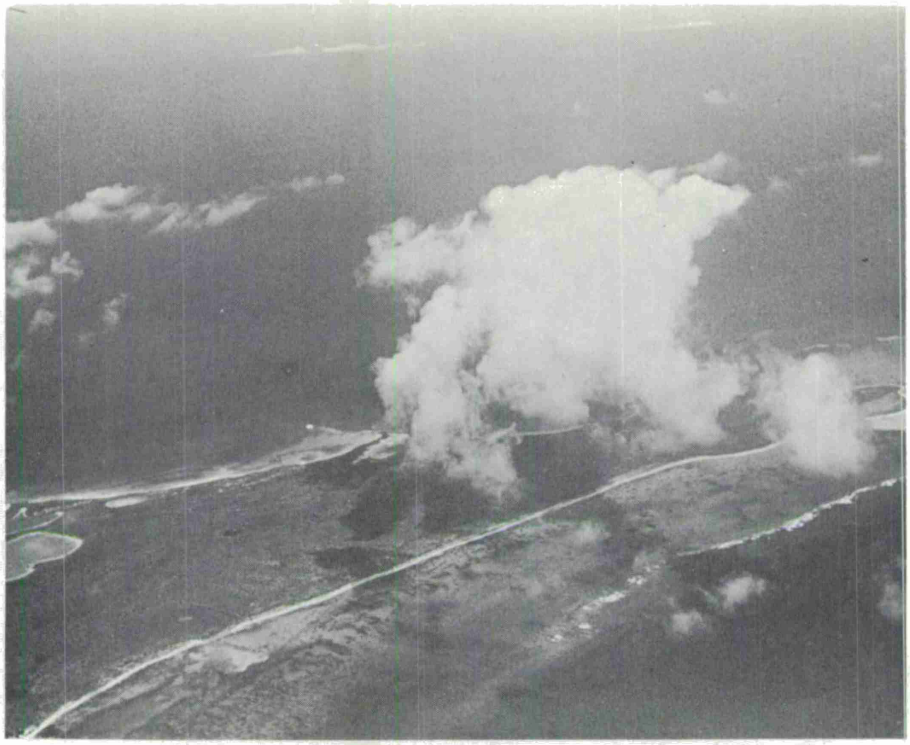

8A 18 March 1969-SPIRAL B

8B 18 March 1969-SPIRAL B-7K

A7036

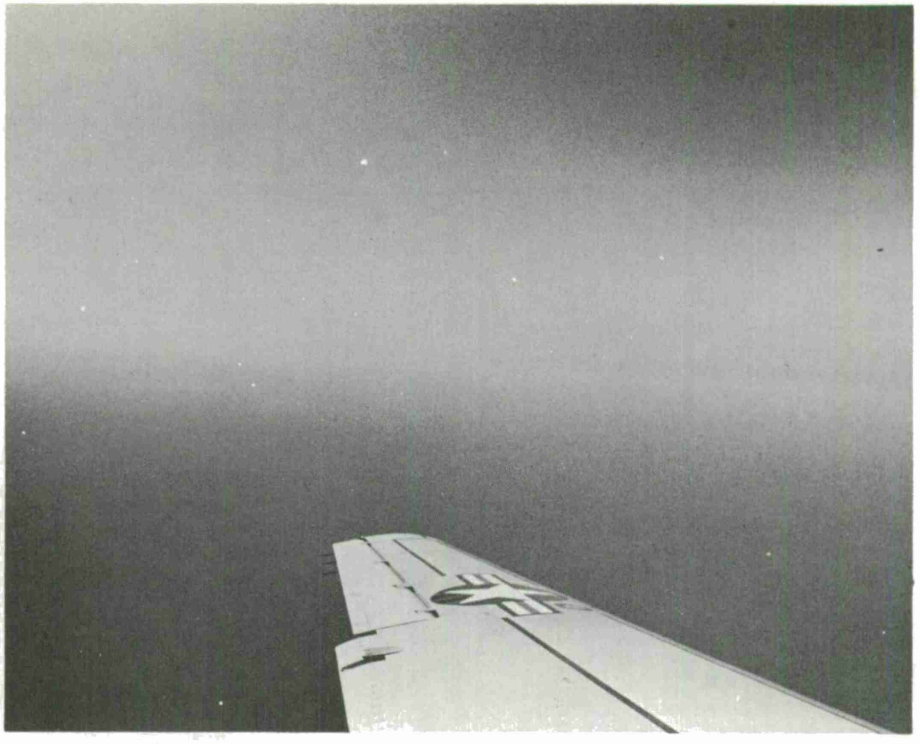

8C 18 March 1969-SPIRAL B-7K

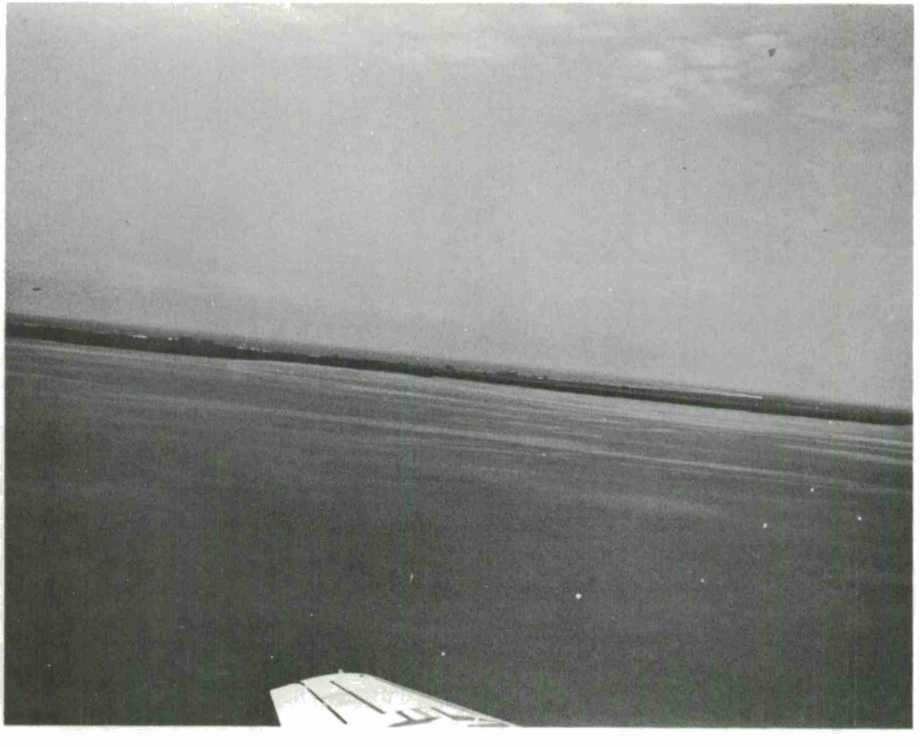

8D 18 March 1969-SPIRAL C-1K

SECTION X

SPATIAL VARIATIONS OF REFRACTIVITY IN THE VICINITY OF KEY WEST
(Missions 9, 10, 11, 21 March)

Figure 34 shows the position of three spirals located along a line extending east from Key West, for Mission 9.

Spiral	Location	Spiral Start Time Z	Local
A	a. Key West	1135	0635
B	b. 24-06 N, 81-51 W	1200	0700
Climb 1	b-c	1218	0718
C	c. 24-06 N, 81-08 W	1235	0735

These spirals were made over a short interval of time in which case the spatial variation of refractivity is fairly easy to define. The surface chart, Figure 35, shows a high pressure ridge advancing southeastward in the area. The low, which affected the previous mission, is leaving the area and heading up along the coast. The area, on 18 March, was partly under the influence of the high to the northeast. As discussed before, the effect of this high at Nassau should be more evident.

Therefore, the area of Key West to Nassau is not only becoming more influenced by the new high off the continent, but is greatly affected by the high pressure system already present to the east. One would, therefore, expect the inversion to be well formed and intensifying with time.

Figure 36 shows the profiles for Mission 9. The Trade Wind Duct (or Inversion) exhibits its characteristic features. The height of the inversion shows some slight variation and is weakening toward the east. At Key West, the radiosonde profile compares very well with the aircraft measurements. Except for some loss of detail the radiosonde profile could be used to show the average behavior of the refractivity with height.

Figure 37 shows the profiles of refractivity approximately five hours later. With the increase in thermal convection the height of the layer is greater but it shows a tendency to lift toward the east. As the high pressure system intensifies over Key West and the high to the east moves out, one could expect such a sloping tendency to occur. In comparison with the 1200 Z radiosonde, one can see the increase in elevation of the underlying moisture layer which is produced by thermal convection.

SCALE 1:5,702,400 OR 90 MILES TO 1 INCH

100 50 0 100 200 300

STATUTE MILES

100 50 0 100 200 300 400

KILOMETERS

FLIGHT PATH I

MISSIONS 1 AND 2 — 6 MARCH 1969

MISSIONS 9, 10, AND 11 — 21 MARCH 1969

FIGURE 34

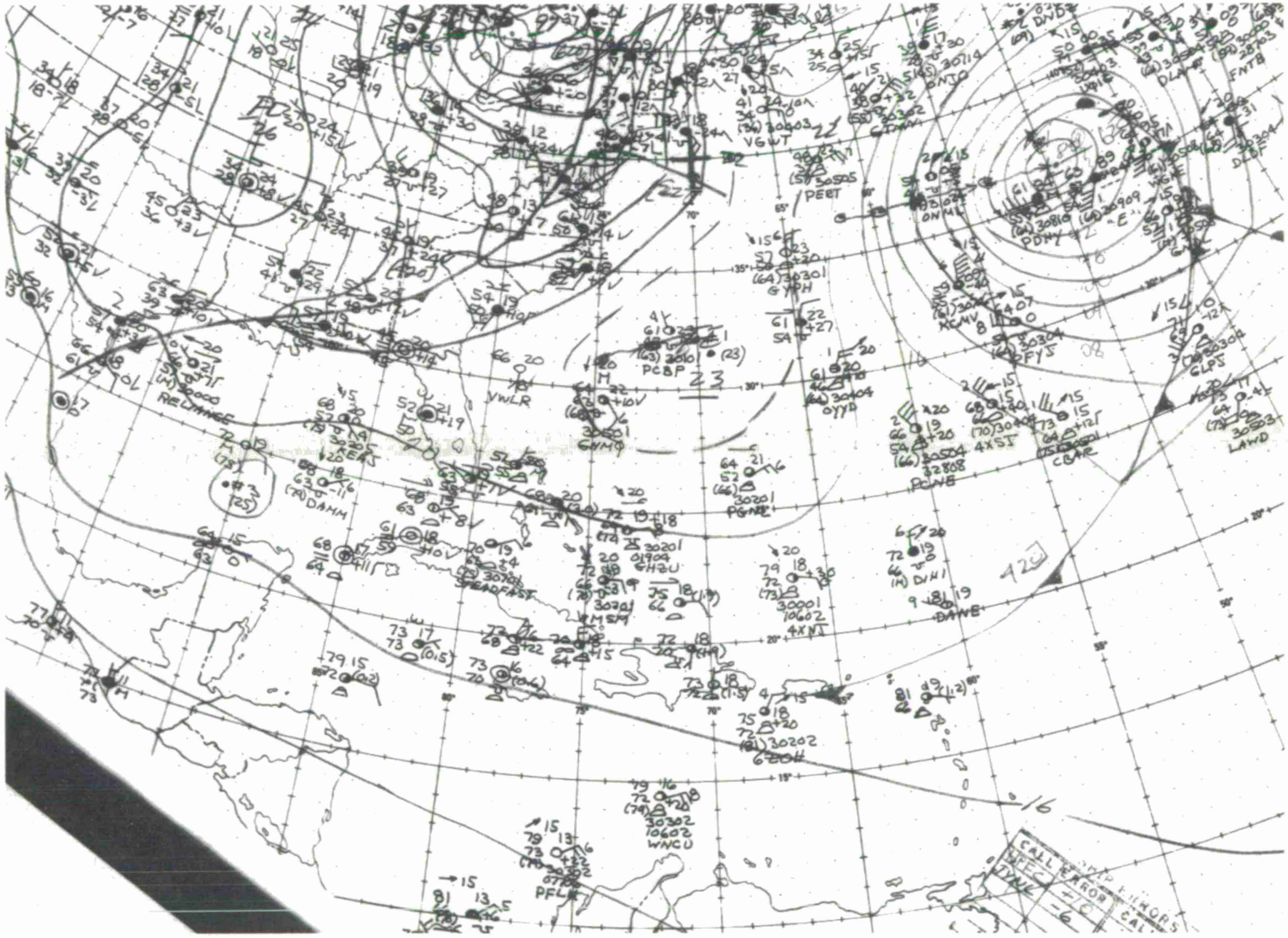

FIGURE 35.

SURFACE CHART 21 March 1969

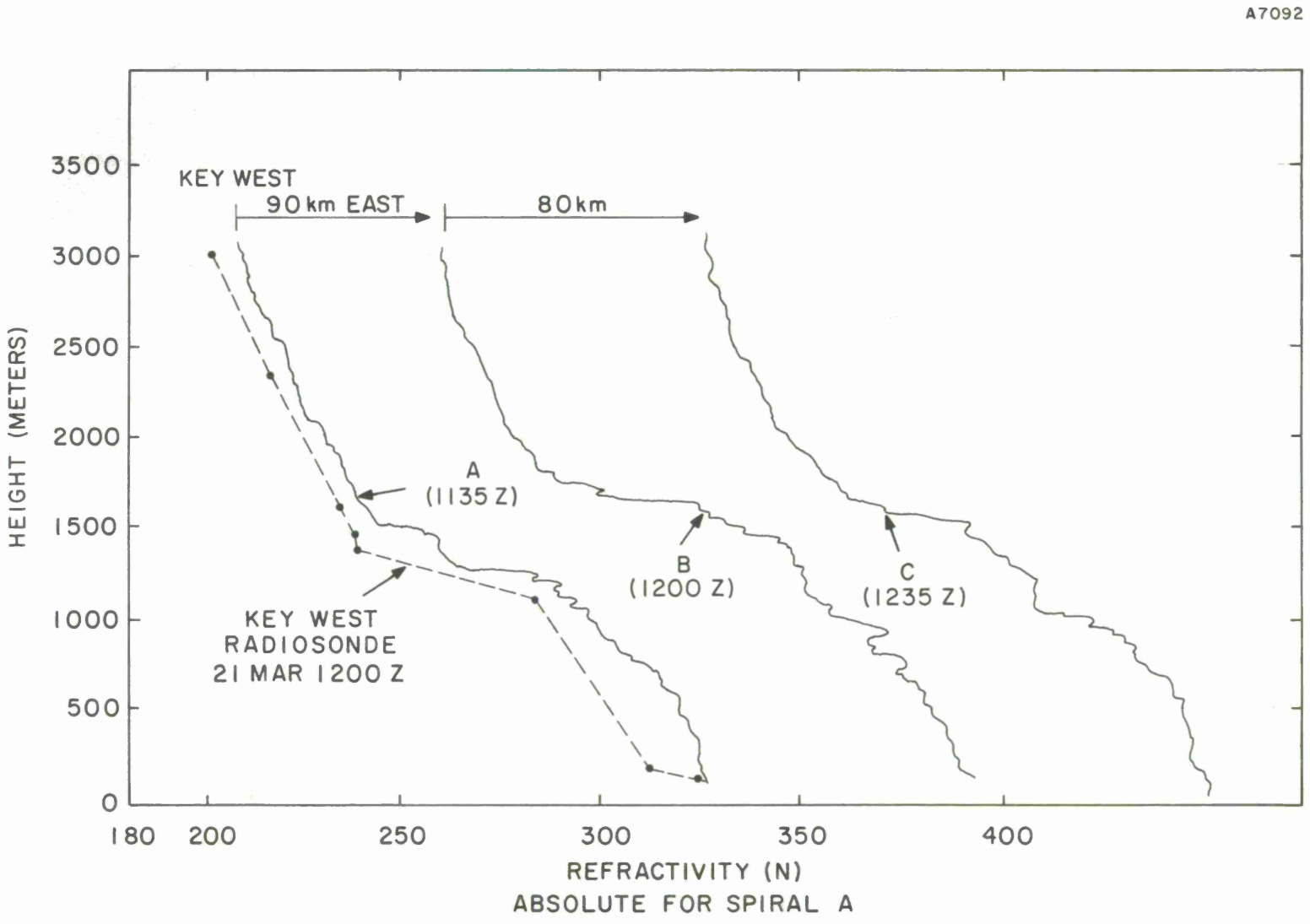
A7092
KEY WEST
90 km EAST
80 km
A
(1135 Z)
B
(1200 Z)
C
(1235 Z)
KEY WEST
RADIOSONDE
21 MAR 1200 Z
HEIGHT (METERS)
3500
3000
2500
2000
1500
1000
500
0
180
200
250
300
350
400
REFRACTIVITY (N)
ABSOLUTE FOR SPIRAL A

FIGURE 36.

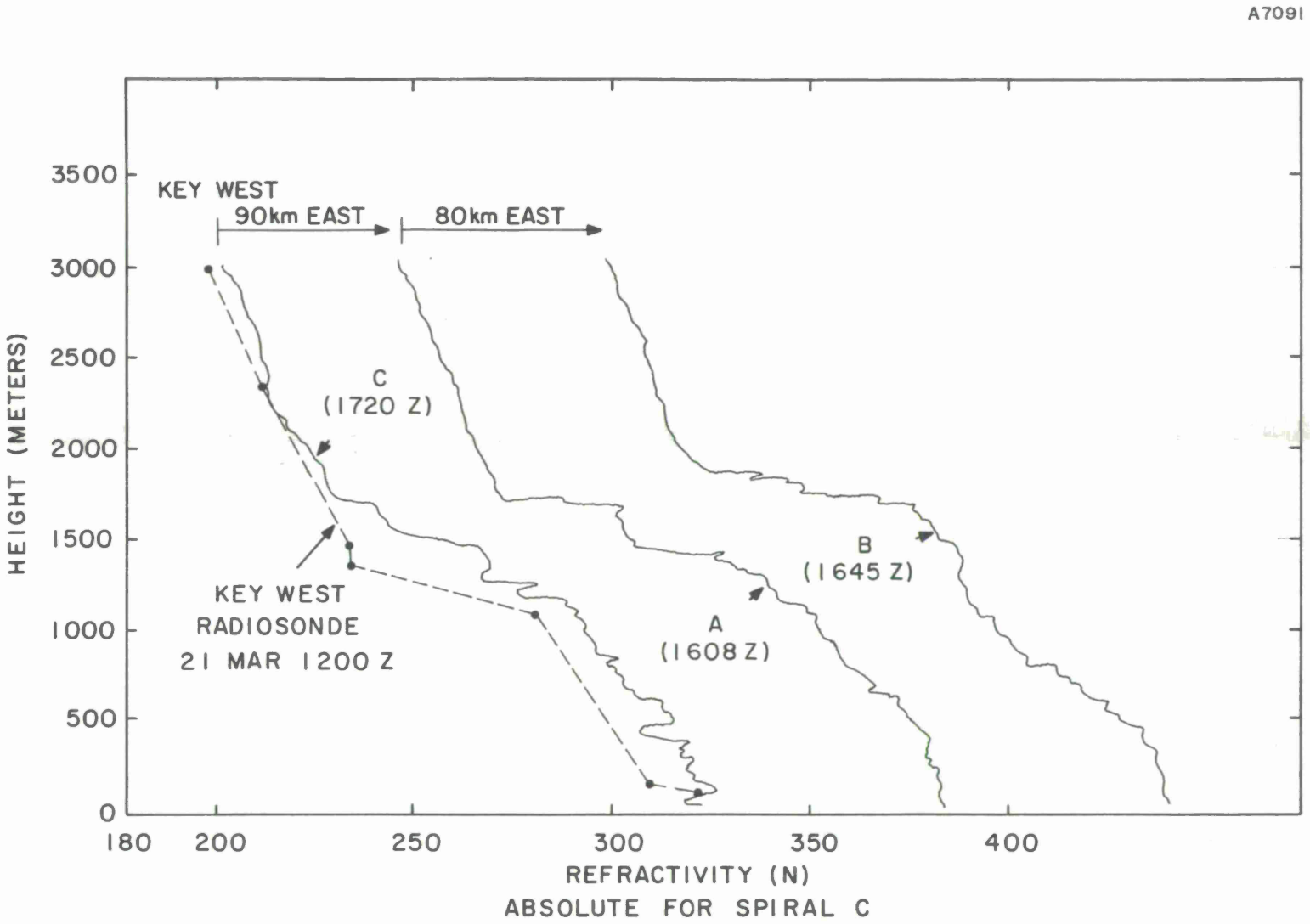
A7091
KEY WEST
90km EAST
80km EAST
C
(1720 Z)
B
(1645 Z)
A
(1608 Z)
KEY WEST
RADIOSONDE
21 MAR 1200 Z
HEIGHT (METERS)
3500
3000
2500
2000
1500
1000
500
0
180
200
250
300
350
400
REFRACTIVITY (N)
ABSOLUTE FOR SPIRAL C

FIGURE 37.

Figure 38 shows the refractivity structure some five hours later. The layer is still intense and as evening arrives, the thermal convection subsides. The only significant effect is to observe the rising and lowering of the air by thermal convection. Near the land, as the air cools in the evening, a cloud deck forms as the maritime air mass begins to sink.

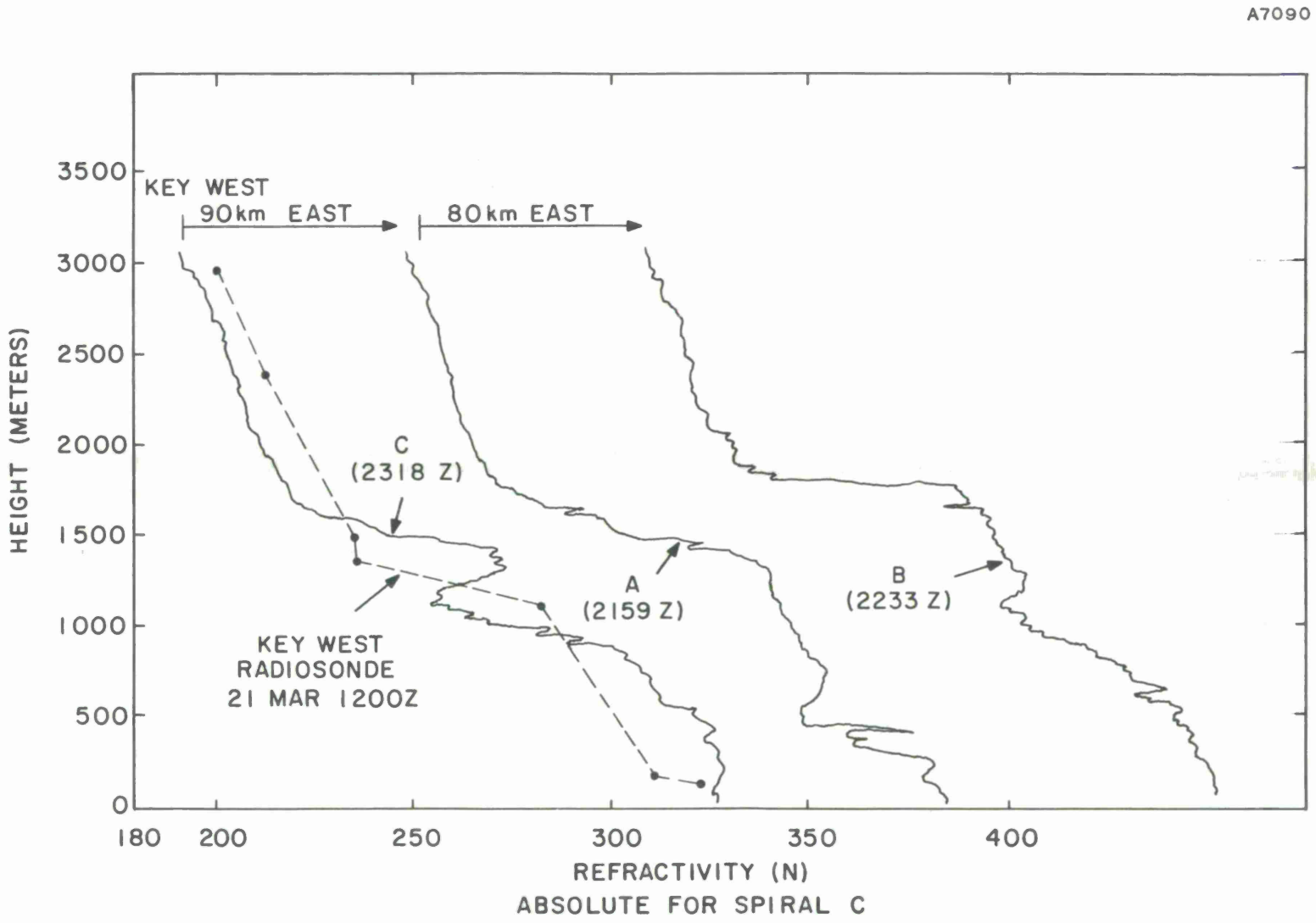
A7090
KEY WEST
90km EAST
80km EAST
C
(2318 Z)
A
(2159 Z)
B
(2233 Z)
KEY WEST
RADIOSONDE
21 MAR 1200Z
HEIGHT (METERS)
3500
3000
2500
2000
1500
1000
500
0
180
200
250
300
350
400
REFRACTIVITY (N)
ABSOLUTE FOR SPIRAL C

FIGURE 38.

SECTION XI

VARIATIONS OF REFRACTIVITY IN THE KEY WEST AREA
(Missions 12, 13, and 14)

11.1 Mission 12

Figure 39 shows the flight plan for Mission 12, which was flown during the afternoon of 23 March.

Spiral	Location	Spiral Start Time Z	Local
A	a. Key West	0712	0212
B	b. 24-35 N, 82-37 W	0748	0248
Climb 1	b-c	0806	0306
C	c. 24-35 N, 83-32 W	0828	0328
Climb 2	c-d	0845	0345
D	d. 24-35 N, 84-26 W	0909	0409
Climb 3	d-e	0926	0426
E	e. 24-35 N, 83-03 W	0952	0452
Climb 4	e-f	1011	0511
F	f. 24-43 N, 81-04 W	1043	0543
Climb 5	f-a	1101	0601
G	a. Key West	1119	0619

Spiral C actually lies in the plane through d, e, and b, therefore, it is interesting to observe the variations extending through a vertical plane from d to f, which lies north of Key West.

Referring to Figure 40, the surface map shows the area of Key West still under the influence of a high pressure system. A low to the northeast should not be influential. Figure 41 shows the five profiles taken along the d-f plane, all recorded within a few hours. The layer is very strong to the east and weakens in the westward direction. The greater height of the inversion in Spiral B (0748 Z) could be accounted for because of the greater thermal convection produced in the early afternoon. Spiral F, on the other hand, was obtained late in the afternoon when the effect of heating is decreasing.

In Spiral D, the layer is breaking up with a weak lower section around 1.2 km.

B6902

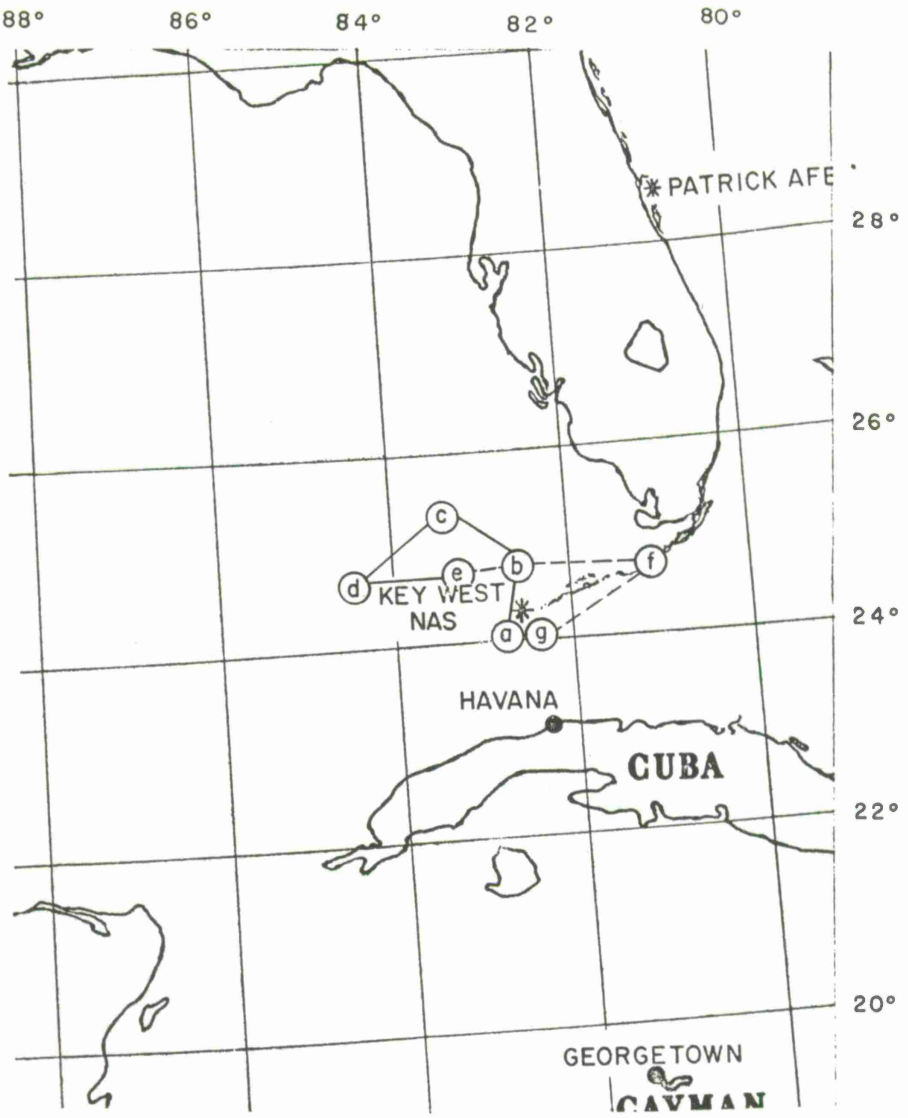

SCALE 1:5,702,400 OR 90 MILES TO 1 INCH

100 50 0 100 200 300
STATUTE MILES
100 50 0 100 200 300 400
KILOMETERS

FLIGHT PATH VIII
MISSION 12 — 23 MARCH 1969
MISSION 13 — 24 MARCH 1969
MISSION 14 — 25 MARCH 1969

FIGURE 39.

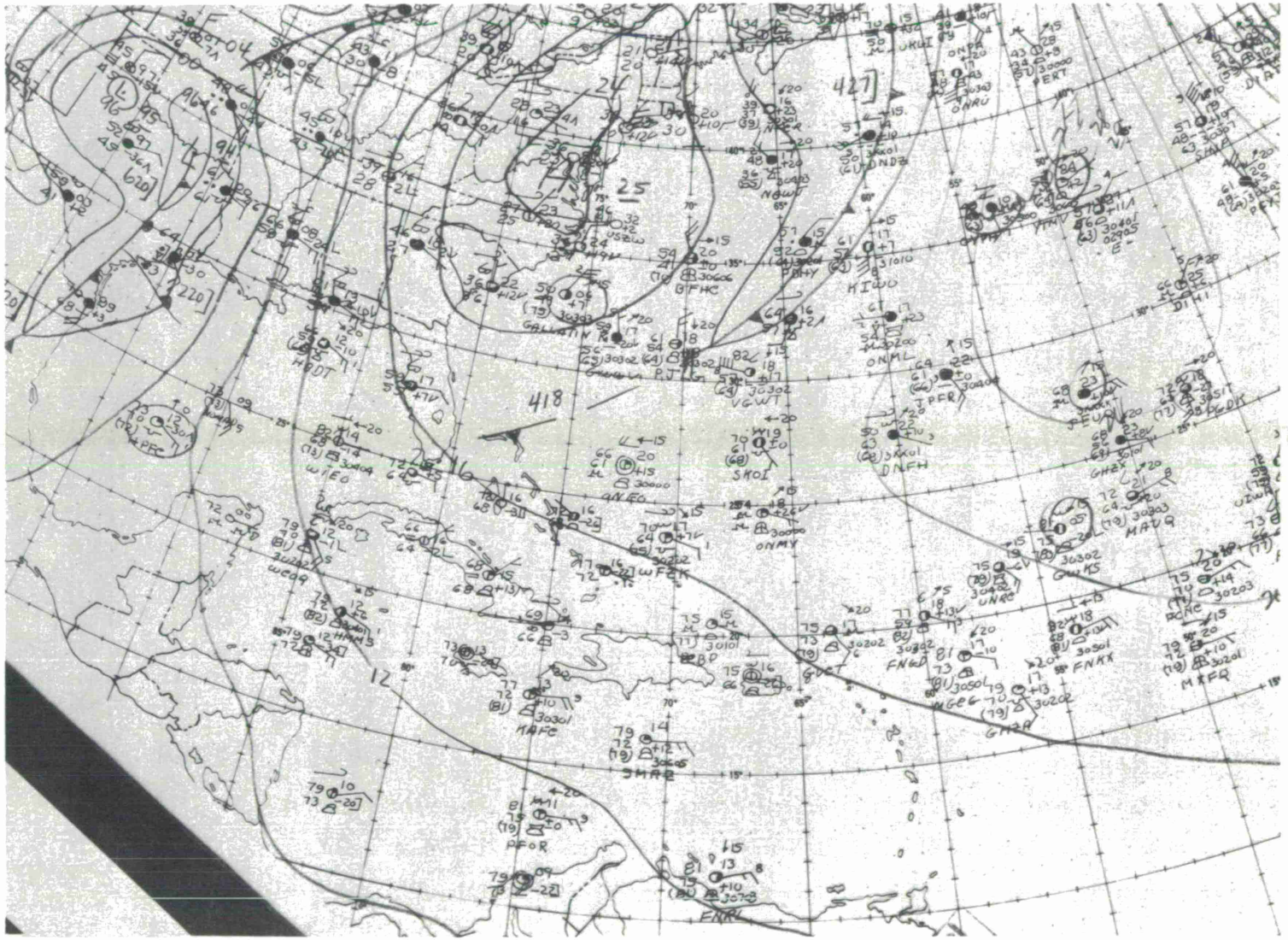

FIGURE 40

SURFACE CHART 23 March 1969

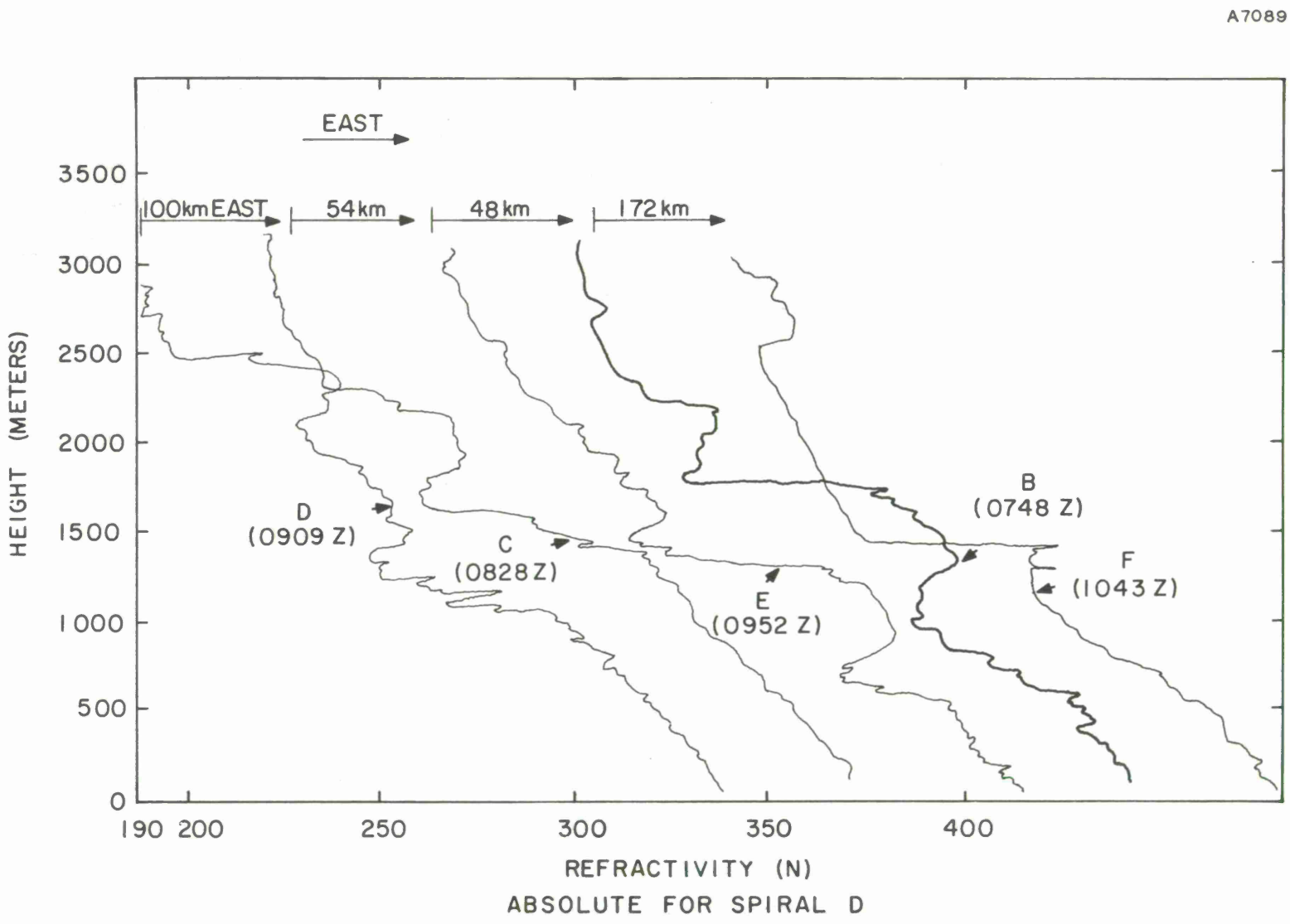
A7089
EAST
100km EAST
54km
48km
172km
3500
3000
2500
2000
1500
1000
500
0
HEIGHT (METERS)
D
(0909 Z)
C
(0828 Z)
E
(0952 Z)
B
(0748 Z)
F
(1043 Z)
190 200
250
300
350
400
REFRACTIVITY (N)
ABSOLUTE FOR SPIRAL D

FIGURE 41.

Comparing D and C, one may observe the increase in moisture above 1.5 km, which produces a layer at 2.5 km in Spiral D.

Figure 42 shows three spirals, C, E, and A, lying along a diagonal roughly forty-five degrees to the d-f plane.

The increased height of the layer at A, which was recorded partly over land, shows the greater thickness of the maritime layer due to thermal conductivity. Both Spirals E and A remain unaffected by the presence of the low pressure system to the northwest.

Figure 43 shows a comparison of Spirals A and G, both taken at Key West but four hours apart. Except for a slight decrease in the height of the layer because of a decrease in thermal convection, there is little variation over this time period. The radiosonde presents the refractivity gradient at the inversion to be less than was measured by the aircraft during Spiral G. During the initial part of the launch, the radiosonde also indicates a bulge, likely due to higher humidity.

The low pressure system is apparently beginning to advect moisture into the area at altitudes around 2 km. This increase in moisture is due to two effects. The low pressure system will cause an advance of cold moist air into the area. The cooler air which flows cyclonically around the low will enhance the vertical transport of water vapor. This would be particularly effective in the mid-northern part of the Gulf where cold air is brought down by the low from the interior of the continent.

These data indicate, as before, that the characteristic Trade Wind Duct survives only under conditions where the air aloft is very dry and of great horizontal extent. The maritime layer is constrained from rising only by a few degrees increase in temperature due to subsidence. This combination of requirements is precarious.

11.2 Mission 13

Mission 13 was flown on 24 March, the day after Mission 12, and during the late afternoon to early evening period. Figure 44 shows the flight plan was the same as for Mission 12.

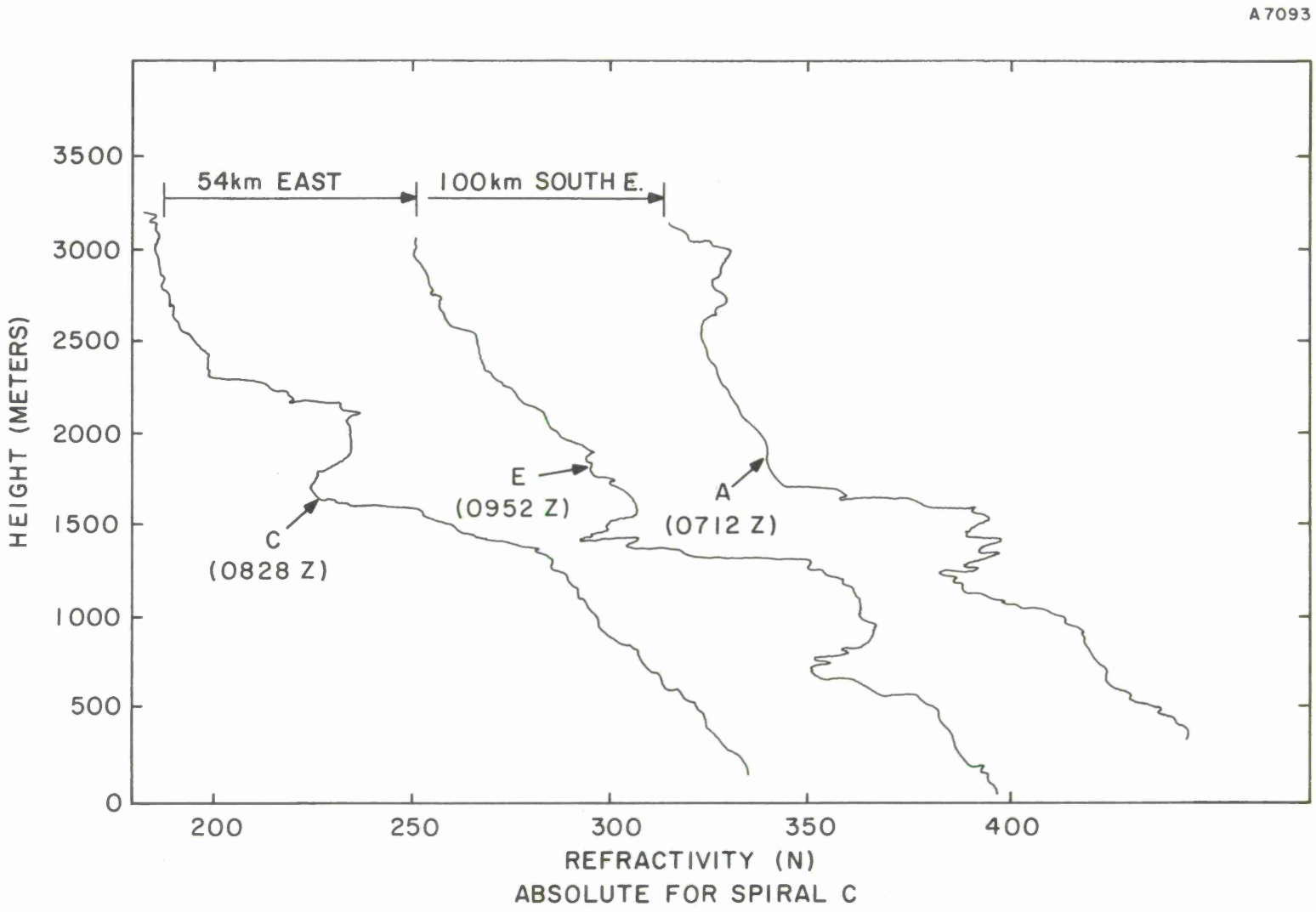
A 7093
3500
3000
2500
2000
1500
1000
500
0
HEIGHT (METERS)
54km EAST
100km SOUTH E.
E
(0952 Z)
A
(0712 Z)
C
(0828 Z)
200
250
300
350
400
REFRACTIVITY (N)
ABSOLUTE FOR SPIRAL C

FIGURE 42.

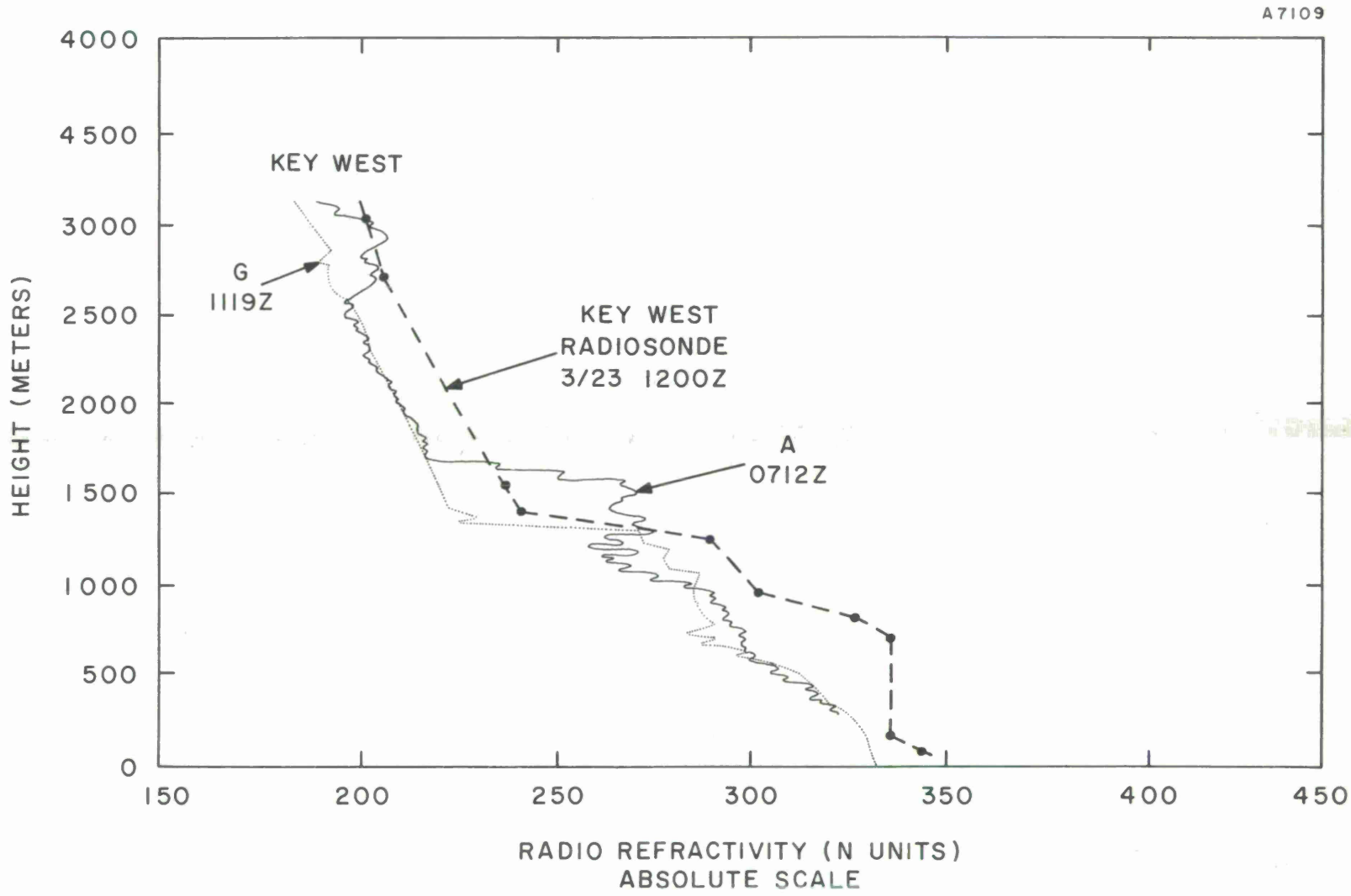
A7109
4000
4500
3000
2500
2000
1500
1000
500
0
HEIGHT (METERS)
KEY WEST
G
1119Z
KEY WEST
RADIOSONDE
3/23 1200Z
A
0712Z
150
200
250
300
350
400
450
RADIO REFRACTIVITY (N UNITS)
ABSOLUTE SCALE

FIGURE 43

B6902

SCALE 1:5,702,400 OR 90 MILES TO 1 INCH

100 50 0 100 200 300

STATUTE MILES

100 50 0 100 200 300 400

KILOMETERS

FLIGHT PATH VIII

MISSION 12 — 23 MARCH 1969

MISSION 13 — 24 MARCH 1969

MISSION 14 — 25 MARCH 1969

FIGURE 44

Spiral	Location	Spiral Start Time Z	Local
A	a. Key West	1132	0632
B	b. 24-35 N, 82-37 W	1212	0712
Climb 1	b-c	1236	0736
C	c. 24-35 N, 83-32 W	1257	0757
Climb 2	c-d	1321	0821
D	d. 24-35 N, 84-26 W	1348	0848
Climb 3	d-e	1406	0906
E	e. 24-35 N, 83-03 W	1430	0930
F	a. Key West	1511	1011

The surface map, Figure 45, shows that the low pressure system is intensifying and moving rapidly eastward. The cold wave is across the northern part of Florida and a trough extends eastward from the Carolinas. The flow of air is now from the south in the Key West area but the upper air flow would be tending eastward.

From Figure 46 along the plane d-e-b, all spirals tend to show that the inversion is destroyed. This has been produced largely due to the loss of subsidence of dry air which would normally create the temperature inversion and constrain the maritime layer. Although surface winds are from the south, the moisture carried into the air is raised as the flow continues northward. Photograph 13C, at 3 km on Spiral B (Figure 46), shows substantial moisture aloft and developing cumulus on the horizon.

Figure 47 shows Spirals E, A, and F, with A and F flown some hours apart at Key West. One may observe an indication of the inversion around 700 meters, but it is very weak. Temporal and spatial variations are not great and the radiosonde profile represents the conditions reasonably well below 1000 meters. The lapse rate of refractivity shown by the radiosonde is much greater than is shown by the aircraft data for heights from 800 to 2500 meters. A lack of data from the radiosonde in the interval between 800 and 1000 meters would account in part for the seemingly greater lapse rate. On Figure 47, Photographs 13A, B, and D show clouds with indications of stratus to light cumulus aloft. The cloud pictures clearly show that large quantities of moisture are aloft through 13 March as the low pressure system passes across the northern part of Florida.

11.3 Mission 14

Mission 14 was flown during the morning of 25 March. As shown on Figure 48, the flight plan was similar to Missions 12 and 13 with the exception

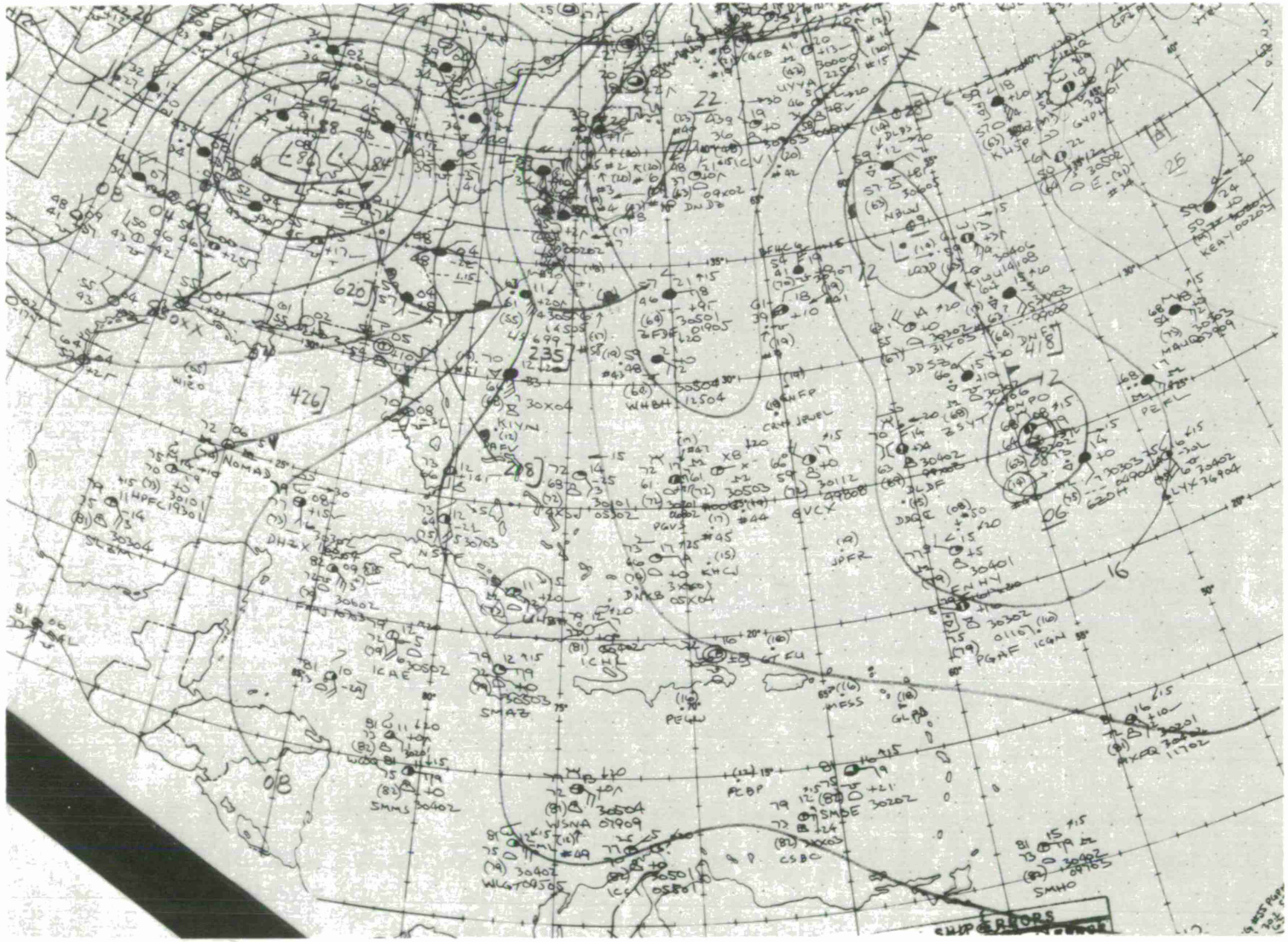

FIGURE 45

SURFACE CHART 24 March 1969

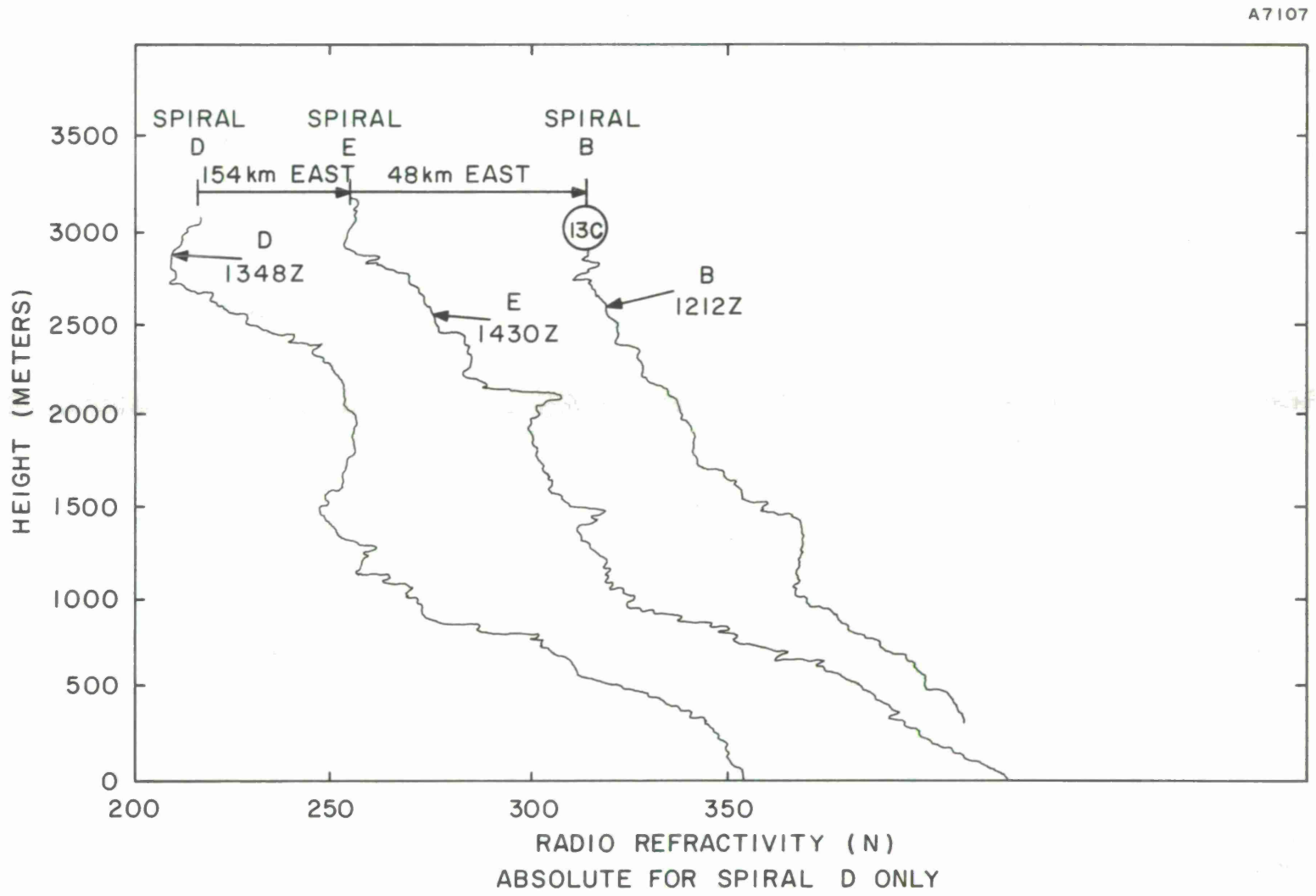
A7107
SPIRAL D
SPIRAL E
SPIRAL B
154 km EAST
48 km EAST
13C
D
1348Z
E
1430Z
B
1212Z
HEIGHT (METERS)
3500
3000
2500
2000
1500
1000
500
0
200
250
300
350
RADIO REFRACTIVITY (N)
ABSOLUTE FOR SPIRAL D ONLY

FIGURE 46.

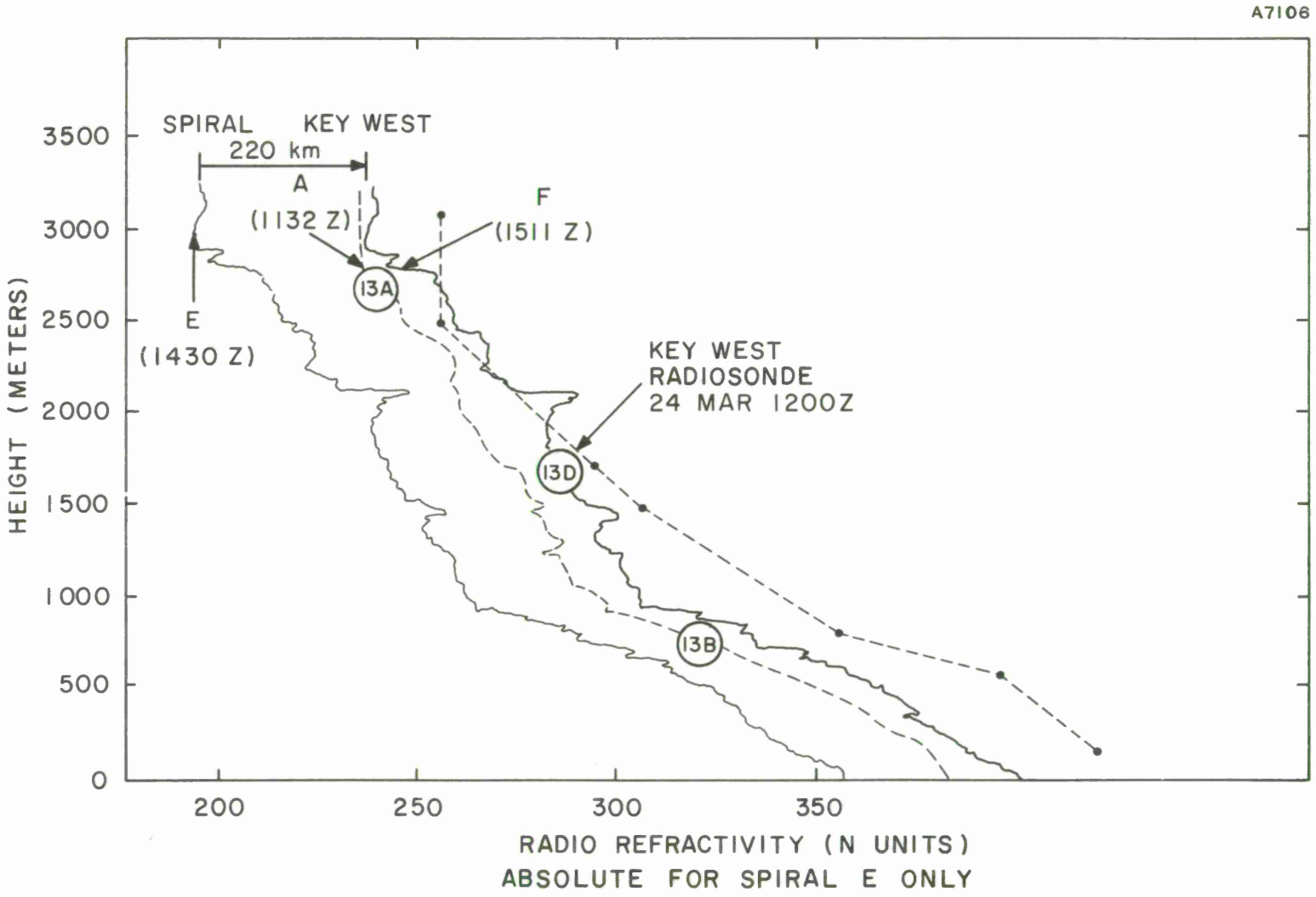
A7106
SPIRAL
KEY WEST
220 km
A
(1132 Z)
F
(1511 Z)
E
(1430 Z)
13A
13D
13B
KEY WEST
RADIOSONDE
24 MAR 1200Z
HEIGHT (METERS)
3500
3000
2500
2000
1500
1000
500
0
200
250
300
350
RADIO REFRACTIVITY (N UNITS)
ABSOLUTE FOR SPIRAL E ONLY

FIGURE 47.

SCALE 1:5,702,400 OR 90 MILES TO 1 INCH

100 50 0 100 200 300

STATUTE MILES

100 50 0 100 200 300 400

KILOMETERS

FLIGHT PATH VIII

MISSION 12 — 23 MARCH 1969

MISSION 13 — 24 MARCH 1969

MISSION 14 — 25 MARCH 1969

FIGURE 48

A7037

13A 24 March 1969-SPIRAL A

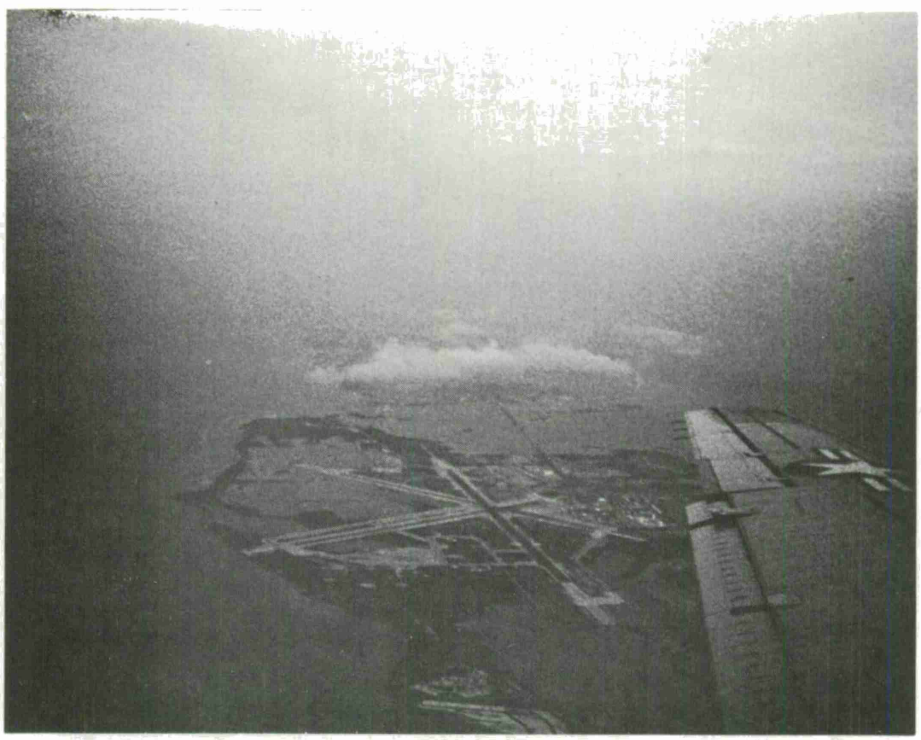

13B 24 March 1969-SPIRAL A-8.5K

A7038

13C 24 March 1969-SPIRAL B-10K

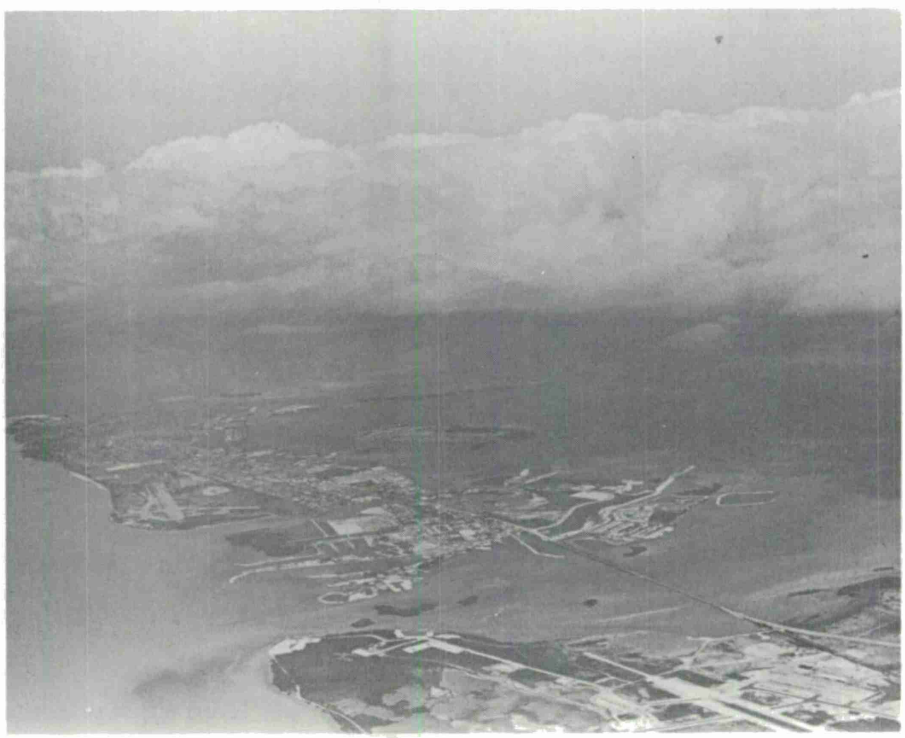

13D 24 March 1969-SPIRAL F

that Spiral G was deleted. This deletion permitted the aircraft to refuel and return to Boston within the allowable flight hours.

Spiral	Location	Spiral Start Time Z	Local
A	a. Key West	1154	0654
B	b. 24-35 N, 82-37 W	1238	0738
Climb 1	b-c	1257	0757
C	c. 24-35 N, 83-32 W	1320	0820
Climb 2	c-d	1343	0843
D	d. 24-35 N, 84-26 W	1403	0903
Climb 3	d-e	1421	0921
E	e. 24-35 N, 83-03 W	1444	0944
F	a. Key West	1527	1027

Figure 49 shows that the low pressure system is intense and extends over the eastern seaboard and the northeast. The associated cold air ridge is further advanced into Florida. Winds are now from northwest and west in the Key West area. To the east, the winds are from the south and southeast, partly influenced by a weak high pressure cell east of the Keys.

Figure 50 shows that the inland storm system has less effect on the area and one may detect a partial restoration of the layer in Spirals C and E. Further to the west, in Spiral D, the increased presence of cool air from the northwest prevents the formation of an inversion. Spiral C shows evidence of the layer forming but spatial variations are obviously still present over the area. Photograph 14B indicates a heavy cloud deck around 2500 meters which accounts for the bulge in the refractivity profile. This appears to be a local effect since the other spirals on Figure 50 have a more uniform lapse rate at this height.

Figure 51 shows that the inversion is more intense in the direction southward and away from the cold ridge. Comparing Spiral F with A and the radiosonde profile one may see the effect of thermal convection. The radiosonde presents the layer in good agreement with simultaneous data recorded in Spiral A. In the overland launch area, the atmosphere was obviously much less moist than over the sea where the aircraft measurements were made.

Photograph 14A, taken in Spiral A at 3000 meters, shows the cloud deck lying below and along the inversion. This cloud structure is characteristic of an intense inversion where stratus clouds are thick and extensive. Because of convection, some clouds puff through the layer.

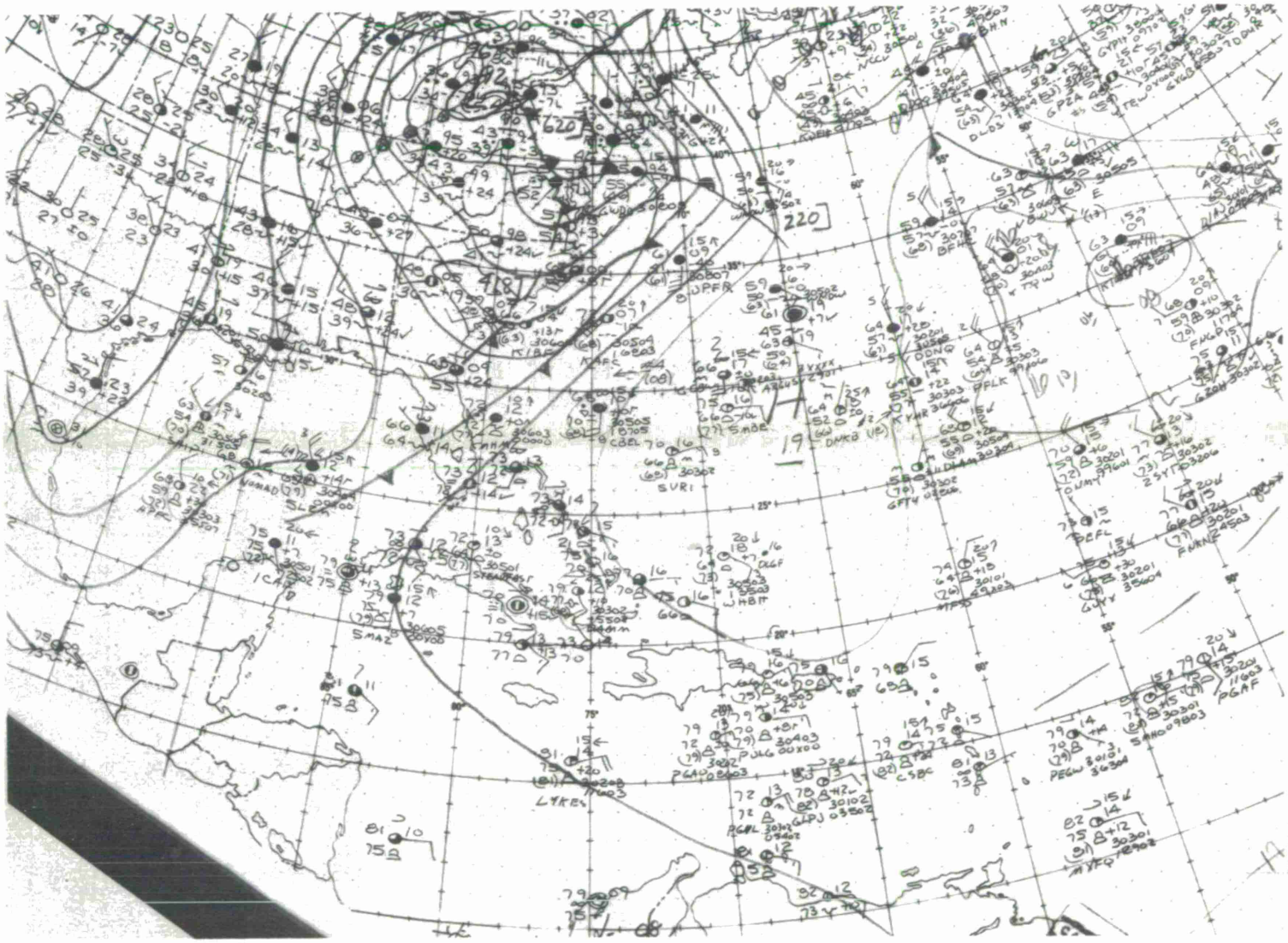

FIGURE 49

SURFACE CHART 25 March 1969

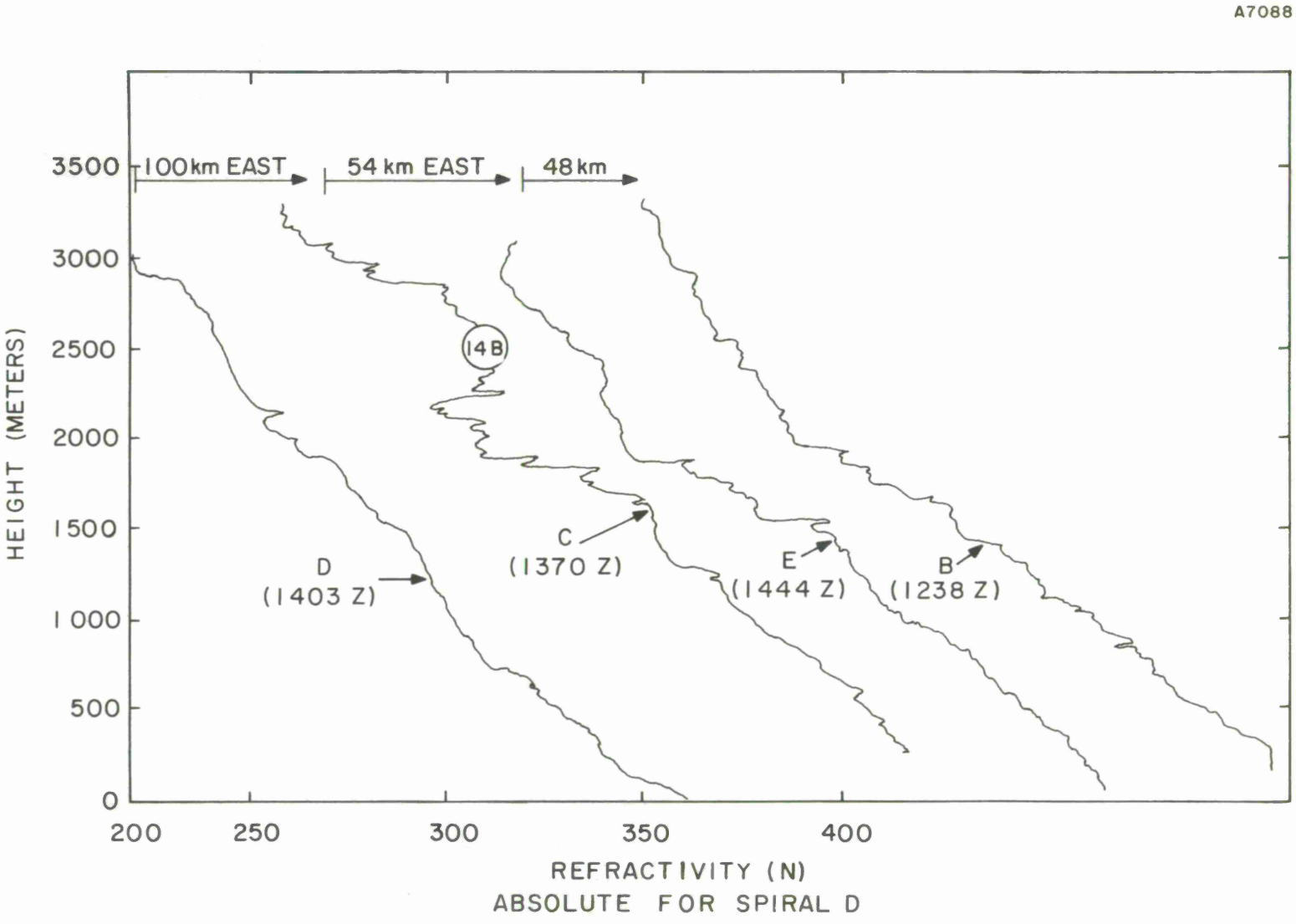
A7088
100km EAST
54 km EAST
48km
3500
3000
2500
2000
1500
1000
500
0
HEIGHT (METERS)
14B
C
(1370 Z)
D
(1403 Z)
E
(1444 Z)
B
(1238 Z)
200
250
300
350
400
REFRACTIVITY (N)
ABSOLUTE FOR SPIRAL D

FIGURE 50.

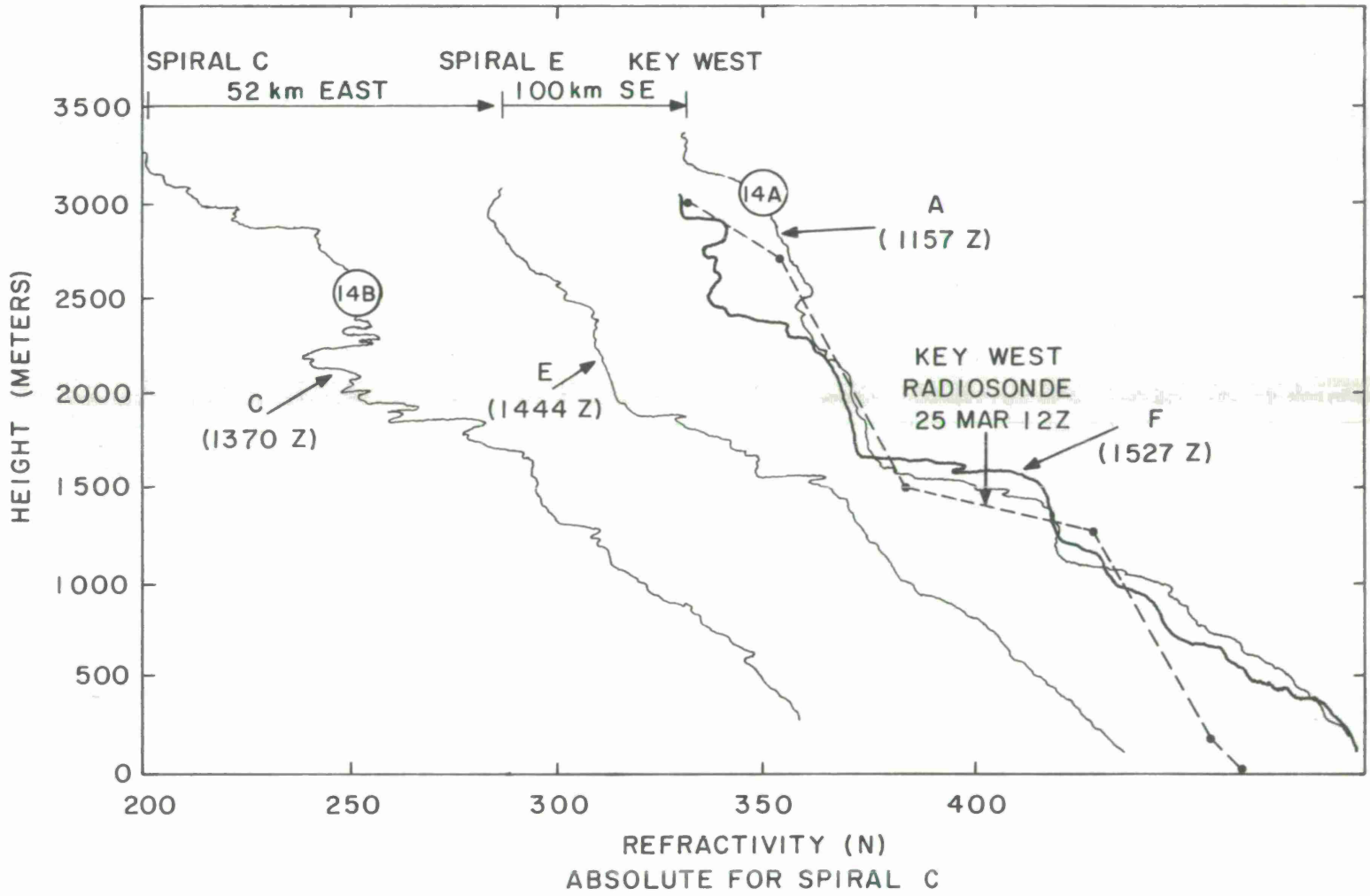
SPIRAL C
52 km EAST
SPIRAL E
100 km SE
KEY WEST
14A
A
(1157 Z)
14B
C
(1370 Z)
E
(1444 Z)
KEY WEST
RADIOSONDE
25 MAR 12Z
F
(1527 Z)
HEIGHT (METERS)
3500
3000
2500
2000
1500
1000
500
0
200
250
300
350
400
REFRACTIVITY (N)
ABSOLUTE FOR SPIRAL C

FIGURE 51.

A7039

14A 25 March 1969-SPIRAL A

14B 25 March 1969-SPIRAL C

It is rather surprising how rapidly the characteristics of the profiles change in moving southward and away from the cold ridge. As was mentioned before, these results further indicate how conditions are delicately balanced to produce the inversion and the Trade Wind Duct.

SECTION XII

THE CHARACTERISTICS OF ELEVATED LAYERS MEASURED DURING THE TEST PERIOD

During the period from 6 March through 25 March, a total of 105 separate soundings were made of the vertical variation of refractivity. This total includes both spirals and the climbs made between spirals. The total number of appearances of elevated layers was approximately 97. These 97 layers were selected on the basis that the M profile showed a negative gradient, dM/dh, and this gradient persisted over at least 50 meters in height.

Figure 52 shows the parameters used to define the layer including its height, thickness, and the magnitudes of the gradients on its lower and upper sides. From the layer characteristics one may calculate a maximum radio wavelength which could propagate in the layer. The layer model and procedure is based on the analysis by Skillman [July 1969], where for E mode propagation,

$$\lambda^{E}_{max} = \lambda^{S}_{max} \cdot F_E \tag{6}$$

and λ^{S}_{max} is the maximum wavelength for propagation in a surface duct, where

$$\lambda^{S}_{max} = 8/5\ K \cdot (S_L)^{\frac{1}{2}} \cdot d_T{}^{3/2} \tag{7}$$

where

$$K = \frac{2\ (0.2)^{\frac{1}{2}}}{3} \times 10^{-4} \tag{8}$$

and

$$F_E = 1.5\ (1 + \frac{|Su|}{S_L}) \tag{9}$$

and Su and S_L is the gradient of the upper and lower boundaries (Figure 52) and d_T is the thickness of the duct. Also, as shown, S_L is the gradient of the surface duct.

The following table summarizes the characteristics of the 97 layers which were selected from all the profiles. The maximum propagation wavelength is also calculated for each layer.

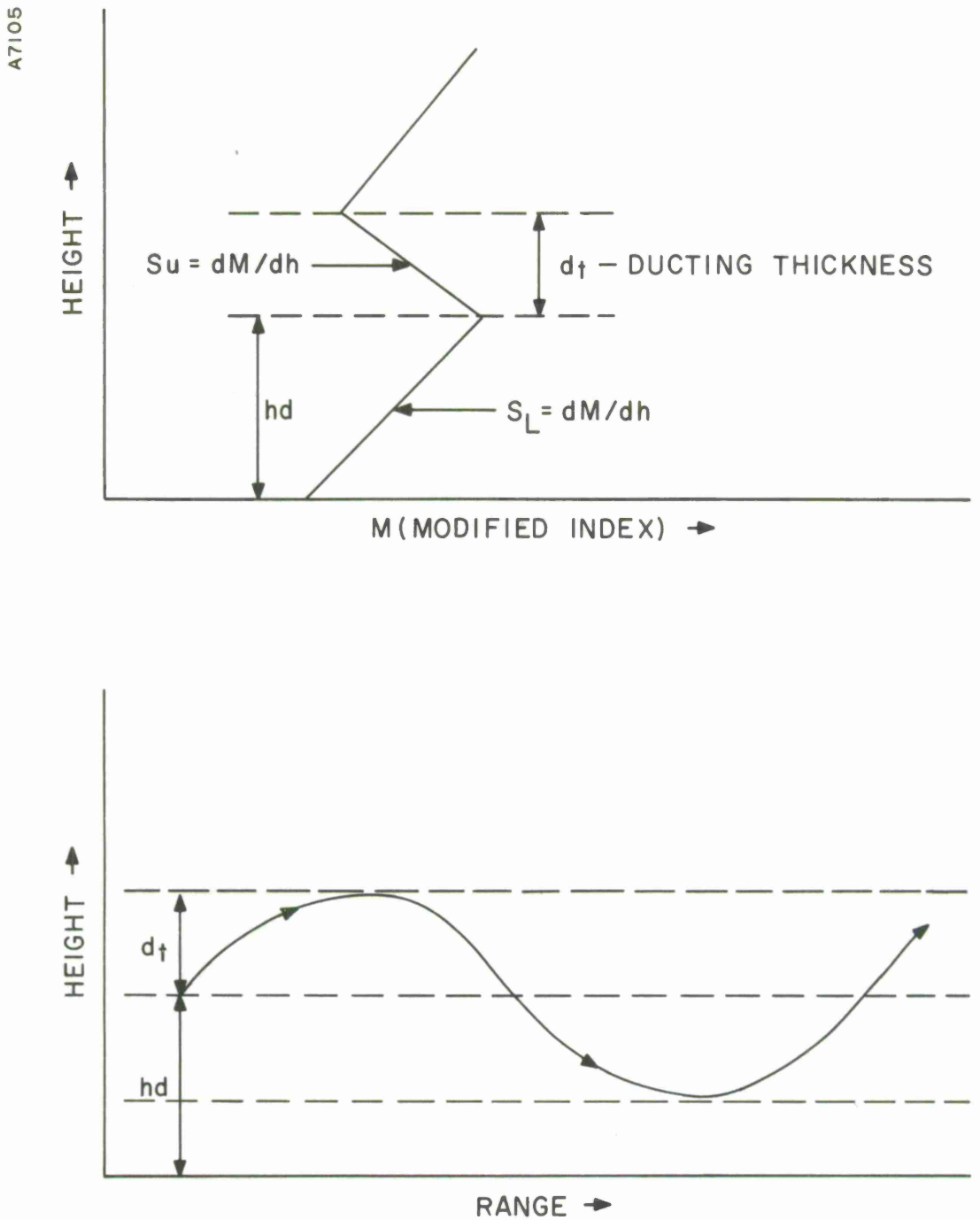
A7105
HEIGHT
Su = dM/dh
d_t – DUCTING THICKNESS
hd
S_L = dM/dh
M(MODIFIED INDEX)
HEIGHT
d_t
hd
RANGE

FIGURE 52.

TABLE I

SUMMARY OF ELEVATED DUCT CHARACTERISTICS

Mission (Spiral/Climb)	Height - h_d (Meters)	Thickness - d_t (Meters)	S_L (M/km)	S_u (M/km)	λ^E_{max} (Meters)
Mission 1					
Spiral A	2450	50.	67.	182.	3.85
Spiral B	2380	50.	70.	210.	4.23
Climb 1	2250	150.	70.	8.	6.13
Spiral C	1050	50.	66.	230.	4.61
Spiral C	2000	50.	70.	156.	3.42
Mission 2					
Spiral A	1000	50.	65.	450.	8.08
Climb 1	900	100.	52.	64.	5.76
Climb 1	2200	75.	64.	140.	5.93
Spiral B	1000	150.	70.	10.	6.28
Climb 2	1000	40.	70.	296.	3.96
Spiral C	950	150.	50.	80.	12.08
Climb 3	1000	150.	55.	20.	6.65
Climb 3	2400	100.	200.	53.	6.40
Spiral D	1000	110.	60.	62.	6.50
Spiral E	1000	50.	20.	300.	9.05
Mission 3					
Climb 1	900	260.	46.	42.	19.46
Spiral C	700	210.	65.	63.	17.29
Climb 2	650	100.	71.	260.	14.05
Spiral D	640	120.	83.	100.	9.45
Climb 3	700	80.	60.	156.	7.14
Mission 4					
Spiral A	600	150.	70.	35.	8.25
Climb 1	850	50.	64.	132.	3.10
Spiral B	1650	90.	50.	50.	4.32
Climb 2	1550	90.	55.	112.	6.88
Spiral C	1310	180.	63.	50.	12.30
Climb 3	1300	90.	63.	138.	7.74

TABLE I (Cont'd.)

Mission (Spiral/Climb)	Height - h_d (Meters)	Thickness - d_t (Meters)	S_L (M/km)	S_u (M/km)	λ^E_{max} (Meters)
Mission 5					
Spiral B	2450	150.	96.	32.	8.59
Spiral C	2250	50.	64.	120.	2.91
Climb 3	2100	80.	64.	77.	4.51
Spiral D	1100	150.	71.	34.	8.19
Mission 6					
Spiral B	1900	300.	59.	12.	17.18
Spiral C	1600	40.	60.	255.	3.68
Climb 2	600	30.	60.	280.	2.58
Spiral D	500	10.	52.	500.	.87
Spiral D	1550	50.	76.	55.	1.90
Spiral D	1900	20.	72.	500.	2.16
Spiral E	270	50.	64.	210.	4.33
Spiral E	1800	270.	61.	24.	17.27
Climb 4	310	10.	110.	500.	.66
Spiral F	2130	120.	81.	20.	5.28
Mission 7					
Spiral A	2400	200.	53.	44.	13.48
Spiral B	2550	20.	47.	392.	2.05
Spiral C	1450	100.	66.	170.	10.39
Spiral C	2100	210.	76.	26.	12.74
Climb 2	1000	80.	75.	143.	6.44
Climb 2	2140	30.	70.	300.	2.60
Climb 2	2300	100.	60.	80.	6.47
Spiral D	1150	25.	60.	162.	1.28
Spiral D	2500	25.	35.	500.	4.04
Climb 3	575	50.	75.	102.	2.59
Climb 3	1050	75.	75.	62.	3.68
Climb 3	2450	150.	62.	16.	6.51
Spiral E	700	150.	70.	22.	7.23
Spiral E	2000	100.	111.	20.	4.45
Spiral F	1280	380.	63.	12.	25.04

TABLE I (Cont'd.)

Mission (Spiral/Climb)	Height - h_d (Meters)	Thickness - d_t (Meters)	S_L (M/km)	S_u (M/km)	λ^E_{max} (Meters)
Mission 8					
Spiral A	1630	180.	58.	102.	18.15
Spiral B	1570	110.	60.	246.	16.31
Climb 1	1460	150.	40.	38.	8.11
Spiral C	480	50.	58.	131.	3.14
Spiral C	1100	170.	54.	55.	11.76
Climb 2	480	40.	36.	169.	3.09
Climb 2	1080	130.	55.	96.	10.80
Spiral D	1000	140.	65.	47.	8.23
Climb 3	900	130.	81.	78.	9.37
Mission 9					
Spiral A	1260	10.	54.	500.	.85
Spiral A	1450	90.	74.	26.	3.55
Spiral B	1600	190.	65.	40.	12.20
Climb 1	1550	140.	65.	46.	8.16
Spiral C	1550	100.	57.	74.	6.21
Mission 10					
Spiral A	1400	100.	54.	68.	5.94
Spiral A	1620	130.	75.	44.	7.29
Climb 1	1550	320	52.	8.	17.04
Spiral B	1680	160.	55.	44.	9.67
Climb 2	1550	250.	74.	21.	15.62
Spiral C	1500	100.	50.	70.	6.07
Mission 11					
Spiral A	1350	150.	70.	35.	8.25
Climb 1	1400	300.	48.	11.	15.83
Spiral B	1740	130.	64.	192.	16.97
Spiral C	850	260.	65.	12.	14.33
Spiral C	1400	150.	71.	50.	9.44

TABLE I (Cont'd.)

Mission (Spiral/Climb)	Height - h_d (Meters)	Thickness - d_t (Meters	S_L (M/km)	S_u (M/km)	λ^E_{max} (Meters)
Mission 12					
Spiral A	1550	150.	102.	90.	12.50
Spiral B	1700	110.	46.	192.	14.48
Climb 1	1580	140.	53.	127.	14.65
Spiral C	1600	50.	39.	265.	6.16
Climb 2	1360	140.	69.	151.	15.70
Spiral D	1140	100.	50.	112.	8.20
Spiral D	2400	110.	75.	123.	9.44
Climb 3	1230	120.	57.	80.	8.53
Spiral E	1300	80.	35.	216.	10.86
Climb 4	700	50.	56.	115.	2.89
Climb 4	1440	160.	56.	177.	22.54
Climb 5	620	70.	85.	112.	4.48
Climb 5	1350	110.	71.	116.	9.16
Spiral G	1280	150.	55.	122.	15.69
Spiral D	750	110.	57.	75.	7.22
Mission 13					
Spiral A	1380	240.	58.	28.	15.02
Climb 4	1500	210.	59.	23.	11.62
Mission 14					
Spiral F	1600	60.	70.	340.	8.15

Figure 53 shows the distribution of ducting gradient values (dM/dh) versus the thickness of each respective duct. For the usual layer, the air below the inversion can at most be saturated with moisture and the air above very dry. Therefore, the vapor pressure reduction , de/dh, through any layer is limited. Then it is reasonable to expect that the M gradient which is almost directly proportional to the vapor pressure gradients will vary inversely with the layer thickness.

From the above figure, an approximate relationship is

$$dM/dh = 12.5/dt \qquad (10)$$

and

dt = the ducting gradient thickness (km)

For these same data, Figure 54 shows the gradient distribution in terms of its probable maximum values.

From Figure 55 it is apparent that there is some apparent correlation between the intensity of the gradients and their heights. On this scatter diagram, there is a tendency for most of the measured gradients to lie within the height interval between 1000 to 1600 meters.

The ducting layer heights are shown in Figure 56 in terms of expected maximum height. The indication is that it is better than 50 percent probable that the layers will lie above 1400 meters. However, very few layers were above 2000 meters.

Dougherty (1967) shows in February that the mean base height of the inversion is about 2500 meters in the approaches to the Caribbean from the east. Our measurements (Rowlandson, et al, 1969, 1970) show the inversion and most other layers to be at a lower level in March. However, climatological conditions change sufficiently from month to month and year to year that it is not unexpected that there would be some differences.

Figure 57 shows the scatter of duct thicknesses versus their respective heights. There appears to be a concentration of thicknesses around 125 meters between 1000 and 1600 meters. Dougherty (1967) gives a mean layer thickness of about 210 meters in the eastern end of the Caribbean. Even attempting to correct for the lag constants in the radiosonde data, Dougherty's results are larger than the measurements made by the microwave refractometer. Of course, Dougherty's results are related to the properties of the inversion, whereas we included the combined effect of all measured layers.

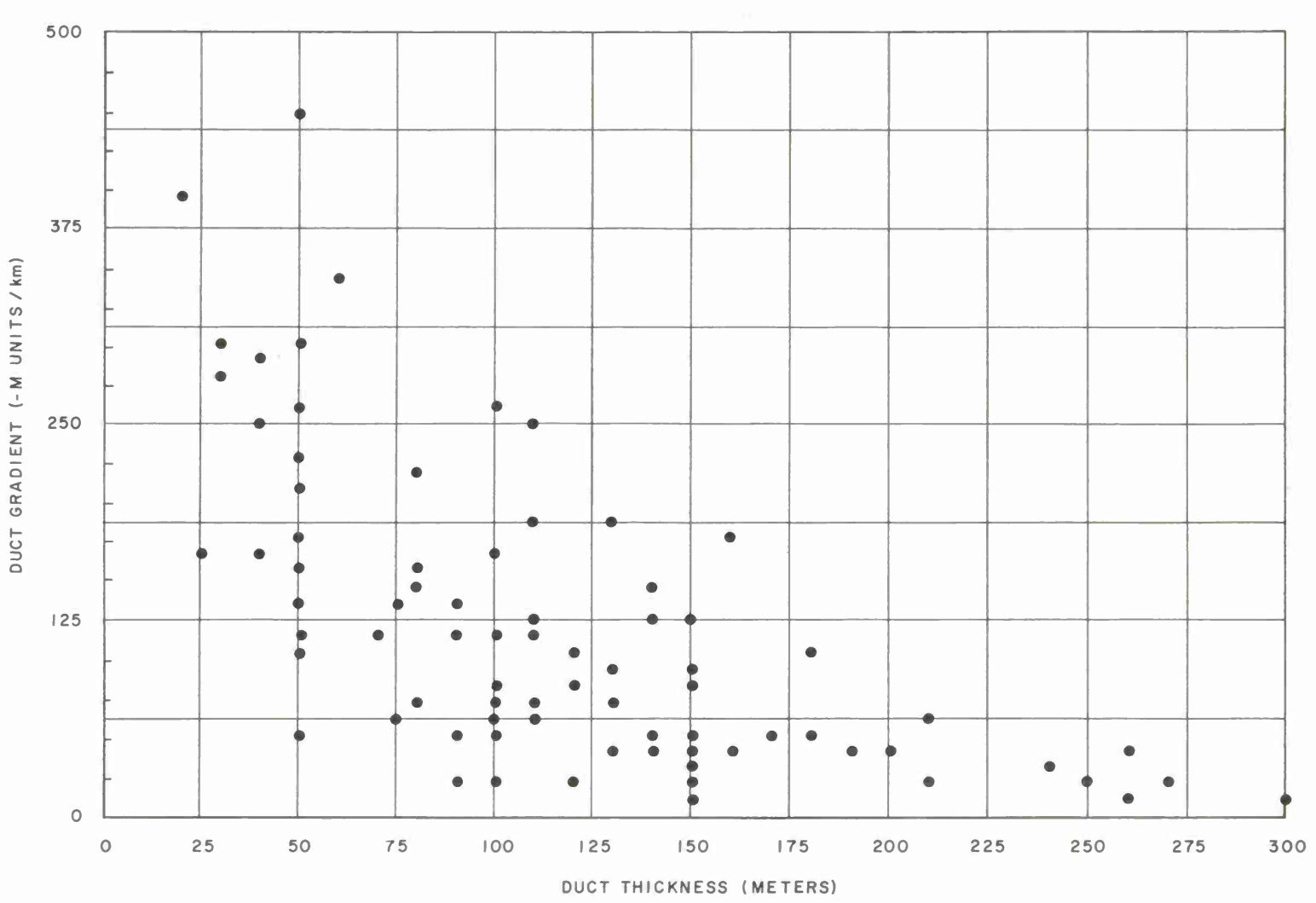
87018
500
375
250
125
0
DUCT GRADIENT (-M UNITS / km)
0
25
50
75
100
125
150
175
200
225
250
275
300
DUCT THICKNESS (METERS)

FIGURE 53.

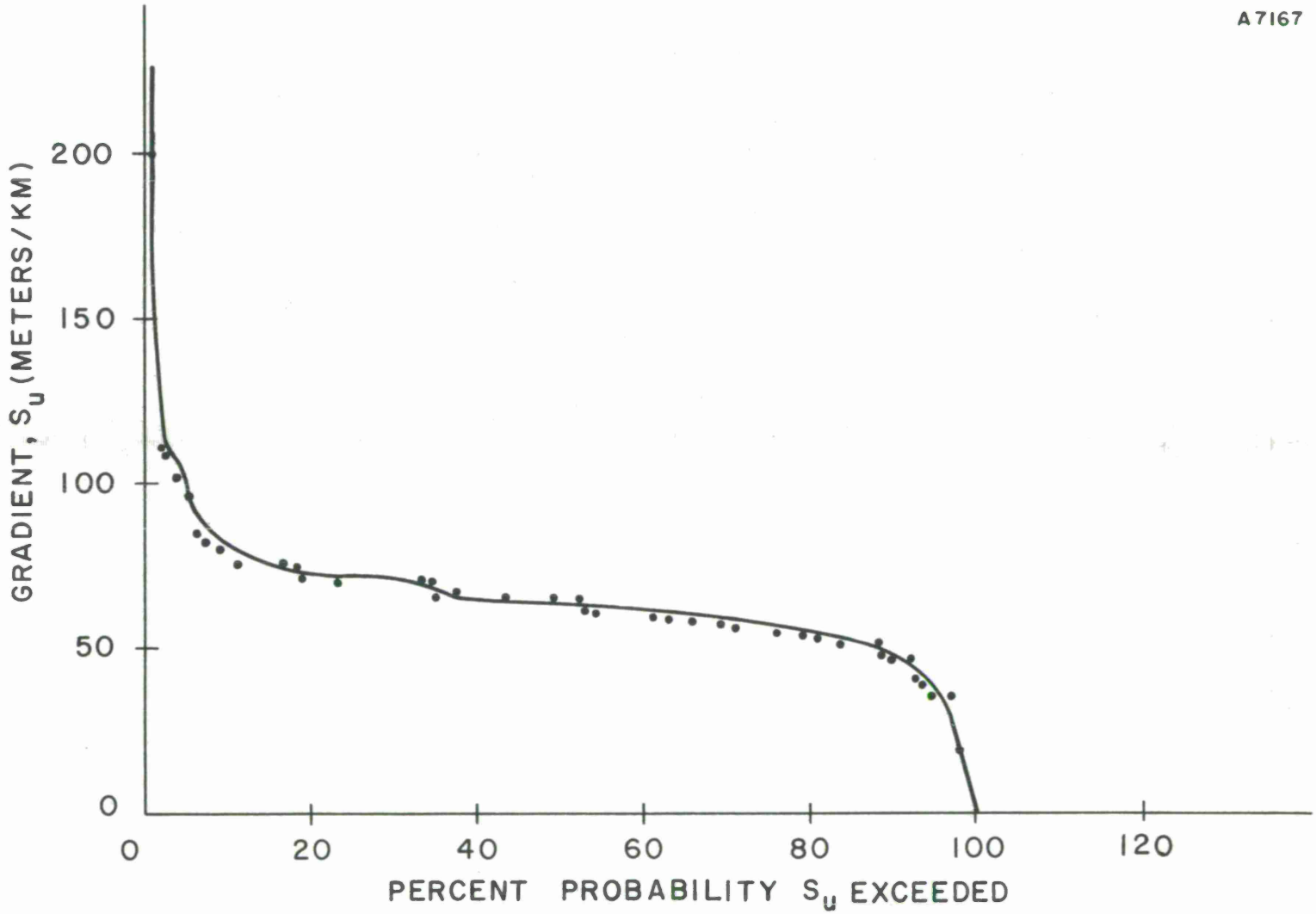
A7167
GRADIENT, S_u (METERS/KM)
200
150
100
50
0
0
20
40
60
80
100
120
PERCENT PROBABILITY S_u EXCEEDED

FIGURE 54.

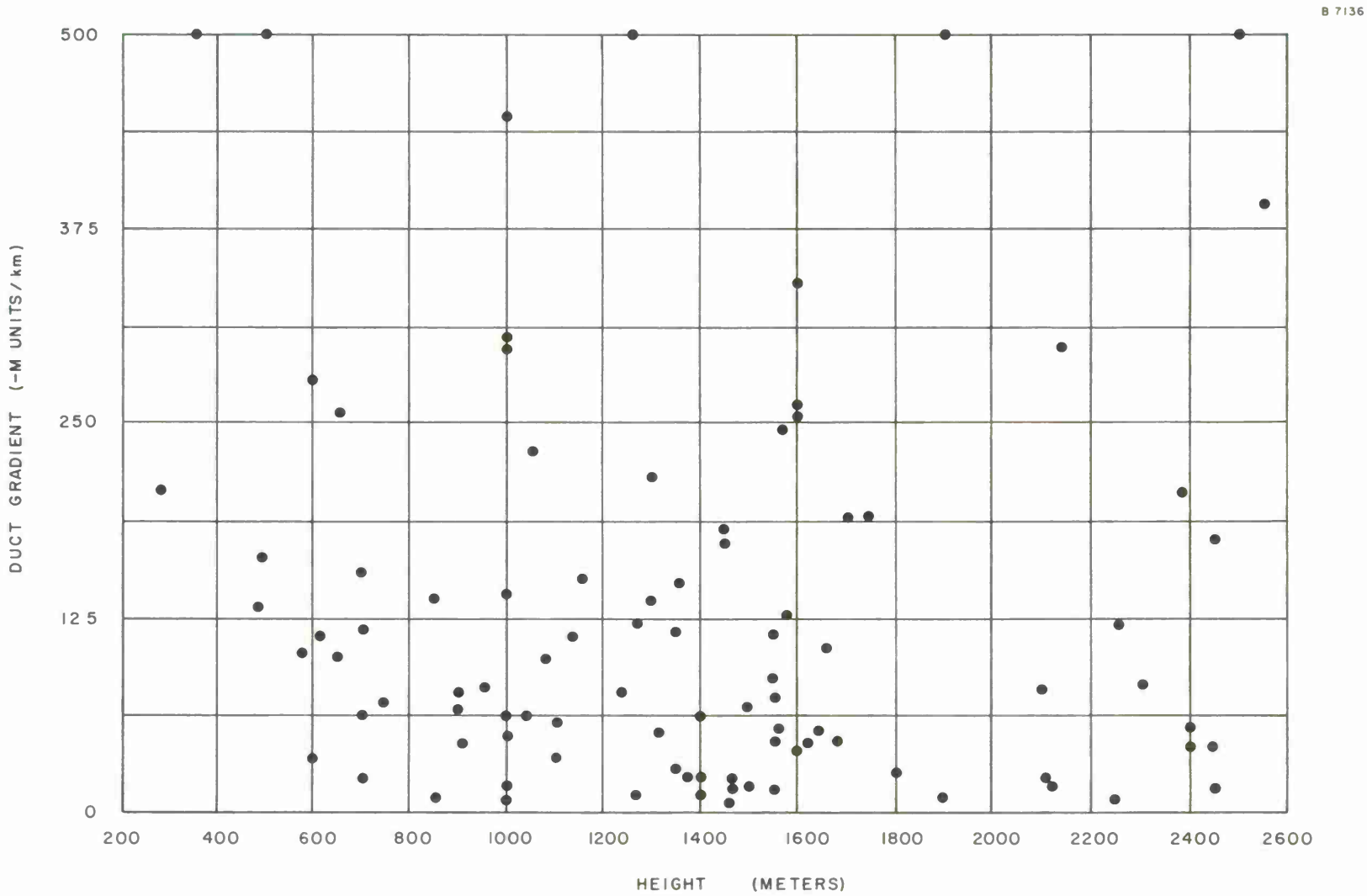
B 7136
500
375
250
125
0
DUCT GRADIENT (-M UNITS/km)
200
400
600
800
1000
1200
1400
1600
1800
2000
2200
2400
2600
HEIGHT (METERS)

FIGURE 55.

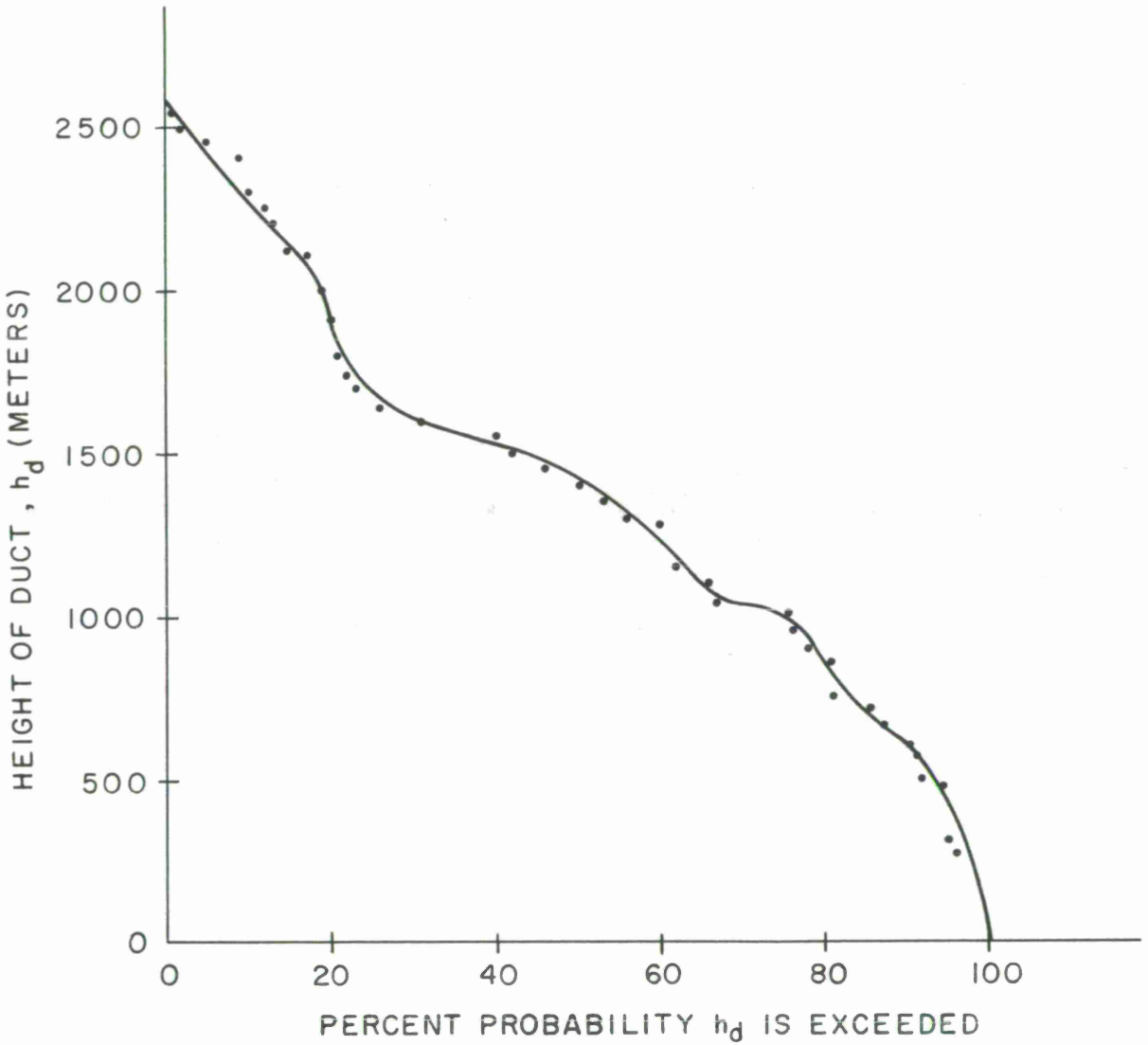
A7169
2500
2000
1500
1000
500
0
HEIGHT OF DUCT, h_d (METERS)
0
20
40
60
80
100
PERCENT PROBABILITY h_d IS EXCEEDED

FIGURE 56.

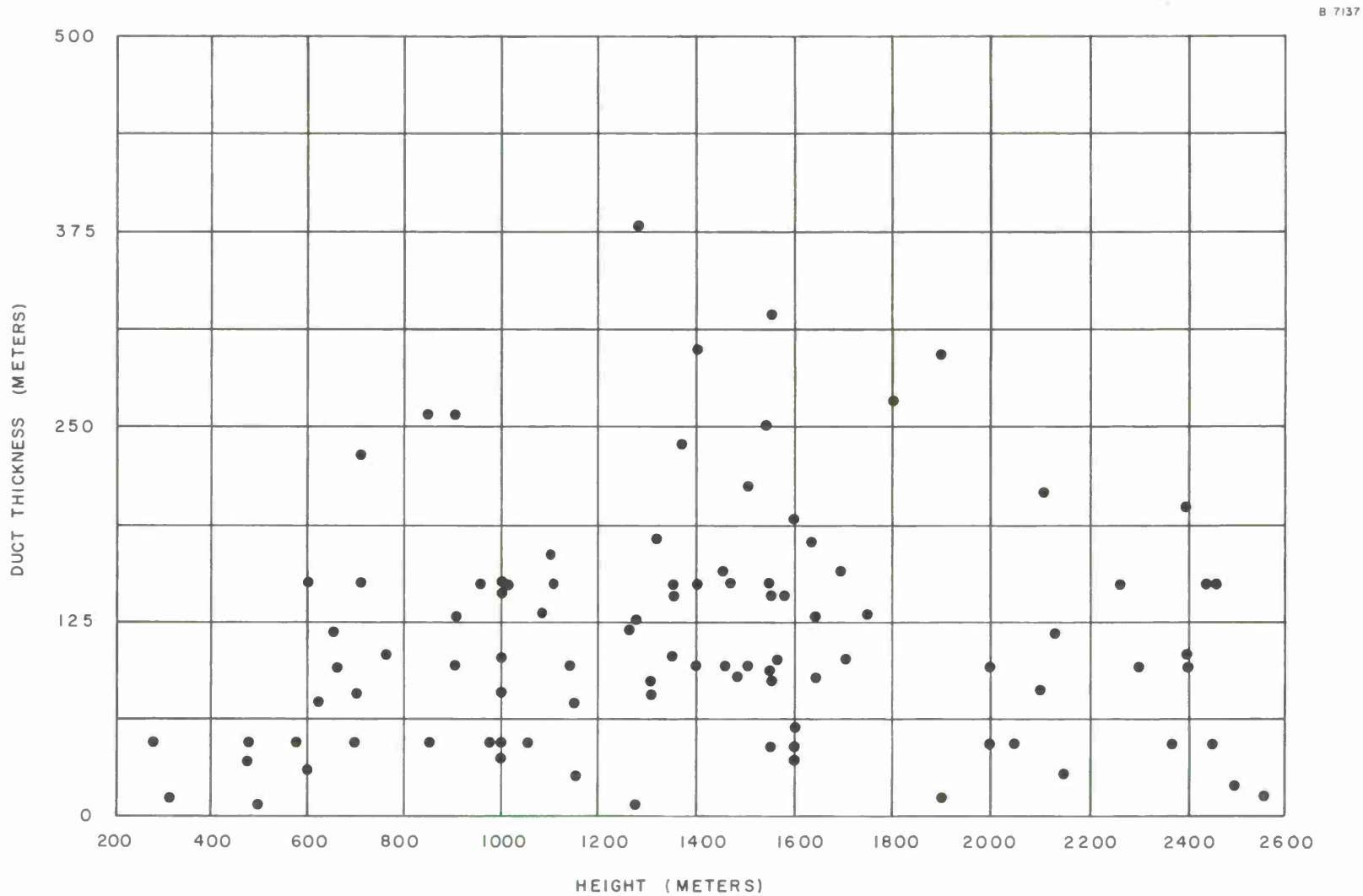
B 7137
500
375
250
125
0
DUCT THICKNESS (METERS)
200
400
600
800
1000
1200
1400
1600
1800
2000
2200
2400
2600
HEIGHT (METERS)

FIGURE 57.

Figure 58 shows the layers, in total, were hardly ever thicker than 300 meters and that only 50 percent of the cases exceeded about 100 meters.

For radio propagation, we are very interested in the critical wavelengths which can be propagated in these ducts. Figure 59 shows the probability that a given wavelength exceeds some critical value. For example, the results show that for 50 percent of the cases a wavelength of eight meters (or less) could be used for ducting propagation.

From CRPL ray-traced data (Bean and Thayer, 1050), the local elevation angle of a ray, launched at zero initial elevation angle, is around 14.6 mr at a height of one kilometer. This is for a surface refractivity value of 344.5 N units not unlike the surface conditions experienced in the Caribbean.

For a layer within which the gradient is constant, one may determine the magnitude of this gradient to produce ducting (Bean and Dutton, 1966, p. 82).

If θ_1 is the local elevation angle into the layer, then the exit angle, θ_2, is given approximately by

$$\theta_2 \approx \left[\theta_1^2 + \frac{2\ DH}{r_o} + \frac{2\ DN}{10^6}\right]^{\frac{1}{2}} \tag{11}$$

where angles are in radians and

DH = the thickness of the layer

DN = the change in refractivity, N, through the layer

r_o = the earth radius

Setting θ_2 equal to zero, for ducting to be produced, then

$$\frac{-dN}{dh} = \frac{\theta_1^2 \times 10^6}{2\ DH} + \frac{10^6}{r_o} \tag{12}$$

On the average, the elevated layer thickness is about 100 meters. For a local elevation angle of 14.6 mr, then from Equation (12) we can compute the gradient required to produce ducting, assuming the wavelength is small enough. This gives

$$\frac{-dN}{dh} = 73 + 157 \text{ N units/km} \tag{13}$$

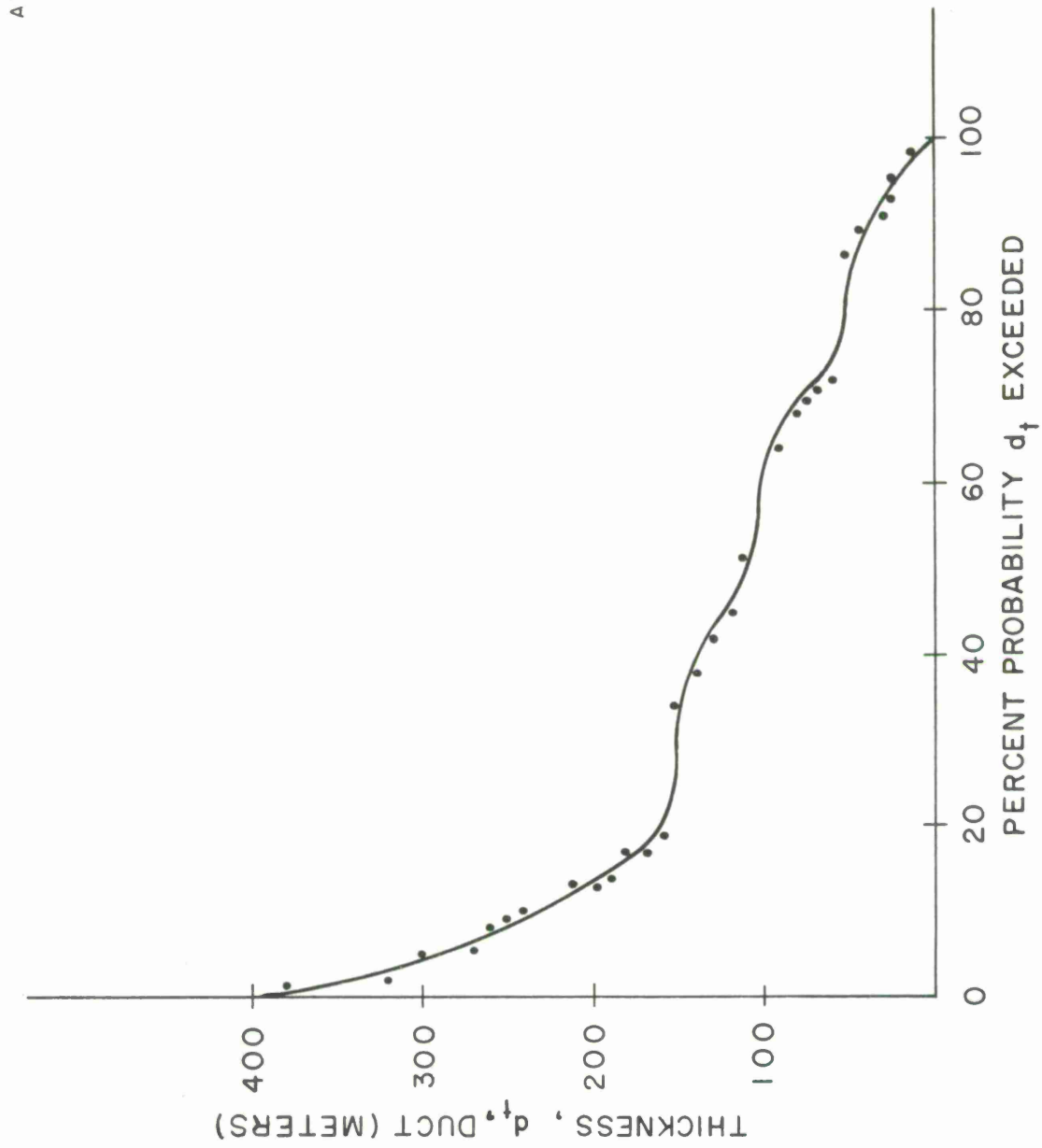
A7168
THICKNESS , d_t, DUCT (METERS)
400
300
200
100
0
20
40
60
80
100
PERCENT PROBABILITY d_t EXCEEDED

FIGURE 58.

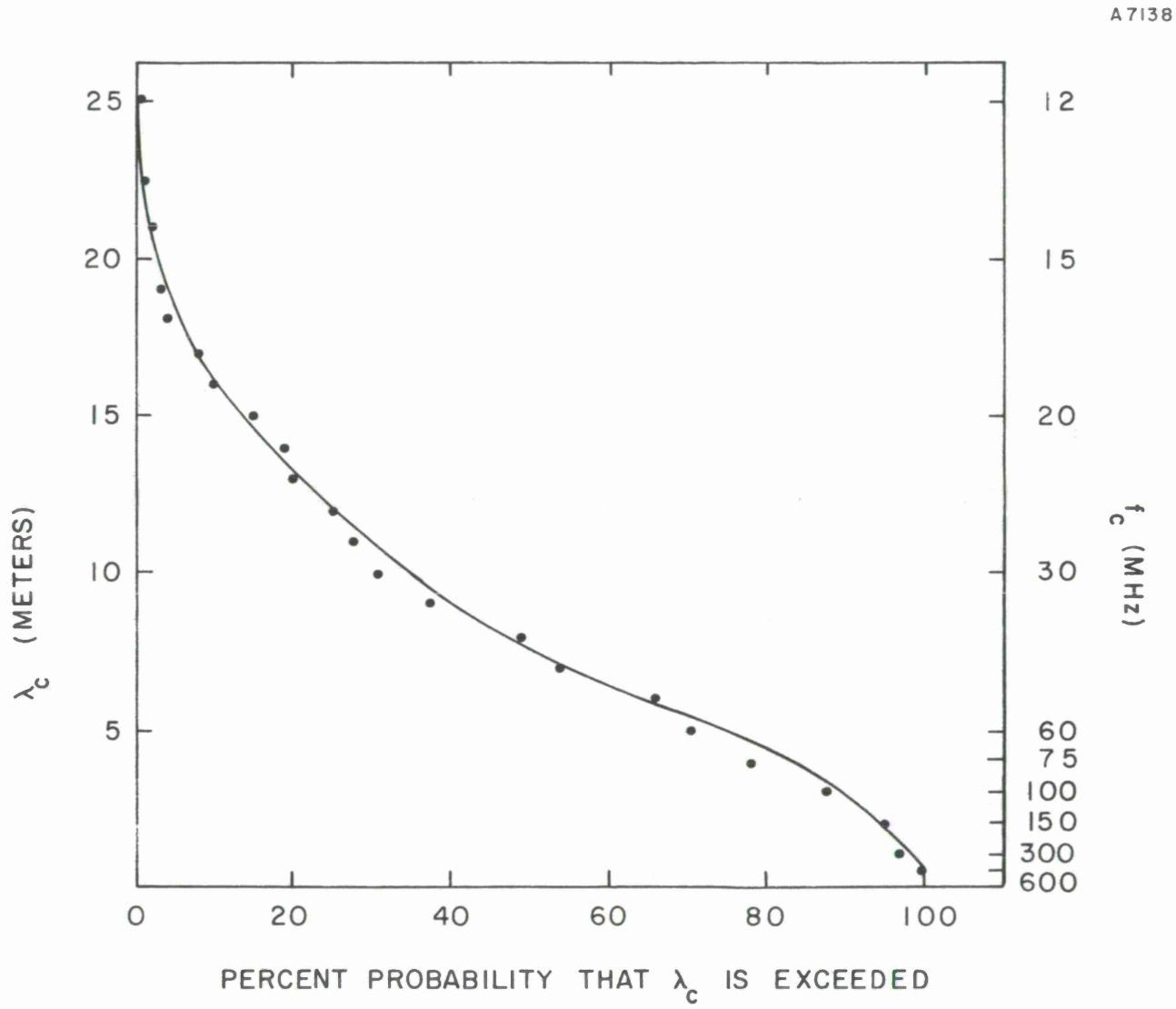
A7138
25
20
15
10
5
λ_c (METERS)
12
15
20
30
60
75
100
150
300
600
f_c (MHz)
0
20
40
60
80
100
PERCENT PROBABILITY THAT λ_c IS EXCEEDED

FIGURE 59.

The 157 value is commonly known as the magnitude of the gradient required to trap a signal entering the layer tangentially. That is, the ray continues to propagate with a radius of curvature essentially equal to that of the true earth. In the above calculation, an additional negative gradient of 73 N/km is required to turn the ray downward and direct it tangential to the layer.

From Figure 54, for a 100 meter layer thickness, it may be seen that half of the cases have gradients sufficiently large to produce ducting for a ray launched tangentially from the earth and providing from (6) the wavelength is sufficiently small. From (12) it is apparent that the gradient required to produce a tangential ray into the layer increases as the square of the initial local elevation angle when the ray enters the layer. Therefore, from the results shown on Figure 54, it is highly unlikely that any ray would be trapped other than an earth-tangent ray. The most consistent method for beyond-the-horizon propagation mode, for a ground-to-ground radio link, then appears to be by reflections of part of the radio signal from these elevated layers.

SECTION XIII

RADIOSONDE LAG CONSTANTS

The index of refractivity, N, obtained from radiosonde measurements is in error for two reasons. The absolute accuracy of measurements of air pressure, temperature, and relative humidity is limited. The International Radiosonde Comparison Tests [Cline, 1957], indicated the following probable absolute errors.

Air Temperature	$\pm 1.5^{\circ}$ C for night flights $\pm 3.5^{\circ}$ C for day flights
Air Pressure	Negligible error below 1 km ± 1.5 mb above 9 km ± 2.5 mb above 16 km
Relative Humidity	15% standard deviation about the mean for all flights

The U. S. Air Force and U. S. Army Signal Corps report different operation for American radiosondes, giving

Air Temperature	0.8° C standard deviation to 6 km 1.0° C standard deviation above 6 km
Air Pressure	2.2 mb standard deviation below 9 km 1.1 mb standard deviation above 9 km
Relative Humidity	5% standard deviation for the lithium chloride sensors under ideal conditions.

Ideal conditions are defined where the relative humidity is less than 95%, there is no direct wetting of the element, and the air temperature is above freezing.

Bean and Dutton (1966) show a three-dimensional presentation of the effect of these combined errors in the accuracy of radio refractivity, N. This diagram is reproduced in Figure 60 and is constructed for the above American radiosonde error data, below 6 km.

To a first approximation, the error in the vapor pressure can be found from

$$\Delta e \simeq [e_s (T)] \cdot \Delta RH \qquad (14)$$

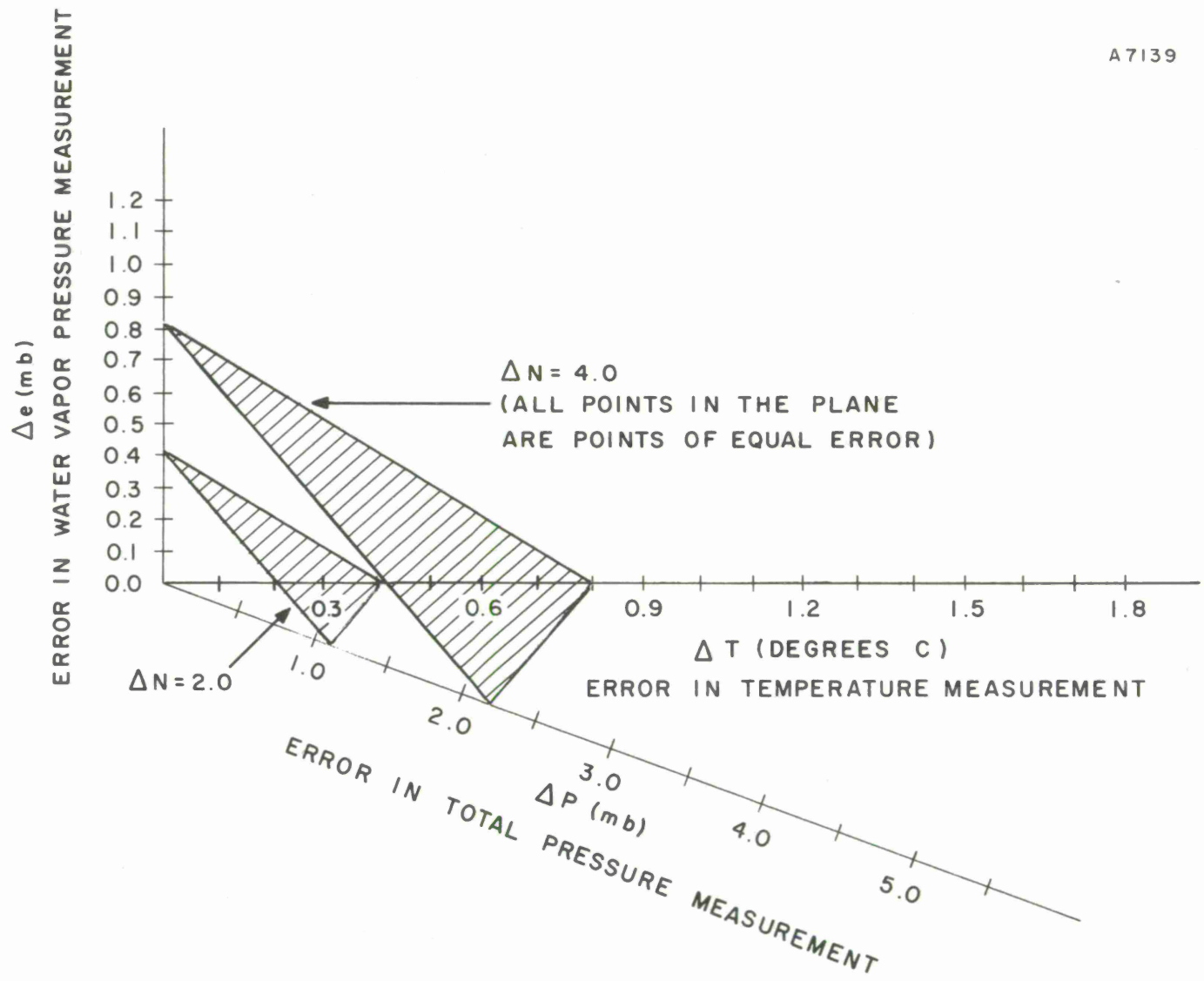
A7139
Δe (mb)
ERROR IN WATER VAPOR PRESSURE MEASUREMENT
1.2
1.1
1.0
0.9
0.8
0.7
0.6
0.5
0.4
0.3
0.2
0.1
0.0
ΔN = 4.0
(ALL POINTS IN THE PLANE
ARE POINTS OF EQUAL ERROR)
.03
0.6
0.9
1.2
1.5
1.8
Δ T (DEGREES C)
ERROR IN TEMPERATURE MEASUREMENT
ΔN = 2.0
1.0
2.0
3.0
Δ P (mb)
4.0
5.0
ERROR IN TOTAL PRESSURE MEASUREMENT

FIGURE 60.

where e_s (T) is the saturated vapor pressure for air at temperature, T, and one may write [Skillman, 1969],

$$e_s(T) \simeq 6.032 \exp(0.0689T) \tag{15}$$

where the air temperature, t, is in degrees Centigrade.

13.1 Absolute Errors

For the flights made during March in the Caribbean area, let the average height of the inversion be 2 km with an air temperature of 15 degrees Centigrade. Then, from (15) take the saturated vapor pressure, e_s (15) to be 16.3 mb. Smithsonian Tables give a value of 17 mb, which is close enough in agreement.

Then, for a 5% standard deviation, using American data for the lithium chloride element, the vapor pressure error, from (14) is

$$\Delta e \text{ (standard deviation)} \simeq 0.815 \text{ mb}$$

From the equation for N, one may write

$$dN = \frac{\partial N}{\partial T} \cdot dT + \frac{\partial N}{\partial e} \cdot de + \frac{\partial N}{\partial P} \cdot dP \tag{16}$$

The partials are replaced by constants which were derived from the ICAO, standard atmosphere and assuming a 60 percent relative humidity.

At one km, altitude (Bean and Dutton, 1966, Table 1.5, p 11)

$$a = \frac{\partial N}{\partial T} \simeq -1.09^{\circ} K^{-1} \tag{17}$$

$$b = \frac{\partial N}{\partial e} \simeq 4.72 \text{ mb}^{-1} \tag{18}$$

$$c = \frac{\partial N}{\partial P} \simeq 0.28 \text{ mb}^{-1} \tag{19}$$

Then, for the rms is

$$\Delta N = [(a \cdot \Delta T)^2 + (b\Delta e)^2 + (c \cdot\cdot \Delta p)^2]^{\frac{1}{2}}. \tag{20}$$

For American radiosonde take

$\Delta T = 0.8^{\circ}$ K

$\Delta e = 0.815$ mb

$\Delta P = 2.2$ mb

then from (20)

$\Delta N \simeq 4$ N units, rms

assuming no errors in the equation for N, itself.

The reader is advised to refer to Bean and Dutton's book (1966) for a comprehensive discussion of these absolute errors for a wide range of conditions.

13.2 Relative Errors

Barring erratic operation of the radiosonde elements and their associated electronic circuitry, it is unreasonable to assume that the rms error will be both positive and negative with equal probability. In any one launch the sensor would likely be biased in one direction over a given height interval. The immediate conditions of the environment could produce such a bias, such as occurs when the lithium chloride element becomes wetted.

For radio propagation studies, the N gradient is of primary importance. Therefore, if the radiosonde elements are biased during the height interval of a layer the measurement of the N gradient would not be seriously affected. The humidity measurement error, from (18) clearly contributes most to the error in N. It is also unfortunate that humidity sensors respond slowly to their environment in comparison with temperature and pressure measuring devices. The lag constant of humidity elements and their compensation in data reduction has been extensively investigated [Middleton and Spilhaus, 1953].

If it is assumed that the lag constant is not a function of the environment, but is some constant, for example, three or five seconds, then it is shown that

$$\frac{d\theta_i}{dt} = \frac{1}{\lambda} (\theta_i - \theta_e) \qquad (21)$$

where

θ_i = the indicated value of a parameter

θ_e = the true free air value

λ = the lag constant.

This equation may be recognized from another field as Newton's law of cooling, where the rate of change, $d\theta_i/dt$, of the temperature of a body is proportional to the difference between the environmental temperature, θ_e, and the instantaneous body temperature, θ_i.

From Bean and Dutton, 1966,

$$\frac{d\theta_i}{dt} = \frac{d\theta_i}{dh} \cdot \frac{dh}{dt} \tag{22}$$

$$= \frac{d\theta_i}{dh} \cdot R \tag{23}$$

where R is the supposedly uniform ascent rate of the radiosonde. Then, from (21), combining and rearranging,

$$\theta_e = \theta_i + R\lambda \cdot \frac{d\theta_i}{dh} \tag{24}$$

The radiosonde reports from point-to-point and within any height interval, dh, we can assume that, $d\theta_i/dh$, is constant. For computational purposes write

$$\theta_{e,k+1} = \theta_{i,k+1} + R\lambda \frac{\theta_{i,k+1} - \theta_{i,k}}{h_{k+1} - h_k} \tag{25}$$

where

$\theta_{e,k+1}$ = the true free air variable at height, k+1

$\theta_{i,k+1}$ = the indicated value at height, k+1

$\theta_{i,k+1} - \theta_{i,k}$ = the change in the indicated value over the height interval, $h_{k+1} - h_k$.

Starting at the launch height, if λ and R are known it should then be possible to adjust the radiosonde data within each height section defined by radiosonde reports.

Wexler, (1949), shows that the lag constant of the humidity sensor is not really constant, but is a function of the environment. Bunker, (1953), reports similar effects.

It is apparent that the correction of radiosonde data through the use of (25) can be thwarted by the dynamic behavior of the lag constant, λ, changes in the ascent rate, R, of the radiosonde and uncertainty in the measurement of indicated data. As noted by Bean and Dutton (1966), "...it is not clear that any correction for sensor lag may be made above the initial layer since, for subsequent layers, the initial indicated and environmental values are not identical and, further, lag constants have not been determined for this case."

However, Dougherty, et al, (1967), reported a correction method which includes the variation of the lag constant for the humidity sensor, λ_{RH}, based on Wexler's studies. The reader is advised to review this approach since it represents a workable method which was used to obtain corrected inversion characteristics in the Trade Wind System. For convenience, the particular method used by Dougherty, et al, is presented in Appendix A.

13.3 Summary

An examination of radiosonde and airborne refractometer profiles presented earlier, clearly shows how difficult it is to obtain a standard against which to compare corrected radiosonde data. The aircraft covers a large horizontal area as it spirals in its ascent. Therefore, horizontal variations in refractivity, which are seen to be many N units, do not permit the refractometer, in this case, to be used as a standard. The large differences between radiosonde and aircraft measurements near the launch altitude may be attributed to these horizontal variations or to not bringing the radiosonde sensors into equilibrium with the local environment prior to launch.

The greatest errors should occur when the relative humidity is high. In this case, the probable occurrence of clouds or haze would restrict the ability of the aircraft pilot to observe the position of the radiosonde as it ascends.

It is virtually impossible to simulate in an environmental chamber the rapidly varying conditions that the radiosonde elements meet in flight.

The approach taken by Dougherty, et al, to correct the data based on the best available behavior of the elements under laboratory conditions would appear to be meaningful. However, there was not, for practical reasons cited above, any attempt to demonstrate that these corrected values agreed with the actual environmental conditions.

It seems reasonable that a comparison can be made by passing ducted air through the refractometer cavity, then into the radiosonde sensors. This package could be carried by an aircraft and the effect of aircraft speed on the radiosonde sensors made part of the calibration study.

SECTION XIV

METEOROLOGICAL ANALYSIS AND RELATED INVERSION CHARACTERISTICS ALONG TWO PLANES IN THE CARIBBEAN

The temperature-moisture characteristics in the lower four kilometers of the atmosphere are related to the sun's heating effects, the land-water geography, and the large and small scale wind flow patterns.

Specifically, the sun's rays are absorbed into a deep layer of water and give slow daily temperature changes, while land masses are heated in a shallow layer with larger diurnal changes. Heat exchange over water in tropical areas is steady and slow except in tropical storms, while over land it is rapid with significant diurnal effects. Wind flow is in the form of air-mass movement and frontal activity, trade winds, convergence, and divergence of specific air streams, and the interim development of tropical disturbances such as easterly waves and tropical cyclones.

The state of the atmosphere over the Caribbean area is undergoing continuous change and exhibits large and small variations in moisture and temperature distribution. Over a five day period, the following cross-sections have been analyzed to show some of the states and changes that are observed. The two planes that are depicted are north-south from Jacksonville, Florida, to Allbrook Air Force Base, Panama, and are west-east from Merida, Mexico, to Guadelupe, by way of Grand Turk. Discussions follow for each route.

14.1 Jacksonville, Florida, to Allbrook Air Force Base, Panama

17 March 1969, 1200 Z. The moist, cloudy, rainy conditions from Jacksonville to Cape Kennedy are related to a cold front. You see a subsidence inversion and dry layer at three kilometers from Miami to the vicinity of Cuba. South of Cuba to the vicinity of Swan Island is an area of convergence and rising air that has lifted moisture above three kilometers. From Swan Island to Allbrook Air Force Base, there is the typical trade wind situation with a temperature inversion and dry air layer about two kilometers.

18 March 1969, 1200 Z. Rapid wave cyclone development over the Gulf of Mexico has surged warm air over a warm front lying north of Miami with relatively moist air to above three kilometers. The relatively light winds and tropical air mass over southern Florida is moist from two kilometers to the surface while a typical dry situation continues to exist above.

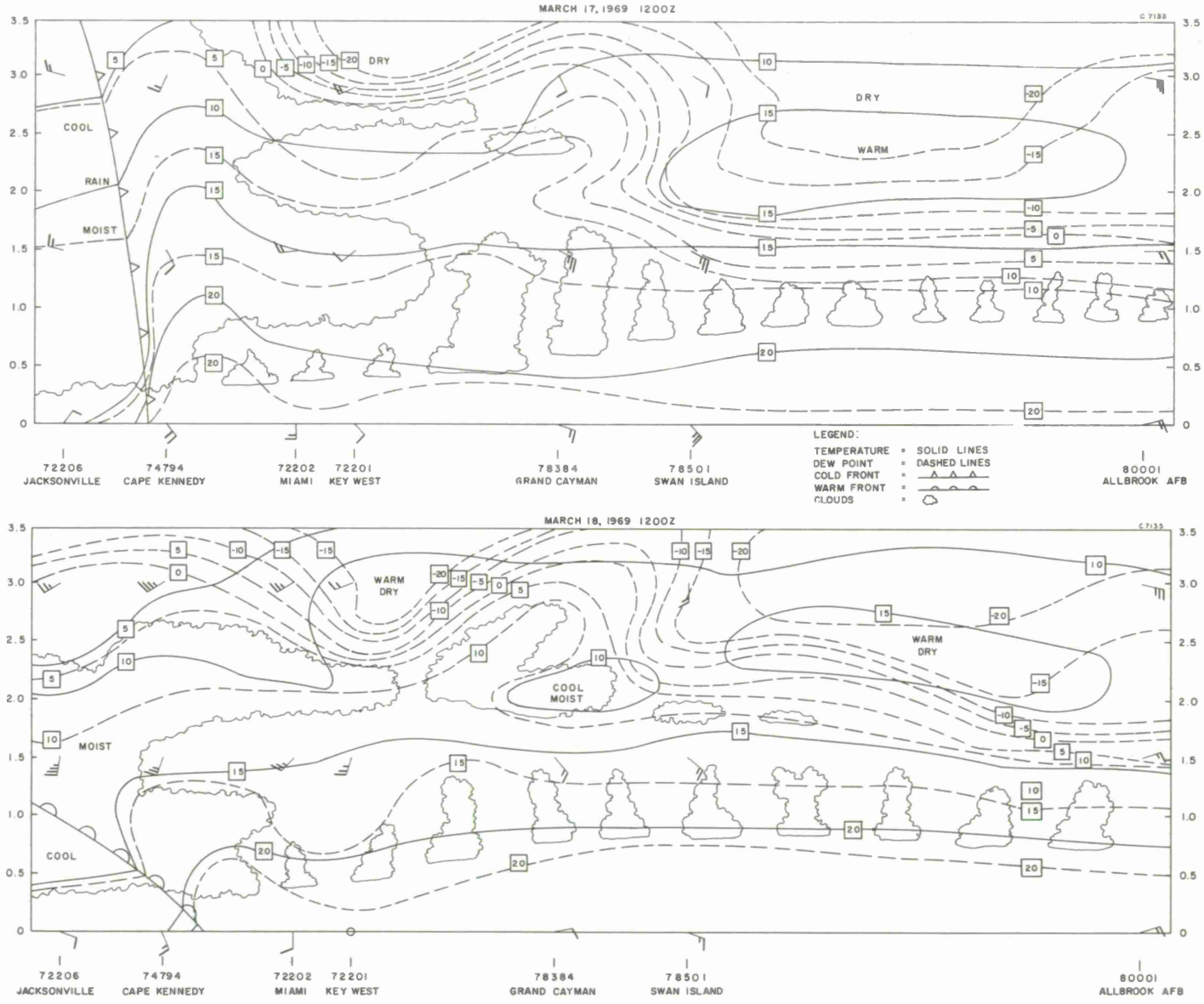
MARCH 17, 1969 1200Z
C 7139
DRY
COOL
RAIN
MOIST
DRY
WARM
LEGEND:
TEMPERATURE = SOLID LINES
DEW POINT = DASHED LINES
COLD FRONT =
WARM FRONT =
CLOUDS =
72206 JACKSONVILLE
74794 CAPE KENNEDY
72202 MIAMI
72201 KEY WEST
78384 GRAND CAYMAN
78501 SWAN ISLAND
80001 ALLBROOK AFB
MARCH 18, 1969 1200Z
C 7135
WARM DRY
COOL MOIST
WARM DRY
MOIST
COOL
72206 JACKSONVILLE
74794 CAPE KENNEDY
72202 MIAMI
72201 KEY WEST
78384 GRAND CAYMAN
78501 SWAN ISLAND
80001 ALLBROOK AFB

FIGURE 61.

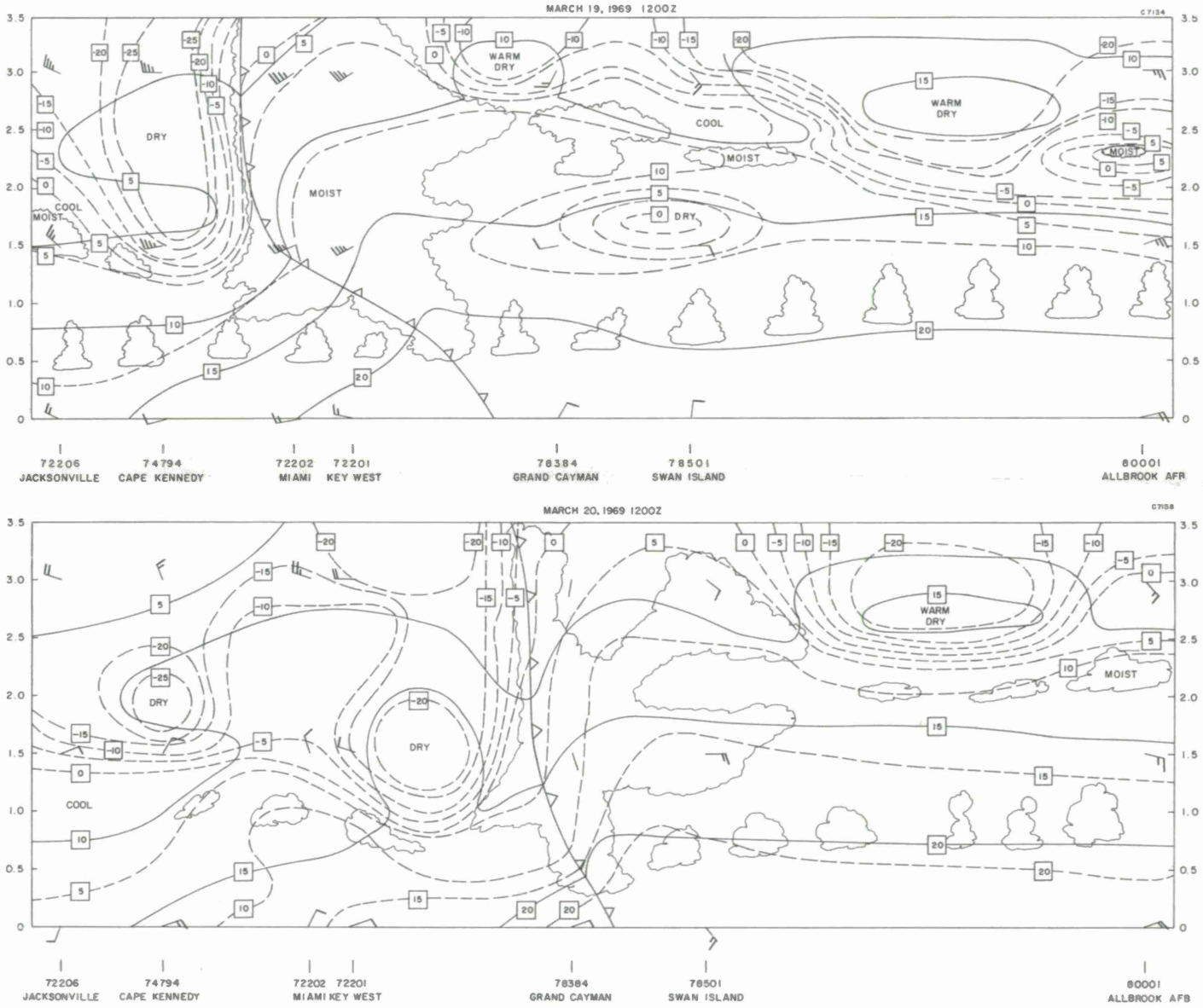
MARCH 19, 1969 1200Z
C7134
WARM DRY
COOL
MOIST
DRY
WARM DRY
MOIST
COOL MOIST
DRY
MOIST
72206 JACKSONVILLE
74794 CAPE KENNEDY
72202 MIAMI
72201 KEY WEST
78384 GRAND CAYMAN
78501 SWAN ISLAND
80001 ALLBROOK AFB
MARCH 20, 1969 1200Z
C7158
WARM DRY
MOIST
DRY
DRY
COOL
72206 JACKSONVILLE
74794 CAPE KENNEDY
72202 MIAMI
72201 KEY WEST
78384 GRAND CAYMAN
78501 SWAN ISLAND
80001 ALLBROOK AFB

FIGURE 62.

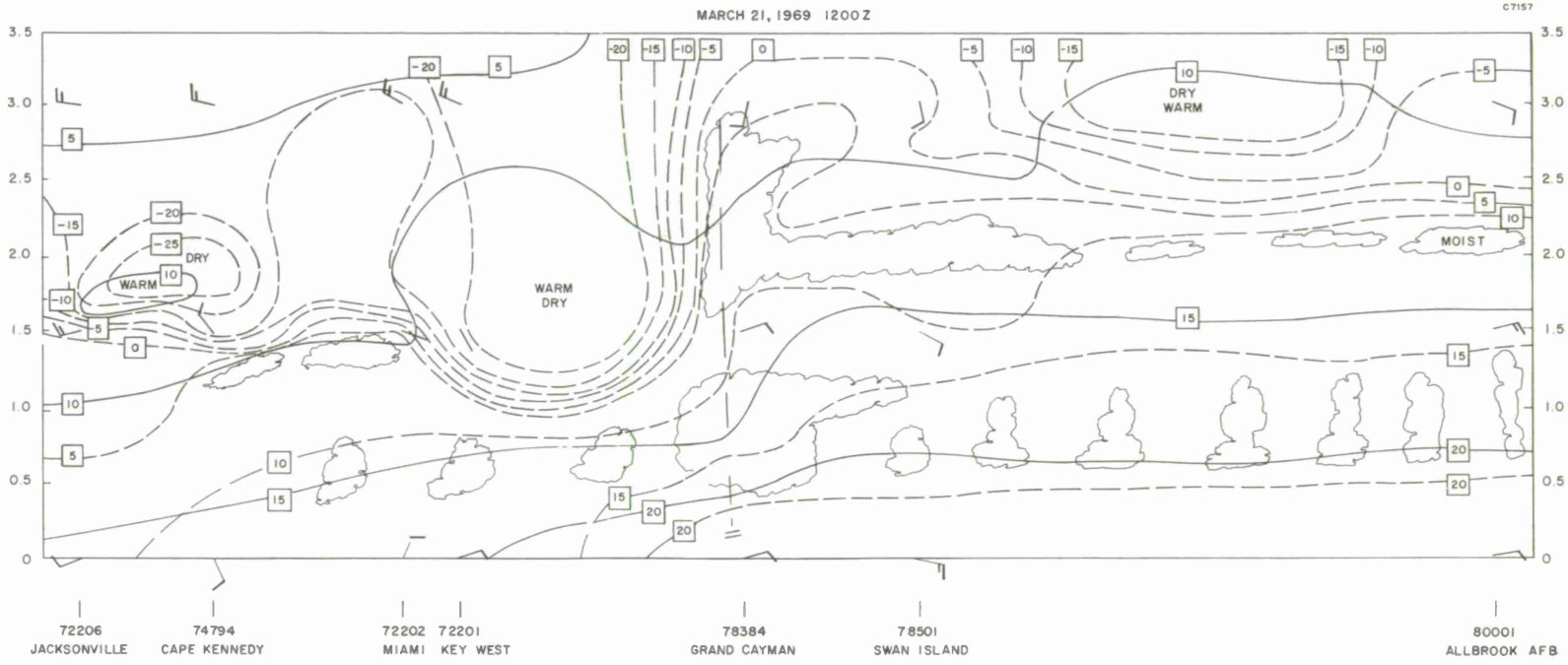
MARCH 21, 1969 1200Z
C7157
3.5
3.0
2.5
2.0
1.5
1.0
0.5
0
DRY
WARM
WARM
DRY
DRY
WARM
MOIST
72206
JACKSONVILLE
74794
CAPE KENNEDY
72202
MIAMI
72201
KEY WEST
78384
GRAND CAYMAN
78501
SWAN ISLAND
80001
ALLBROOK AFB

FIGURE 63.

A large area south of Cuba continues quite moist. Note that the Swan Island three kilometer wind has increased and become southerly. From Swan Island to Allbrook Air Force Base there continues to be a warm dry layer above 1.5 kilometers.

19 March 1969, 1200 Z. A cold front has pushed across Florida and rests over Cuba. Dry continental air is in evidence over northern Florida while warm, moist air remains aloft over southern Florida with the previous dry air pushed southward and aloft. Moist air continues over Grand Cayman while moisture has made inroads into the air over Swan Island. The typical structure of the Trade Winds over Allbrook Air Force Base is now broken by a moist layer from 2 to 2.5 kilometers.

20 March 1969, 1200 Z. Over all of Florida and Cuba there is dry continental polar air with moistening beginning to develop below 1.5 kilometers. The cold front is becoming weak and slow moving to the south of Cuba and leaves this area in deep moisture. The southerly components to the 3 kilometer winds at Swan Island and Allbrook Air Force Base are evidence of convergence and show expected increase in moisture.

21 March 1969, 1200 Z. The dry air over Florida and Cuba continues to moisten at low levels and the cold front is washing out near Grand Cayman. The Trade Winds are now quite weak and the tropical inversion is now poorly defined and relatively high.

14.2 Merida, Mexico, to Guadelupe by Way of Grand Turk

17 March 1969, 1200 Z. On this date this lengthy route is primarily in tropical easterly winds and deep moisture. Swan Island is dry above 1.5 kilometers but southeasterly winds can be expected to thicken the moist layer. The land chain of Cuba, Haiti, and Puerto Rico divides a zone of convergence and deep moisture as found at Grand Cayman and divergence and very dry air from 1.5 kilometers and above as seen at Grand Turk. The remainder of the route has a typical Trade Wind subsidence layer above 2 kilometers.

18 March 1969, 1200 Z. A cold front with deep moisture is over Merida and the south to southeast winds have not yet lifted the dry air over the Swan Island area. The great contrast of moisture distribution continues on the south and north sides of the land chain. The eastern portion of the route maintains typical Trade Wind characteristics.

19 March 1969, 1200 Z. The cold front is well east of Merida and is washing out over the warm Caribbean waters. The moisture is increasing at Swan Island. Ahead of the front, winds aloft at Grand Cayman have shifted to southwest and the air mass is dryer. Also at Grand Turk, westerly winds are breaking the dry air into layers. The eastern part of the route has increased subsidence that is lowering the level of dry, warm air and this is associated with a shift to light northwest winds at 3 kilometers.

20 March 1969, 1200 Z. Dry air has established itself at three kilometers over Merida in a westerly flow aloft, while moisture and clouds have saturated all of the Swan Island and Grand Cayman region. Westerly flow over the Grand Turk area has moistened the air to 2 kilometers and it remains very dry above. The interruption in the easterlies has affected the Puerto Rico area with some decrease in moisture gradients.

21 March 1969, 1200 Z. Easterlies are gradually returning to all sections of the route except Grand Turk with more typical moisture and dry layers prevailing.

12.3 Summary

In a general way, the thermal-moisture characteristics of the lower atmosphere can be analyzed and explained. For small variations in analysis and for forecasting it would be necessary to have more radiosonde observations and/or aircraft spiral data. Regular twice-daily analyses could then keep very close track of the Trade Wind subsidence inversion and other details.

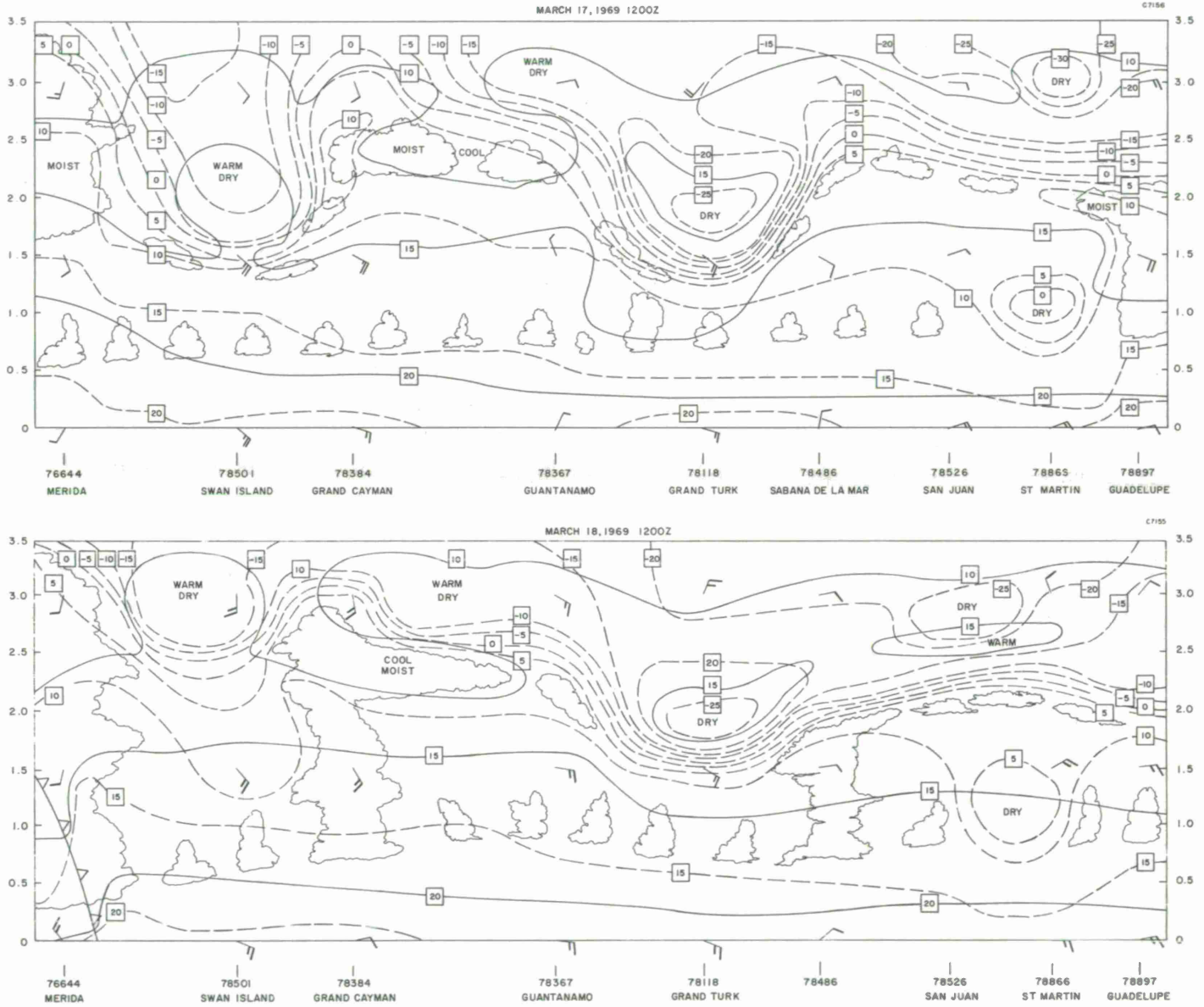
MARCH 17, 1969 1200Z
C7156
MOIST
WARM DRY
MOIST
COOL
WARM DRY
DRY
DRY
DRY
MOIST
DRY
76644 MERIDA
78501 SWAN ISLAND
78384 GRAND CAYMAN
78367 GUANTANAMO
78118 GRAND TURK
78486 SABANA DE LA MAR
78526 SAN JUAN
78865 ST MARTIN
78897 GUADELUPE
MARCH 18, 1969 1200Z
C7155
WARM DRY
WARM DRY
COOL MOIST
DRY
DRY
WARM
DRY
76644 MERIDA
78501 SWAN ISLAND
78384 GRAND CAYMAN
78367 GUANTANAMO
78118 GRAND TURK
78486
78526 SAN JUAN
78866 ST MARTIN
78897 GUADELUPE

FIGURE 64.

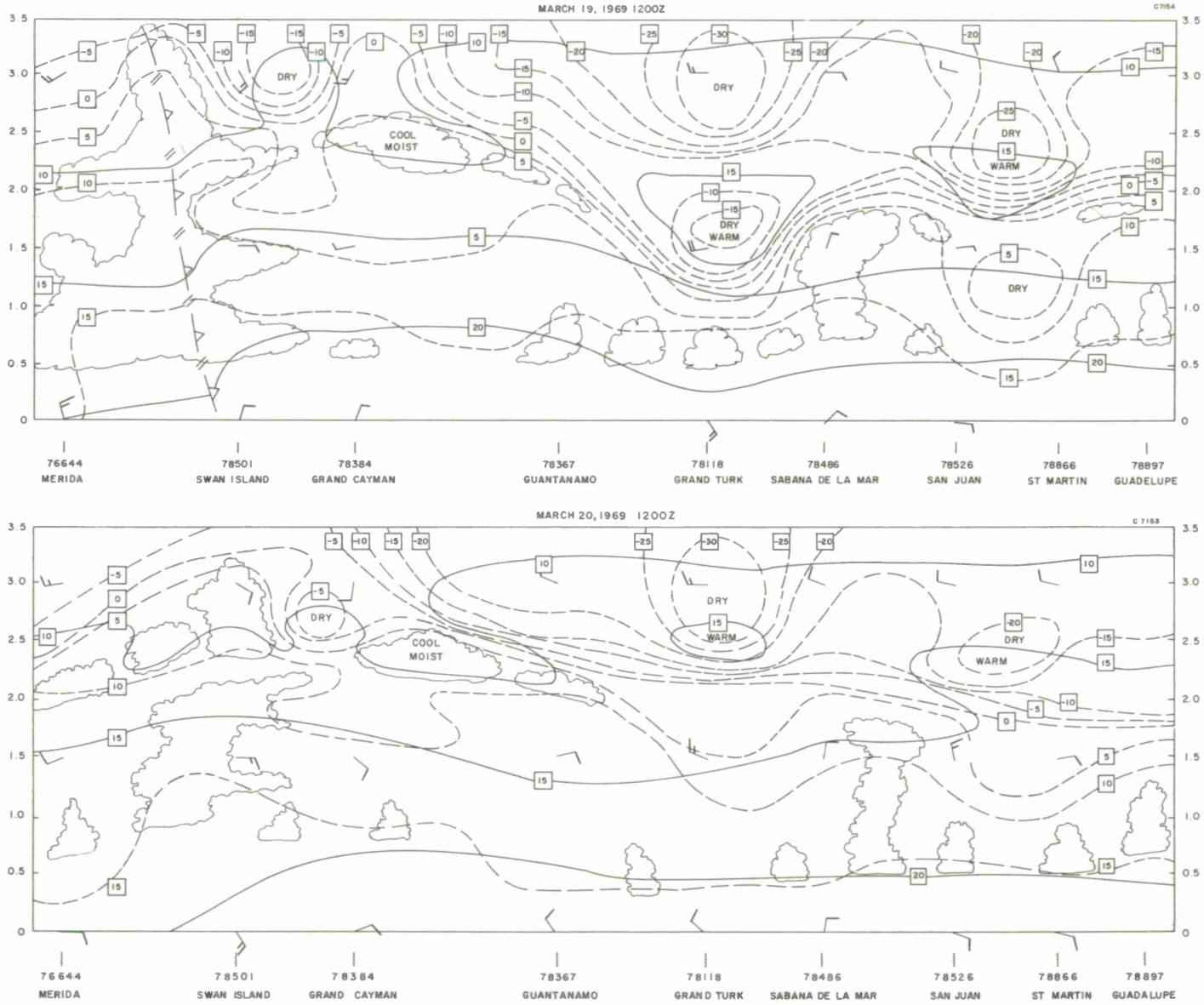
MARCH 19, 1969 1200Z
C7154
DRY
COOL MOIST
DRY
DRY WARM
DRY
WARM
DRY
3.5
3.0
2.5
2.0
1.5
1.0
0.5
0
76644 MERIDA
78501 SWAN ISLAND
78384 GRAND CAYMAN
78367 GUANTANAMO
78118 GRAND TURK
78486 SABANA DE LA MAR
78526 SAN JUAN
78866 ST MARTIN
78897 GUADELUPE
MARCH 20, 1969 1200Z
C7183
DRY
COOL MOIST
DRY
WARM
DRY
WARM
76644 MERIDA
78501 SWAN ISLAND
78384 GRAND CAYMAN
78367 GUANTANAMO
78118 GRAND TURK
78486 SABANA DE LA MAR
78526 SAN JUAN
78866 ST MARTIN
78897 GUADALUPE

FIGURE 65.

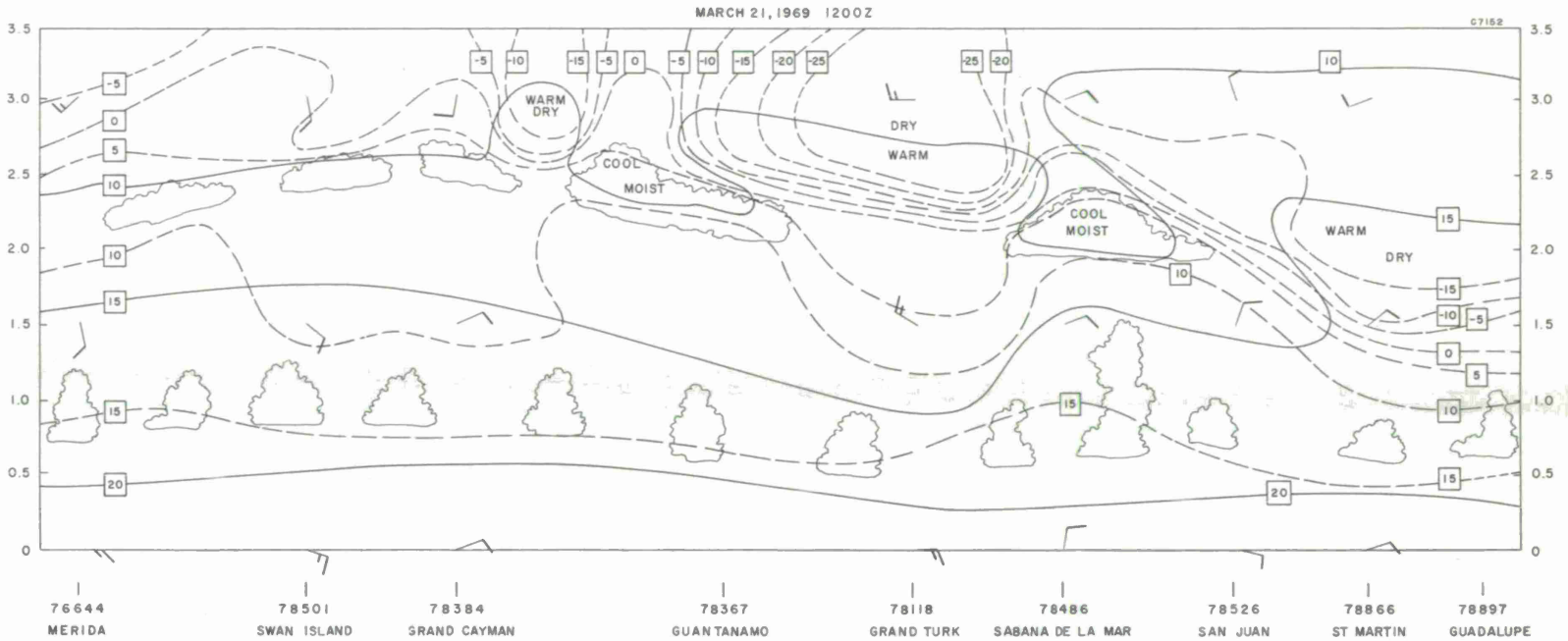
MARCH 21, 1969 1200Z
C7152
WARM DRY
COOL MOIST
DRY WARM
COOL MOIST
WARM DRY
3.5
3.0
2.5
2.0
1.5
1.0
0.5
0
76644 MERIDA
78501 SWAN ISLAND
78384 GRAND CAYMAN
78367 GUANTANAMO
78118 GRAND TURK
78486 SABANA DE LA MAR
78526 SAN JUAN
78866 ST MARTIN
78897 GUADALUPE

FIGURE 66.

SECTION XV

CONCLUSIONS

The microwave refractivity measurements made with the USAF Convair, supplemented by radiosonde data (Rowlandson, et al, 1969, 1970), has permitted an analysis of the temporal and spatial behavior of the Trade Wind Duct for March 1969. From this analysis it is quite clear that the existence of the Duct depends upon a rather delicate balance of thermodynamic forces. Intense subsidence of mid-tropospheric air provides a temperature inversion near sea level which then constrains the upward flow of warm, moist air from the surface. In this case, the Trade Wind Duct is intense and generally stratified over large geographical areas.

It was demonstrated in the analyses of the individual missions that two conditions have the most devastating effect on this thermodynamic balance. The first occurs when cool, Continental air, overruns the warmer water of the Caribbean. Instability is then produced at the surface and moist air rises with considerable vertical momentum. The release of latent heat of condensation further amplifies this vertical transfer of energy and moisture can be driven aloft to heights far exceeding the normal height of the inversion. A second noticeable effect occurs when a low pressure trough, if not over the Caribbean, skirts past the northern part of the Sea. As moist air is lifted by the convergence near the surface it is then carried southward by the anticyclonic flow of air around the center of the low. This type of frontal system tends to move to the east since the level of non-divergence is at low altitudes and the high altitude pattern predominates. As was shown during the last three missions, the effect of this type of disturbance is felt at extremely great distances from the center.

Measurements in the Key West and Puerto Rico areas showed the orographic and thermal (convective) effects produced by land masses. One might consider these effects to be sufficiently localized as not to have any significant consequence. However, if one is attempting to propagate radio signals from these land areas these local effects then become important. If the Duct is made to oscillate in altitude by these effects (Rowlandson, 1966), it may become possible to couple radio signals into the Duct because at certain points in space the local elevation angles become sufficiently small. (Guignard, et al, 1965)

Of course, using the Duct to reflect signals presents a different interpretation of the effect of losing the stratified properties of this layer.

In view of the widely varying properties of the Trade Wind Duct, it would appear that a statistical presentation of its charactistics is most meaningful. For detailed measurements of orographic and thermal effects mentioned above, it is imperative that an instrumented airborne system be used. However, with a sensible distribution of radiosonde stations, augmented by launches from ships, it is economically more reasonable to use this type of information for a large area. Therefore, if confidence can be placed on the accuracy of radiosonde data, the statistical presentation used by Dougherty, et al (1967) is meaningful. It is well known that propagation by tropospheric scatter can never be defined other than by consideration of the statistical behavior of median signal level, fading rate, depth of fade, etc.

Within certain periods of time, and over defined areas, one may associate the statistical behavior with meteorological conditions and changes in the transmission parameters (Tagliaferri, et al, 1966).

Similarly, it is reasonable to know statistically the probability for a given location and period of time such information as:

If I have a choice of equipment, the one operating at 30 centimeters wavelength and the other at two meters, which would be more effective to receive and/or communicate beyond the horizon?

Certainly, the choice depends upon the relative advantages of duct propagation versus reflection by layers. The statistical information on the properties of these layers coupled with ray-traced data could provide information to resolve such a question.

Now, let us return to the question of the usefulness of radiosonde data. During the March experiment only a few opportunities were available where aircraft measurements could be compared with radiosonde data. As mentioned in the preceding sections, it is virtually impossible to make any meaningful comparisons because the aircraft measurements are usually not located close to the position of the radiosonde in flight. Furthermore, the balloon tends to be affected less by horizontal variations of the free air variables than do the aircraft measurements. If the radiosonde instruments could be co-located with the refractometer on the aircraft, and if the dynamic effects were compensated, a useful comparison could be made. The correction method described by Dougherty, et al (1967), and included herein, could then be evaluated.

It may also be possible to modify the present radiosonde operating procedures to enhance the quality and usefulness of the data. For those stations where launch control can be exercised it should be requested that the radiosonde elements be brought into equilibrium with the environment prior to release. The transmissions recorded at release would be checked against psychometric data to verify that the prescribed launch procedures were followed. Such procedures are imperative to make effective corrections for the lag in sensors (Bean and Dutton, 1966, pp 40-41). In addition, all significant data should be recorded and reported.

SECTION XVI

RECOMMENDATIONS

The prevalence of elevated layers in the subtropical areas of the world provide a statistically dependable method to receive and/or communicate radio signals far beyond the horizon.

For any particular area, it is possible to develop the statistical probability that a given type of propagation mode can be effectively employed.

Considering, for example, the Caribbean Sea, the radiosonde data available from all cooperative sources should be used to statistically define the properties of elevated layers on a seasonal and geographical basis.

This data could be enhanced by requesting psychometric measurements at launch and stressing the importance of bringing the sensors to equilibrium with the environment prior to launch.

Correction methods would be applied in an attempt to compensate for sensor time lags. This correction procedure should be tested by a confrontation of data obtained from an airborne microwave refractometer and co-located radiosonde sensors.

Together with ray-tracing methods, the statistical response of a propagation technique to radio parameters, such as wavelength, geometry, propagation mode (ducting versus reflections) should be determined. This determination would, of course, be related to seasonal effects which is substantially the meteorological conditions, and to geographical features.

Mode-coupling considerations should be investigated such as the effect of orographic and convective effects on the normally stratified Trade Wind Duct. Radio considerations would be included such as the effect of wavelength, beamwidth and scanning mode in relation to thedegree of coupling.

A comprehensive experiment should include actual radio transmissions and records of received signal characteristics over selected paths. As previously recommended (Rowlandson, 1966, pp 50-51) an attempt to separate the coherent and non-coherent signal characteristics would reveal information on the relative merits of duct versus reflection propagation modes within selected time frames. The evaluation of the effectiveness of mode-coupling using radio experimentation should also be included.

APPENDIX A

CORRECTION PROCEDURES FOR THE SENSOR TIME LAG IN RADIOSONDE DATA
(After Dougherty)

BACKGROUND

For several years, radiosonde data have been used to determine the vertical distribution of the radio refractive index without considering the inherent errors in the transmitting element. Wagner (1960) concluded that of all the errors in the sensing elements, data transmission cycling procedures, and significant level selection criteria, it is the time lag of the temperature and humidity sensors which constitute the most serious error. All of the data considered here were from stations using the lithium chloride humidity sensor.

CORRECTION FACTORS

If θ^* and θ are, respectively, the corrected and indicated values of the parameter, then

$$\theta_i^* = \theta_i + R\lambda \left[\frac{\theta_i - \theta_{i-1}}{h_i - h_{i-1}}\right] \tag{A-1}$$

where $R = 0.005$ km/sec, the assumed ascention rate of the balloon

λ = lag constant in seconds

h = height in km

i = level reported

If the same procedure is applied to changes of the parameter through the layer, then

$$\Delta\theta_i^* = \Delta\theta_i + R\lambda \left[\frac{\Delta\theta_i}{\Delta h_i} - \frac{\Delta\theta_{i-1}}{\Delta h_{i-1}}\right] \tag{A-2}$$

For temperature, T, the $\lambda_T = 3$ seconds; for relative humidity, RH, $\lambda_{RH} = 5$ seconds, where

$$\Delta\theta_i = \theta_i - \theta_{i-1} \tag{A-3}$$

The λ_{RH} varies with temperature, but since the range of temperature for this particular problem (Trade Wind Inversion refractive layers) is usually 0 to 30° C, the approximate room temperature value of λ_{RH} obtained by Wexler, et al, (1955), is used.

For thin layers, this procedure is believed to over-correct the relative humidity. Therefore, the factor δ is used:

$$\delta = 1 \qquad \text{if } \Delta h_i > 0.1 \text{ km}$$

$$\delta = 10\,\Delta h_i \qquad \text{if } \Delta h_i < 0.1 \text{ km} \tag{A-4}$$

Substituting the numerical values of the constants, the correction term for relative humidity is

$$C_{RH} = 0.025\delta \left[\frac{\Delta RH_i}{\Delta h_i} - \frac{\Delta RH_{i-1}}{\Delta h_{i-1}} \right] \tag{A-5}$$

The correction term for temperature is

$$C_T = 0.015\delta \left[\frac{\Delta T_i}{\Delta h_i} - \frac{\Delta T_{i-1}}{\Delta h_{i-1}} \right] \tag{A-6}$$

The change in refractivity due to changes in relative humidity and temperature is given by

$$\Delta N = \frac{\partial N}{\partial T}\ \Delta T + \frac{\partial N}{\partial RH}\ \Delta RH \tag{A-7}$$

so that the correction term for the refractivity gradient, $\Delta N/\Delta h$ is

$$C_N = \left[C_T \frac{\partial N}{\partial T} + C_{RH} \frac{\partial N}{\partial RH} \right] / \Delta h_i \tag{A-8}$$

Since the effect of the temperature lag on the refractive index gradient is negligible, (for the range of temperatures generally encountered) relative to that of relative humidity, the correction term generally used for the refractivity gradient is

$$C_N = \frac{K_{RH}\, C_{RH}}{\Delta h_i} \tag{A-9}$$

where

$$K_{RH} = 3733 e_s / T^2 \approx 0.3 \text{ at } 0^\circ \text{ C} \tag{A-10}$$

The T is the absolute temperature, 273 plus degrees centigrade. However, the complete correction term for correcting the refractivity gradient is

$$C_N = \frac{C_{RH} K_{RH}}{\Delta h_i} + \frac{[K_w - K_d][C_T]}{\Delta h_i} \tag{A-11}$$

where

$$K_{RH} = \frac{\partial N}{\partial RH} \tag{A-12}$$

$$K_d = 77.6 P / T^2 \tag{A-13}$$

$$K_w = \frac{3.73 \times 10^6 RH}{T^2} \left[\frac{de_s}{dT} - \frac{2e_s}{T}\right] \tag{A-14}$$

where K_w and K_d are "wet" and "dry" components of $\partial N/\partial T$, respectively, and T is the absolute temperature. These coefficients K_{RN}, K_d, and K_w are plotted in Figures A-1, A-2, and A-3.

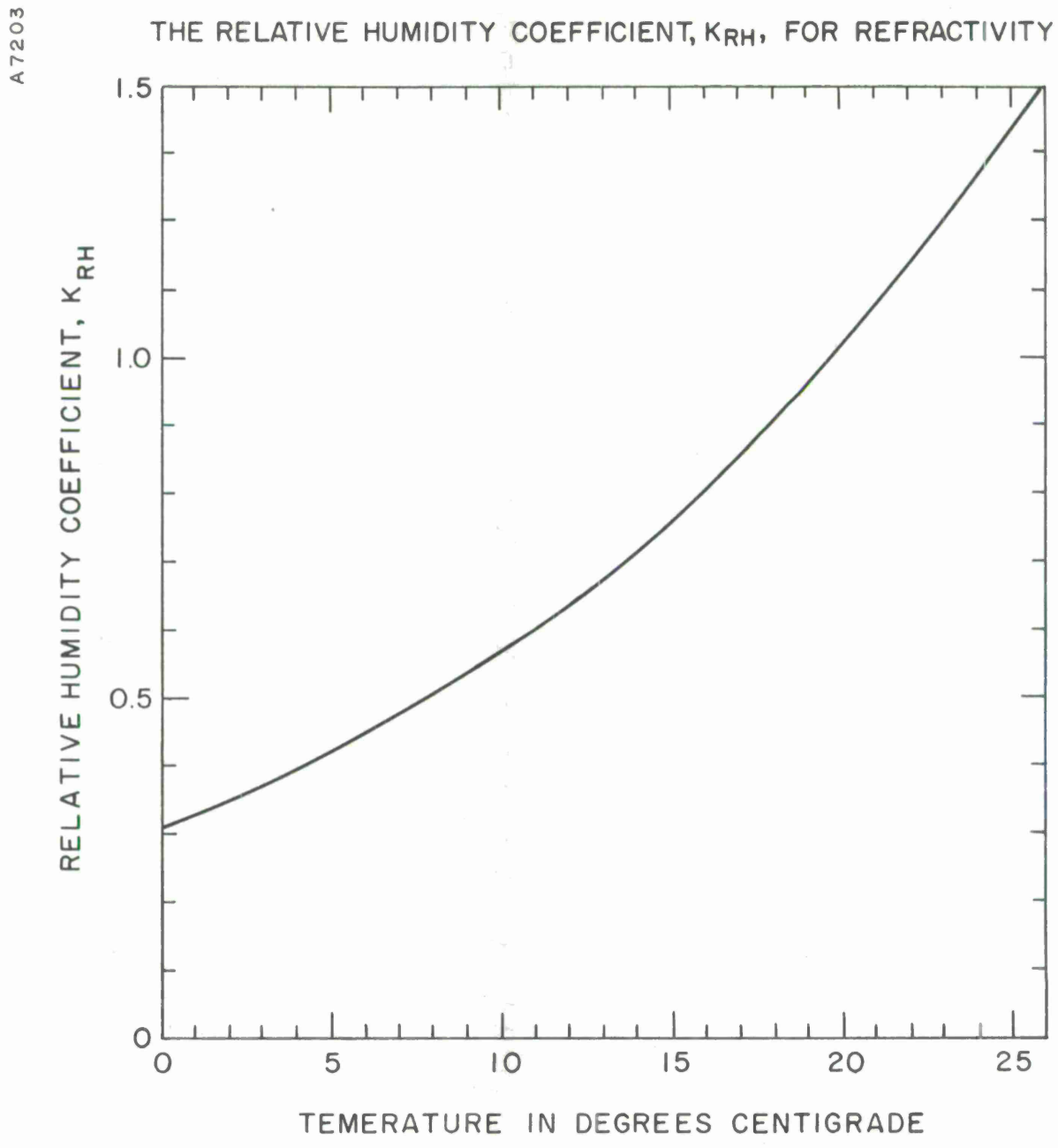
A7203
THE RELATIVE HUMIDITY COEFFICIENT, K_{RH}, FOR REFRACTIVITY
RELATIVE HUMIDITY COEFFICIENT, K_{RH}
1.5
1.0
0.5
0
0
5
10
15
20
25
TEMERATURE IN DEGREES CENTIGRADE

FIGURE A-1.

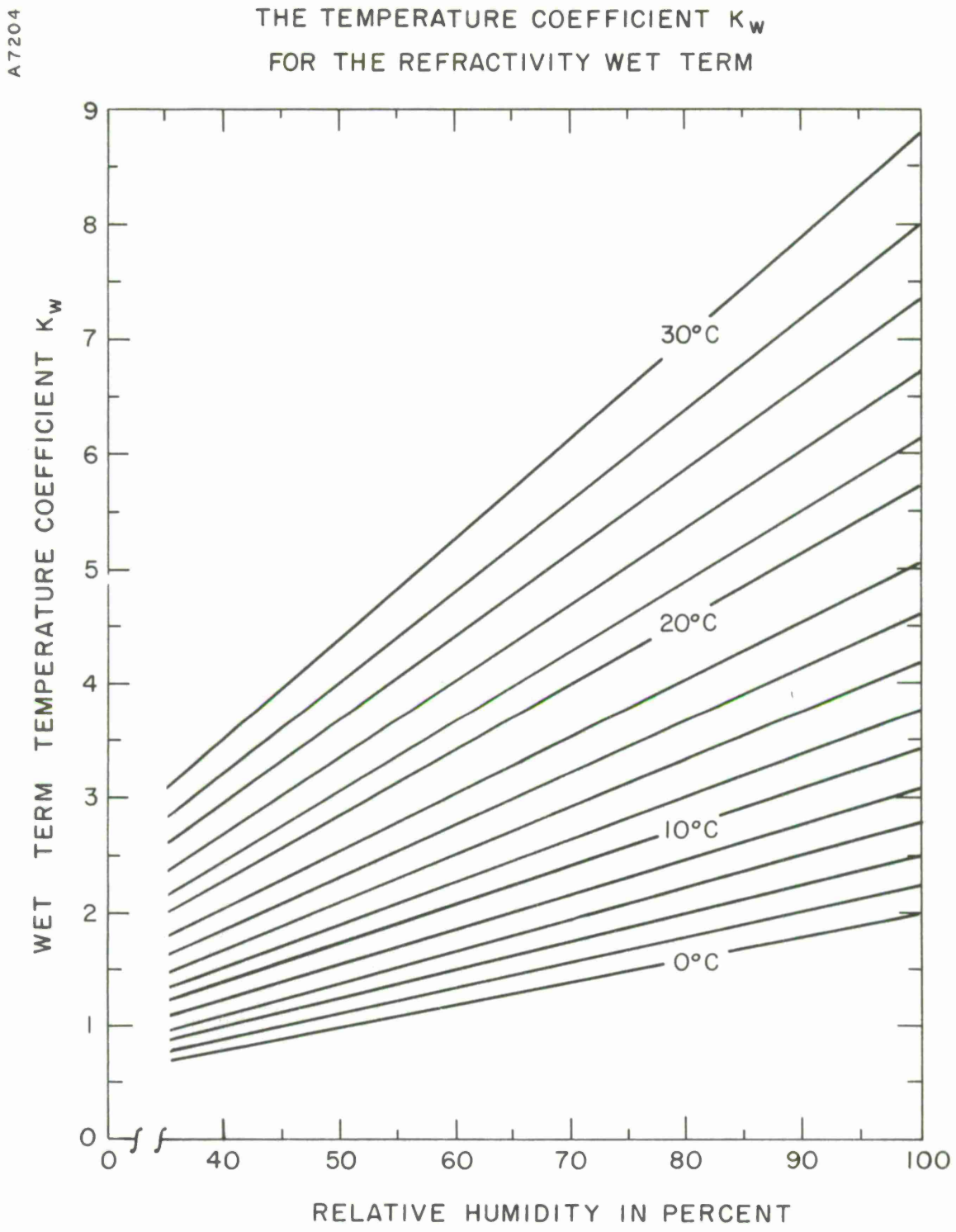
A7204
THE TEMPERATURE COEFFICIENT K_w
FOR THE REFRACTIVITY WET TERM
WET TERM TEMPERATURE COEFFICIENT K_w
9
8
7
6
5
4
3
2
1
0
30°C
20°C
10°C
0°C
0
40
50
60
70
80
90
100
RELATIVE HUMIDITY IN PERCENT

FIGURE A-2.

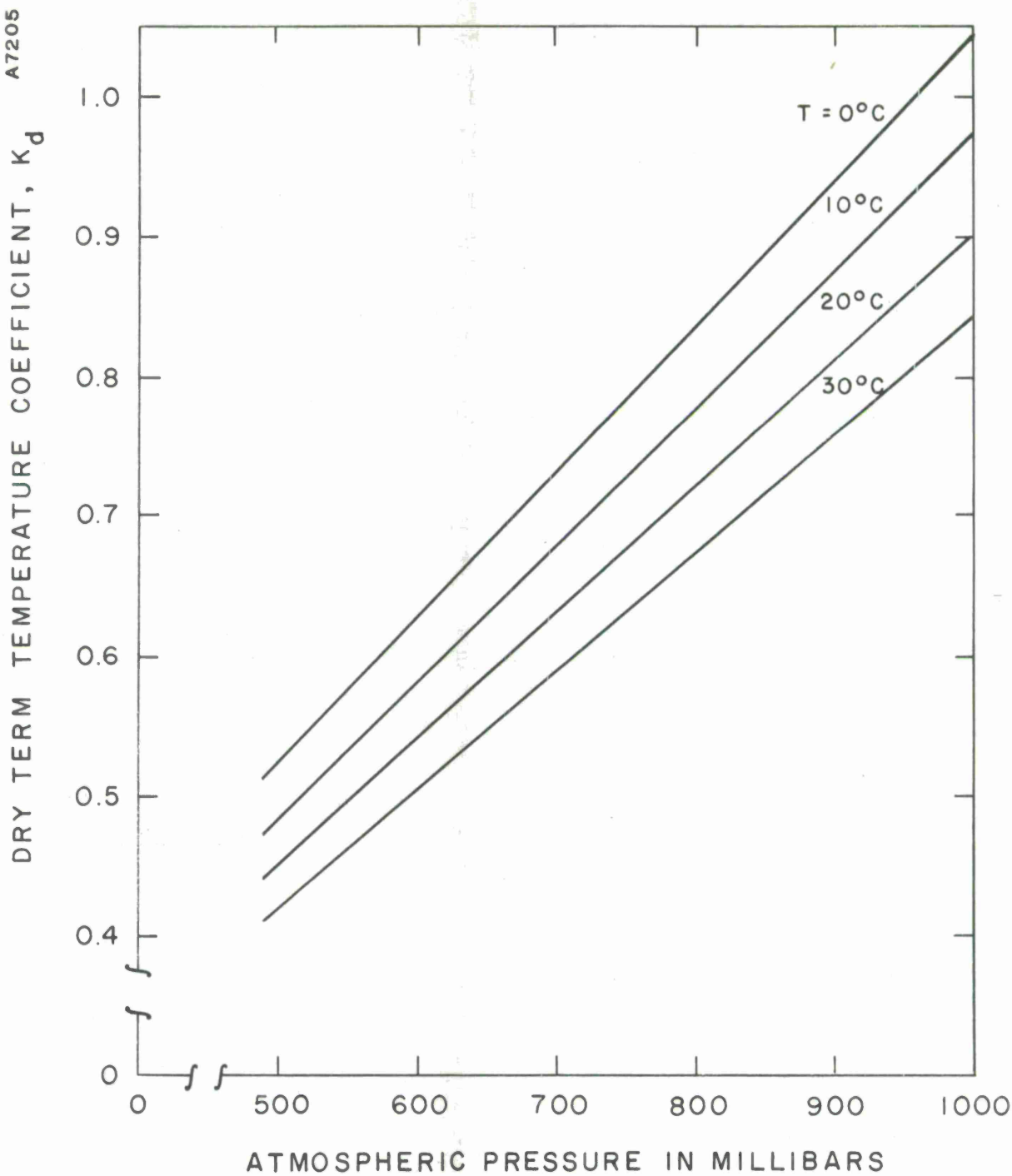
A7205
DRY TERM TEMPERATURE COEFFICIENT, K_d
1.0
0.9
0.8
0.7
0.6
0.5
0.4
0
T = 0°C
10°C
20°C
30°C
0
500
600
700
800
900
1000
ATMOSPHERIC PRESSURE IN MILLIBARS

FIGURE A-3.

REFERENCES

1. Bean, B. R. and Thayer, G. D. (1959), "CRPL Exponential Reference Atmosphere," NBS Monograph 4, Sup. of Doc., U. S. Government Printing Office, Washington, D. C.

2. Bean, B. R. and Dutton, E. J. (1966), "Radio Meteorology," National Bureau of Standards Monograph 92, Sup. of Doc., U. S. Government Printing Office, Washington, D. C.

3. Bénard, H. (1900), "Les Tourbillons Cellulaires Dans une Nappe Liquid," Rev. Gen. Sci. Pures Appl. 11, 1261-1271, 1309-1328.

4. Bunker, A. F. (1953), "On the Determination of Moisture Gradients From Radiosonde Records," Bull. Am. Meteorol. Soc. 34, 406-409.

5. Cline, D. E. (1957), "International Radiosonde Comparison Tests," Tech. Memo NRM-1907, U. S. Army Signal Eng. Lab. Task NR 3-36-11-402.

6. Dougherty, H. T., Riggs, L. P. and Sweezy, W. B. (1967), "Characteristics of the Atlantic Trade Wind System Significant for Radio Propagation," ESSA Technical Report IER 29-ITSA 29, Clearing House for Federal Scientific and Technical Information, Springfield, Virginia.

7. Fleagle, R. G. and Businger, J. A. (1963), "An Introduction to Atmospheric Physics," International Geophysics Series, Vol. 5, Academic Press, New York.

8. Gentilli, J. (1958), "A Geography of Climate," The University of Western Australia.

9. Guinard, N. W., Laing, M. B., and Morin, K. W. (1965), "Ray-Tracing in Rising and Falling Ducts," NRL Report 6253.

10. Hill, M. N. (1962), "The Sea," Vol I; Physical Oceanography, Interscience Publishers, John Wiley and Sons, New York.

11. Middleton, W. E. K. and Spilhaus, A. F. (1953), Book, "Meteorological Instruments," University of Toronto Press, Toronto, Ontario, Canada.

12. Montgomery, R. B. (1936), "On the Momentum Transfer at the Sea Surface," Part II, Papers Phys. Oceanog, Meteorol. 4, No. 3, 21-22.

13. Montgomery, R. B. (1948), "Vertical Eddy Flux of Heat in the Atmosphere," J. Meteorol. 5, 265-274.

14. Roll, H. U. (1965), "Physics of the Marine Atmosphere," International Geophysics Series, Vol. 7, Academic Press, New York.

15. Rowlandson, L. G. (1966), "Measurements on the Trade Wind Inversion at Aruba, N. A.," MTR 116, The Mitre Corporation, Bedford, Massachusetts (Contract AF 19(628)-5165).

16. Rowlandson, L. G., Aldrich, R. J., and Herlihy, J. R. (1969), "Measurements of Meteorological Parameters and Radio Refractivity in the Caribbean," ESD-TR-69-374, Aerospace Instrumentation Program Office, Electronic Systems Division, USAF, Bedford, Massachusetts.

17. Rowlandson, L. G. and Schwarz, J. S. (1970), "Radio Refractivity and Meteorological Data Plots from Radiosonde Launches," ESD-TR-70-60, Aerospace Instrumentation Program Office, Electronic Systems Division, USAF, Bedford, Massachusetts.

18. Skillman, J L. (1969), "The Effects of Elevated Tropospheric Layers on Radio Wave Propagation," Technical Report No. R42/002/69, National Security Agency, Fort George G. Meade, Maryland.

19. Smith, E. K. and Weintraub, S. (August 1953), "The Constants in the Equation for Atmospheric Refractive Index at Radio Frequencies," Proc. IRE 41, 1035-1037.

20. Tagliaferri, O. A. (1966), and the Radio-Meteorological Test Committee, "Support to DCA Tropospheric Scatter Tests," RADC Final Report, TR-66-609, Rome Air Development Center, Rome, New York.

21. Wagner, N. K. (1960), "An Analysis of Radio Effects on the Measured Frequency of Occurrence of Ducting Layers," J. Geophys. Res. 65, 2077-2085.

22. Wexler, A. (1949), "Low Temperature Performance of Radiosonde Electric Hygrometer Elements," J. Res. NBS 43, 49-56.

23. Wexler, A., Garfinkel, S., Jones, F., Hasegawa, S., and Krinsky, A., (1955), "A Fast Responding Electric Hygrometer," J. Res. NBS 55, 71-78.

Security Classification

DOCUMENT CONTROL DATA - R & D

(Security classification of title, body of abstract and indexing annotation must be entered when the overall report is classified)

1. ORIGINATING ACTIVITY *(Corporate author)*
Syracuse University Research Corporation
Merrill Lane, University Heights
Syracuse, New York 13210

2a. REPORT SECURITY CLASSIFICATION
UNCLASSIFIED

2b. GROUP
N/A

3. REPORT TITLE
THE EFFECT OF METEOROLOGICAL CONDITIONS ON THE TRADE WIND DUCT AND RELATED RADIO WAVE PROPAGATION

4. DESCRIPTIVE NOTES *(Type of report and inclusive dates)*
None

5. AUTHOR(S) *(First name, middle initial, last name)*
L. G. Rowlandson
H. W. Meredith

6. REPORT DATE	7a. TOTAL NO. OF PAGES	7b. NO. OF REFS
February 1970	151	23

8a. CONTRACT OR GRANT NO.	9a. ORIGINATOR'S REPORT NUMBER(S)
F19628-69-C-0208	ESD-TR-70-123
b. PROJECT NO.	
c.	9b. OTHER REPORT NO(S) *(Any other numbers that may be assigned this report)*
d.	

10. DISTRIBUTION STATEMENT
This document has been approved for public release and sale; its distribution is unlimited.

11. SUPPLEMENTARY NOTES	12. SPONSORING MILITARY ACTIVITY
	Aerospace Instrumentation Program Office Hq Electronic Systems Division (AFSC) L G Hanscom Field, Bedford, Mass. 01730

13. ABSTRACT

The horizontal extent and the intensity of the Trade Wind Inversion are controlled by meteorological conditions. The subtropical area of the Caribbean is influenced by subsiding air which tends to produce a temperature inversion around one kilometer above the sea surface. The vertical transport of water vapor is thereby inhibited and a boundary forms along the inversion with moist air below and dry air above. The index of radio refraction therefore decreases rapidly with height through this layer to form an elevated duct. The meteorological situation controlling the characteristics of this duct varies from the normal high pressure condition. Interest is therefore centered on the variability of the inversion layer as affected by weather systems and local geographical conditions.

DD FORM 1 NOV 65 1473

Security Classification

14. KEY WORDS	LINK A		LINK B		LINK C	
	ROLE	WT	ROLE	WT	ROLE	WT
Radio Propagation						
Refraction						
Trade Wind Inversion						
Ducting						
Meteorology						